NASA CONTRACTOR REPORT

NASA CR-1190

NASA CR-1

EXPERIMENTAL STUDY OF MULTI-COMPONENT COAXIAL-FLOW JETS IN SHORT CHAMBERS

by Bruce V. Johnson

Prepared by
UNITED AIRCRAFT CORPORATION
East Hartford, Conn.
for

NATIONAL AERONAUTICS AND SPACE ADMINISTRATION • WASHINGTON, D. C. • OCTOBER 1968

EXPERIMENTAL STUDY OF MULTI-COMPONENT

COAXIAL-FLOW JETS IN SHORT CHAMBERS

By Bruce V. Johnson

Distribution of this report is provided in the interest of information exchange. Responsibility for the contents resides in the author or organization that prepared it.

Issued by Originator as Report No. G-910091-16

FOREWORD

An exploratory experimental and theoretical investigation of gaseous nuclear
rocket technology is being conducted by the United Aircraft Corporation Research
Laboratories under Contract NASw-847 with the joint AEC-NASA Space Nuclear
Propulsion Office. The Technical Supervisor of the Contract for NASA is Captain
C. E. Franklin (USAF). Results of the investigation of the characteristics of a
coaxial-flow reactor conducted during the period between September 15, 1966 and
April 15, 1968, and results of investigations of the characteristics of transparent
materials conducted between September 15, 1967 and April 15, 1968, are described
in the following two reports (including the present report) which comprise the
required seventh Interim Summary Technical Report under the Contract:

1. Johnson, B. V.: Experimental Study of Multi-Component Coaxial-Flow Jets in
    Short Chambers. United Aircraft Research Laboratories Report G-910091-16,
    April 1968. (present report)

2. Gagosz, R. M. and J. Waters: Optical Absorption and Fluorescence in Fused
    Silica During TRIGA Pulse Irradiation. United Aircraft Research Laboratories
    Report G-910485-3, April 1968. (NASA CR-1191)

Experimental Study of Multi-Component

Coaxial-Flow Jets in Short Chambers

TABLE OF CONTENTS

TABLE OF CONTENTS (Continued)

Experimental Study of Multi-Component Coaxial-Flow

Jets in Short Chambers

SUMMARY

Fluid mechanics experiments were performed to obtain information applicable to an open-cycle, coaxial-flow, gaseous nuclear rocket engine. In this engine concept, gaseous nuclear fuel and a surrounding stream of seeded hydrogen propellant pass coaxially through a reactor chamber. The flow was simulated in the present experiments by multi-component, constant-temperature, coaxial-flow jets in short chambers. The flow was studied using flow visualization techniques and concentration measurements.

All tests were performed in 10-in.-dia chambers having lengths (from inlet plane to exhaust nozzle throat) between 7.5 and 12.5 in. The following flow and geometric variables were investigated: (1) an intermediate-velocity buffer stream between the high-velocity outer-stream (simulated propellant) and the low-velocity inner jet (simulated fuel), (2) the ratio of average outer-stream and buffer-stream velocity to inner-jet velocity, (3) the absolute inlet velocities of the outer stream, buffer stream and inner jet, (4) the ratio of inner-jet gas density to outer-stream and buffer-stream gas density, (5) the ratios of buffer-gas density to outer-stream gas density and to inner-jet gas density, (6) the ratios of inner-jet inlet radius and buffer-stream inlet radius to chamber radius, (7) the ratio of chamber length to diameter, and (8) the ratio of exhaust nozzle throat diameter to chamber diameter. Air was used as the outer-stream gas; air and Freon-11 were used as buffer-stream gases; and air, Freon-11 and FC-77 were used as inner-jet gases. The tests were conducted at Reynolds numbers up to those expected for a full-scale engine.

The results indicate that the containment of inner-jet gas is strongly affected by the occurrence of recirculation or reverse flow in the inner-jet region. For a high ratio of average outer-stream and buffer-stream inlet velocity to inner-jet inlet velocity, the flow recirculates behind the inner jet like flow behind a bluff body, and the containment is poor. For flow conditions with moderate values of this

velocity ratio (on the order of 20), a reduced level of turbulent mixing occurs between the outer stream, buffer stream and inner jet, and the inner-jet core extends to the exhaust nozzle; under these conditions, the amount of inner-jet gas contained approached the amount that would be contained in a cylinder of radius equal to the inner-jet inlet radius and length equal to the chamber length.

RESULTS

As a standard for comparisons, the following geometry and inlet flow conditions were selected: ratio of inner-jet inlet radius to chamber radius, $r_I / r_0 = 0.5$; buffer-stream inlet radius ratio, $r_B / r_0 = 0.65$; chamber length-to-diameter ratio, $L_N / D = 1.0$; ratio of exhaust nozzle throat diameter to chamber diameter, $D_N / D = 0.6$; average buffer-stream and outer-stream inlet velocity, $V_{BAO} = 80$ ft/sec; outer-stream inlet velocity, $V_0 = 97$ ft/sec; buffer-stream inlet velocity, $V_B = 33$ ft/sec ($V_B / V_{BAO} = 0.4$); inner-jet inlet velocity, $V_I = 4$ ft/sec ($V_{BAO} / V_I = 20$); inner-jet gas, Freon-11; and buffer-stream and outer-stream gas, air ($\rho_I / \rho_{BAO} = 4.7$). For this standard flow condition, the ratio of average inner-jet gas partial pressure to total pressure in the chamber, $\bar{P}_I / P$, was approximately 0.20. Unless specified otherwise, all comparisons referred to in the following results are with respect to this standard flow condition.

1. For $r_I / r_0 = 0.5$, the average inner-jet gas partial pressure ratio, $\bar{P}_I / P$, was greatest for $V_B / V_{BAO} \approx 0.4$; it decreased at higher and lower values of V_B / V_{BAO}. For $r_I / r_0 = 0.7$, $\bar{P}_I / P$ was independent of V_B / V_{BAO}. No concentration measurements were made for $r_I / r_0 = 0.6$; however, flow visualization tests indicated the effect of V_B / V_{BAO} on the containment characteristics was decreased from that obtained for $r_I / r_0 = 0.5$ and greater than for $r_I / r_0 = 0.7$.

2. Increasing the inner-jet inlet velocity, V_I, increased $\bar{P}_I / P$ slightly. Decreasing V_I decreased $\bar{P}_I / P$ approximately proportional to $1 / (V_{BAO} / V_I)$.

3. $\bar{P}_I / P$ was independent of the absolute velocity V_{BAO}.

4. $\bar{P}_I / P$ increased with increasing inner-jet gas density.

5. When the ratios of volume flow rates Q_{AIR} / Q_I were the same, $\bar{P}_I / P$ with Freon-11 as the buffer-stream gas and air as the outer-stream gas was equal to or less than $\bar{P}_I / P$ with air as the buffer-stream and outer-stream gases.

6. $\bar{P}_I / P$ was decreased when recirculation or reverse flow of the inner-jet gas occured. For the standard flow condition, a small region of recirculation occurred immediately upstream of the exhaust nozzle.

7. The maximum velocity ratio V_{BAO} / V_I for which recirculation could be prevented by the proper choice of buffer-stream inlet velocity was dependent upon inner-jet gas density. For a given geometric configuration, the maximum momentum flux ratio $V_{BAO}^2 \rho_{BAO} / V_I^2 \rho_I$ for which recirculation could be prevented was approximately the same for all three inner-jet gases tested.

8. The maximum velocity ratio V_{BAO}/V_1 for which recirculation could be prevented by the proper choice of buffer-stream velocity decreased as the chamber length-to-diameter ratio was increased from $L_N/D = 0.75$ to 1.25.

9. Decreasing the exhaust nozzle throat diameter ratio, D_N/D, from 0.6 to 0.2 decreased $\bar{P}_I/P$ for flow conditions where recirculation occurred in the chamber.

INTRODUCTION

An analytical and experimental investigation of gaseous nuclear rocket technology is being conducted by the United Aircraft Research Laboratories under Contract NASw-847 administered by the joint AEC-NASA Space Nuclear Propulsion Office. The research performed under this contract is applicable to both open-cycle and closed-cycle engines. The open-cycle engine concepts which have been investigated include a vortex-stabilized reactor (described in Ref. 1) and a coaxial-flow reactor proposed by the NASA Lewis Research Center (the subject of the present investigation; see Ref. 2 for details of the concept). The closed-cycle engine concept currently under investigation at UARL is the vortex-stabilized nuclear light bulb (Ref. 1). All three engines are based on the transfer of energy in the reactor chamber by thermal radiation from gaseous nuclear fuel to seeded hydrogen propellant. These engines are theoretically capable of providing specific impulses in the range from 1500 to 3000 sec.

In the coaxial-flow engine concept, the nuclear fuel and the propellant would be injected at one end of the reactor chamber and would flow axially to the nozzle (Fig. 1). Additional propellant would probably be added along the peripheral walls and in the exhaust nozzle. The fluid mechanics requirements for this concept, and for all other open-cycle concepts, are (1) that a large fraction of the reactor chamber volume be filled with the gaseous nuclear fuel, and (2) that the ratio of the propellant weight flow rate to the gaseous-nuclear-fuel weight flow rate be large.

The goal of the current gaseous-core nuclear rocket research programs is to investigate the feasibility of each proposed concept. This is being done by studying the various component processes separately (fluid mechanics, heat transfer, nuclear criticality, materials, etc.). The present study of confined coaxial-flow jets will provide information which may be used to determine the feasibility of meeting the fluid mechanics requirements of the coaxial-flow engine concept.

Background Information

The use of coaxial-flow jets for containment of gaseous nuclear fuel was proposed by Ragsdale and Weinstein (Ref. 3) and was further developed in Refs. 2 and 4. Experimental studies (Refs. 5 through 10) and analytical studies (Refs. 11 through 17) were performed to formulate a suitable model for the coaxial-flow jet which can be used in feasibility studies of the full-scale engine. Thus far, the experiments have been performed in chambers where the axial pressure gradients are negligible and the inner-jet inlet area is a small fraction of the total chamber cross-section

area. Since the gaseous nuclear rocket engine requires a large volume fraction of nuclear fuel in the chamber, i.e., 15 to 40 percent, the inner-jet inlet area must be an appreciable fraction of the chamber cross-section area, or else another suitable technique must be developed to obtain a large volume fraction.

In a confined coaxial-flow system, where the inlet jet velocities are not equal, mixing will occur with one stream accelerated and the other decelerated. If this mixing occurs in a constant area duct, a momentum pressure balance on the flow shows that a pressure rise will occur with increasing distance downstream of the inlet. At present, the effect of a nonuniform axial pressure distribution on the coaxial-flow jet has not been determined analytically or experimentally.

Previous analytical and experimental studies have shown that the inlet flow conditions affect the containment characteristics of the coaxial-flow jet. Increasing the inner-jet inlet velocity for a constant outer-stream velocity increased the amount of inner-jet gas in the region behind the inner-jet inlet for the experiments reported in Refs. 5 and 8. Increasing the ratio of inner-jet gas density to outer-stream gas density also increased the concentration of inner-jet gas downstream of the inlet plane for identical inlet velocity ratios (Ref. 8).

Analysis of a three-stream coaxial-flow jet (Ref. 13) indicated that the average concentration of inner-jet gas could be increased, for the same ratio of outer-stream flow rate to inner-jet flow rate, by the use of a "buffer" between the outer stream and inner jet. The buffer consisted of outer-stream gas with a velocity greater than the inner-jet gas. To maintain the same flow rate ratio, the outer-stream velocity was increased to compensate for the slower buffer stream. The effect of a buffer layer on the inner-jet gas containment characteristics had not been determined experimentally until the present study.

Objectives of This Study

There were three primary objectives in the present study. The first was to determine the containment characteristics of confined, isothermal, coaxial-flow jets in short chambers with geometries and flow conditions which simulate the proposed full-scale engine. The second objective was to present these results in a format suitable for use in engine performance studies. The third objective was to investigate a large range of possible geometries and flow conditions to determine which of the ideas proposed in previous analytical studies and experiments for increasing the containment characteristics of jets would apply to confined coaxial-flow jets.

DESCRIPTION OF TEST EQUIPMENT AND PROCEDURES

Coaxial-Flow Test Apparatus, Flow System, and Inlet Flow Conditions

Test Apparatus

A schematic of the coaxial-flow test apparatus is shown in Fig. 2. The chamber inside diameter was 10 in. for all tests in this program. Gas was injected into the chamber through a woven wire screen (0.028-in.-dia wire, 16 mesh, 31 percent nominal open area) at the chamber injection plane. The inlet manifold was divided into three areas. The inner-jet extended from the center to radius r_I , the buffer-stream annulus extended from r_I to r_B , and the outer-stream annulus extended from r_B to r_O . Photographs of the inlet manifold are shown in Fig. 3 and a summary of the inlet manifold geometric configurations tested is presented in Table I. The flow was exhausted from the chamber through a nozzle at the lower end of the chamber (Fig. 2). The distance from the inlet plane to the exhaust nozzle throat, L_N , was adjusted using a spacer. The diameters of the exhaust nozzles, D_N , and the chamber lengths, L_N , used in the tests are also tabulated in Table I.

Photographs of the lucite chamber with an inlet manifold and exhaust nozzle used for the flow visualization tests and the steel chamber used for the gas concentration measurement tests are shown in Figs. 4a and 4b, respectively. The details of the flow visualization optical system and the light absorptometer will be discussed in a following section.

Flow System

A photograph of the coaxial-flow test facility is shown in Fig. 5. To supply the desired combinations of inner-jet, buffer-stream and outer-stream gases and inlet gas velocities to the inlet manifold, a combination of gas generators, heaters and compressors were used. For air flow rates in the outer-stream and the buffer-stream up to 2 lb/sec, air was drawn into the chamber using the Research Laboratories' vacuum system. For air flow rates between 2 and 4 lb/sec, air was obtained from the Research Laboratories' 400 psi supply. In both cases, the air flow rate was measured with a nozzle not shown in the photograph. In most tests, the outer-stream and buffer-stream air was heated to approximately 260 deg F using the "light-gas" supply system described in Ref. 18. The inner-jet gases used were air, Freon-11 and FC-77. The air was obtained from the 400 psi air supply and heated to 260 deg F in a conventional tube-and-shell heat exchanger. The Freon-11 was vaporized in the shell side of a tube-and-shell heat exchanger and superheated in the air superheater. The air and Freon-11 flow rates were measured with the variable-area flow meters shown in Fig. 5. The FC-77 was vaporized and metered with the "heavy-gas" supply system

7

described in Ref. 18. For tests with Freon-11 as the buffer-stream gas, the Freon-11 was vaporized and superheated in the same manner as the Freon-11 inner-jet gas, and was metered with the buffer-stream variable-area flow meters shown in Fig. 5. The densities of air, Freon-11 and FC-77 at the operating conditions of 260 deg F and 10.8 psia are 0.041, 0.191 and 0.568 lb/ft^3, respectively. The dynamic viscosities for air and Freon-11 at these conditions are 1.54 x 10^{-5} and 0.985 x 10^{-5} lb/ft-sec, respectively. The dynamic viscosity of FC-77 has not been determined thus far; therefore, the dynamic viscosity of air was used for FC-77 in calculations.

Inlet Flow Conditions

The original design for the inlet manifold incorporated a 1/16-in. hexagonal honeycomb, a fine screen, and two layers of porous plates in all the plenums. However, the fraction of open area of the honeycomb and the fine screen varied, due to manufacturing technique and dirt from the air. When initial measurements were made at a distance $z = 2\ 3/8$ in. downstream of the inlet plane it was found that the velocity varied by approximately 20 percent. Because of these nonuniformities in the velocity distribution, the inlet manifold was modified by removing the honeycomb, fine screen and porous plates upstream of the inlet plane and by replacing them with the woven wire screen. A porous plate with approximately 25 percent open area was installed in the inner-jet manifold to increase the pressure drop in that duct system.

Flow visualization tests and measurements of the total pressure distribution downstream of the inlet plane indicated that the flow through the modified inlet manifold had no major asymmetries. For these tests, the inner-jet, buffer-stream and outer-stream velocities, based on the nominal inlet dimensions, were 6.7, 70 and 66 ft/sec, respectively. Total pressure distributions were measured in planes at $z = 3/8$ in. and $2\ 3/8$ in., and local velocity distributions were calculated using the local total pressure and the peripheral wall static pressure as the local static pressure (Fig. 6). The velocity distribution at $z = 2\ 3/8$ in. (Fig. 6b) was obtained from total pressure measurements made at twenty-one different radial stations at each of twelve different azimuthal stations. Eight of these azimuthal stations were midway between the eight struts of the inlet manifold ($\theta = 22.5, 67.5$ deg, etc.), two azimuthal stations were directly under the struts ($\theta = 0$ and 180 deg), and two azimuthal stations were 11 1/4 deg from the struts ($\theta = 11.2$ and 191.2 deg). The calculated velocities varied in a random manner across the measurement plane. At $z = 3/8$ in., the velocity varied up to 35 percent from the average velocity along the radius on which the measurements were made (Fig. 6a). However, at $z = 2\ 3/8$ in., the velocity varied by only 6 to 7 percent from the average, indicating that the local disturbances caused by the screen at the inlet plane were nearly dissipated.

The conclusion derived from these measurements was that the flow distribution was sufficiently uniform to proceed with the containment tests.

Optical Equipment

Flow Visualization

A schematic of the optical system used for flow visualization photography is shown in Fig. 7. Light was supplied by quartz-iodine lamps and diffused with frosted glass or opal glass to provide a uniform background illumination. Iodine was used for coloring the inner-jet gas for all of the flow visualization tests. For black and white photography, a Kodak Wratten Filter No. 58 was used to obtain maximum contrast in the photographs. For color photography, no filter was used.

Chordal Absorptometer

The theory of the chordal absorptometer is given in Refs. 19 and 20. An outline of the theory adapted from Ref. 21 is presented in the APPENDIX for reference. A schematic of the chordal light absorption system used in this study is shown in Fig. 8 and a photograph of the chordal absorptometer is shown in Fig. 9. Seventy-two fiber optics (thirty-six from each of two units) were connected to the chamber, twelve at each of six axial locations. Eleven of the light carriers were used to transmit light from the lamp to the chamber and one was used to transmit light from the chamber to a photomultiplier. As shown in Fig. 9, light from a tungsten-ribbon lamp was collimated and passed through a chopper wheel located in front of the fiber optic holder. The light passed through the chopper wheel and struck only one fiber optic at a time. There was a short time between illumination of successive fiber optics in which no light entered the chamber. Light was transmitted through the fiber optics to the chamber wall where a lens and adjustment mechanism (see Detail "A" in Fig. 8) was used to focus the transmitted light. The light traversed chords of the chamber which were oriented such that light emanating from each of the eleven fiber optics at one axial location struck the receiver fiber optic. The perpendicular distances from the chords to the chamber centerline were 0, 0.5, 1.0, 1.5, 2.0, 2.5, 2.83, 3.16, 3.5, 4.0 and 4.5 in. Light was transmitted through the receiving fiber optic, through an interference filter (bandwidth 50Å and peak transmission at 5250Å) and into a photomultiplier tube. An absorption coefficient calibration was required for each light path because the geometric arrangement caused the incidence angle of light from each chord into the receiver fiber optic to be different. The transmitted angle of light from a fiber optic is a function of the incidence angle. The incidence angle of the light through the interference filter affects the wave length passed by the filter. This is important since the iodine absorption coefficient varies with wave length near the wave length of the filter.

A calibration was obtained with the chordal absorptometer in place using the inlet absorptometer (described in Ref. 21) for the inner-jet gas as a reference.

During tests, the light intensities on the receiver fiber optic fluctuated due to concentration fluctuations of the flowing gases. Therefore, eleven photomultiplier output readings were averaged to determine the I and I_0 values at each chordal station. Data were obtained at the axial locations shown in Fig. 1.

The local concentration of inner-jet gas in the chamber was determined from the ratio of the local iodine density to the inner-jet inlet iodine density. The inner-jet gas and the iodine were assumed to be fully mixed at the inlet and in the chamber. The iodine density in the inner-jet gas at the inlet and in the chamber were calculated using Eqs. (A-1) and (A-11) of the APPENDIX.

Parameters used to Define Containment Characteristics

Local and average ratios of inner-jet gas partial pressure to total pressure in the chamber were used to describe the containment characteristics of the coaxial-flow jets. The ratio of local partial pressure of the inner-jet gas to total pressure, $\bar{P}_I / P$, is equal to the ratio of the local iodine concentration in the chamber to the iodine concentration in the inlet duct. Calculation of this ratio from the absorptometer measurements was discussed in the previous paragraph. The ratio of the area-average of inner-jet gas partial pressure to the total pressure, P_I^* / P, was calculated at each axial station, z, from the following equation:

$$\frac{P_I^*}{P} = \frac{2}{r_0^2} \int_0^{r_0} \left(\frac{P_I}{P} \right) \cdot r \cdot dr \qquad (1)$$

The ratio of the average partial pressure of inner-jet gas to the total pressure was calculated for each test from the following equation:

$$\frac{\bar{P}_I}{P} = \frac{2}{L_c r_0^2} \int_0^{L_c} \int_0^{r_0} \left(\frac{P_I}{P} \right) \cdot r \cdot dr \cdot dz = \frac{1}{L_c} \int_0^{L_c} \left(\frac{P_I^*}{P} \right) dz \qquad (2)$$

10

where L_c is the length of the chamber from the chamber inlet plane to the intersection of the nozzle cone with the chamber wall (Fig. 1). A straight-line relationship was assumed in most tests for the variation of P_I^*/P between axial measuring stations.

A containment parameter η_c was used in Refs. 12 through 14 to describe the average amount of inner-jet gas contained in a given volume of a coaxial-flow jet. The parameter was calculated by the equation

$$\eta_c = \frac{2}{L \, r_I^2} \int_0^L \int_0^\infty \left(\frac{P_I}{P} \right) \cdot r \cdot dr \cdot dz \tag{3}$$

For a volume with length $L = L_c$, the containment parameter η_c may be calculated from $\bar{P}_I / P$ by the equation

$$\eta_c = \frac{\bar{P}_I}{P} \left(\frac{r_o}{r_I} \right)^2 \tag{4}$$

In the figures for the section entitled DISCUSSION OF RESULTS OF CONTAINMENT TESTS, the value of $\bar{P}_I / P$ for which $\eta_c = 1$ with $L = L_c$ is identified by the note, "average partial pressure of cylinder of inner-jet gas having volume $\pi \, r_I^2 \, L_c$."

The nondimensional parameters used to describe a given test condition have not been defined previously for all of the flow and geometrical conditions employed in this study. However, for all tests, an inner-jet Reynolds number may be defined by the equation

$$Re_I = 2 V_I \, r_I \, \rho_I / \mu = 2 W_I / \pi \, r_I \, \mu \tag{5}$$

Data were obtained in the tests described herein for a range of inner-jet Reynolds numbers from approximately 2000 for tests with air to 125,000 for tests with Freon-11 as the inner-jet gas.

11

GENERAL DISCUSSION OF FLOW IN COAXIAL-FLOW JETS

Flow Patterns

The flow patterns for confined, one-component coaxial-flow jets vary as the ratio of the average buffer-stream and outer-stream inlet velocity to the inner-jet inlet velocity, V_{BAO}/V_I , increases from 1.0 to a large number (Fig. 10). For $V_{BAO}/V_I \approx 1.0$, the flow is mixed by the turbulence downstream of the inlet. As V_{BAO}/V_I is increased, turbulent mixing due to shear between the inner and outer streams occurs as shown in Fig. 10c. For V_{BAO}/V_I approaching infinity ($V_I = 0$), the flow is similar to that behind a bluff body and has recirculation cells (sometimes denoted counter flow or reverse flow) extending to the inner-jet inlet plane. For high values of the velocity ratio V_{BAO}/V_I , a flow pattern similar to that behind a bluff body is expected (Fig. 10a). In the tests performed during this study, the flow patterns shown in Figs. 10a and 10c were limiting cases. For intermediate inlet velocity ratios, the flow pattern shown in Fig. 10b occurred. As V_{BAO}/V_I was increased sufficiently, a small recirculation cell formed upstream of the exhaust nozzle. Further increase of V_{BAO}/V_I increased the length of the recirculation cell until the limiting condition shown in Fig. 10a was reached. When recirculation occurred locally in a region of the chamber, the concentration of inner-jet gas in that region was considerably lower than in the regions where recirculation did not occur. Flow conditions for onset of recirculation will be discussed for each geometric configuration and combination of gases used.

Pressure Distributions

Static pressure measurements along the chamber wall and centerline were obtained in tests with air as the inner, buffer and outer gas. The effects of velocity ratio V_{BAO}/V_I on the axial distributions of wall and centerline pressures are shown in Fig. 11. The subtitles in this and succeeding figures indicate the parameters varied (V_I in Fig. 11) and held constant (V_B , V_O and V_{BAO} in Fig. 11). The geometric configuration for a set of tests is given as the inner-jet inlet radius ratio, r_I/r_O , the chamber length-to-diameter ratio, L_N/D , and the exhaust nozzle throat diameter ratio, D_N/D . Detailed information about each geometric configuration may be obtained from Table I. The inner-jet, buffer-stream and outer-stream gases and the constant inlet velocities for each set of tests are also given on each figure. Table II presents a summary of the geometric configurations and flow conditions for all tests and indicates the figures on which the results appear.

In Fig. 11, the wall pressure distribution was essentially independent of inner-jet velocity. Other tests indicated the wall static pressure was increased above that shown when the outer-stream velocity was increased and the buffer-stream velocity

decreased to maintain V_{BAO} constant. The centerline pressure distribution for $V_{BAO}/V_I = 4.8$ decreased continuously with increasing z. For $V_{BAO}/V_I = 9.5$, 20.1 and 40, the centerline static pressure increased and then decreased with increasing z. The centerline pressure decrease for $z > 7.5$ in. is due to converging of the flow leaving the chamber through the exhaust nozzle. Note that the pressure rise for $V_{BAO}/V_I = 9.5$ was approximately 0.3 lb/ft^2 while the increase for $V_{BAO}/V_I = 20.1$ and 40 was approximately 0.8 lb/ft^2. For air having a density of 0.05 lb/ft^3, the velocities required to provide the equivalent dynamic heads of 0.3 and 0.8 lb/ft^2 are 19.6 and 32 ft/sec, respectively.

The pressure difference between the wall and centerline static pressure was approximately 1.0 lb/ft^2. Calculations were made to estimate the streamline curvature that might be associated with this pressure difference. For outer-stream inlet velocities $V_0 \approx 100$ ft/sec, the average radius of curvature of the stream over a two-inch distance necessary to produce that pressure difference is approximately 2.5 ft. At $z = 6$ in., the pressure difference was approximately 5 lb/ft^2, requiring the average radius of curvature at that axial location be approximately 0.5 ft.

Large-Scale Fluctuations and Vortex Rings

Two sets of high-speed motion picture frames showing fluctuations in the flow are presented in Fig. 12. The average buffer-stream and outer-stream velocity, V_{BAO}, and the inner-jet velocity, V_I, were held constant while the buffer-stream velocity, V_B, and the outer-stream velocity, V_0, were varied. The set of motion-picture frames for $V_B/V_{BAO} = 0.89$ shows a large annular vortex ring forming near the inlet manifold ($t = 0.000$ sec). The disturbance moves downward in the chamber with time and increases in size. The vortex ring is difficult to see in the photographs but observations of many motion-picture sequences confirm this trend. For $V_B/V_{BAO} = 0.45$, the vortex rings are smaller, but are still present. One undesirable feature of the vortex rings was that inner-jet gas was entrained into the higher-velocity region, thus decreasing the average concentration of inner-jet gas in the chamber.

Photographs of oscilloscope traces (Fig. 13) show the time variations of light transmitted through the chamber for a flow similar to that shown in Fig. 12b. The oscilloscope trace shown in Fig. 13a was for a chord with minimum radius ratio $r/r_0 = 0.566$ at $z = 3.75$ in. This radius ratio is slightly larger than the inner-jet inlet radius, $r_I/r_0 = 0.5$. The light transmitted through the chord fluctuates with and without iodine in the inner-jet gas. The fluctuations in $\ln(I/I_0)$ for this chord are large; $I/I_0 \approx 0.8$ and $\Delta I \approx 0.2 I_0$. The fluctuations in I_0 occur because

Freon-11 has a different index of refraction than air. The light transmitted with iodine in the chamber through the chord having $r_I/r_0 = 0.566$ (Fig. 13a) fluctuated more than that transmitted through the chord having $r_I/r_0 = 0.4$ (Fig. 13b). However, the fluctuation of I_0 was approximately the same for both chords.

DISCUSSION OF RESULTS OF CONTAINMENT TESTS

In this section, the major effects on containment of changes in the inlet velocity ratios, absolute velocity levels, inlet gas density ratios, and geometric configurations will be discussed. In order to present the effects of the changes most effectively, a standard flow condition and geometric configuration was chosen which had inner-jet gas containment characteristics between those shown in Figs. 10b and 10c. For the standard condition, the inner-jet gas was Freon-11 and the buffer-stream and outer-stream gas was air; thus, the inner-jet gas density ratio was $\rho_I / \rho_{BAO} = 4.7$. The inner-jet, buffer-stream and outer-stream inlet gas velocities were $V_I = 4$, $V_B = 33$, and $V_O = 97$ ft/sec; the average buffer-stream and outer-stream velocity was $V_{BAO} = 80$ ft/sec. Hence, $V_{BAO} / V_I = 20$ and $V_B/V_{BAO} = 0.41$. The inlet manifold had an inner-jet inlet radius ratio $r_I / r_O = 0.5$ and a buffer-stream radius ratio $r_B / r_O = 0.65$. The chamber length-to-diameter ratio was $L_N / D = 1.0$ and the exhaust nozzle diameter ratio was $D_N / D = 0.6$. Because of the interest in large inner-jet inlet area configurations, the major effects of inlet flow condition changes will also be shown for an inlet radius ratio $r_I / r_O = 0.7$.

Additional information about the geometrical configurations, indicated in the subtitle of each figure by r_I / r_O, L_N / D and D_N / D, may be obtained from Table I. A summary of the flow conditions investigated is presented in Table II; the figure numbers where the effects of the inlet flow condition and geometric variables may be found are also included.

Effects of Inlet Velocity Ratios and Inner-Jet Inlet Radius

Effects of V_B / V_{BAO} for $r_I / r_O = 0.5$

Photographs, local inner-jet gas concentration data and average inner-jet gas concentration data showing the effects on containment of changes in the velocity ratio V_B / V_{BAO} are shown in Figs. 14 through 17. The maximum amount of inner-jet gas contained in the chamber, as indicated by the photographs, appears to occur for $V_B / V_{BAO} = 0.42$ (Fig. 14) which was the standard flow condition. Recirculation occurred immediately upstream of the exhaust nozzle. The photographs show that changes in the buffer velocity had a strong effect on the size of the recirculation cell; for $V_B / V_{BAO} = 0$ and 1.04, the recirculation cell or reverse flow region extended to the inlet manifold plane.

The radial distribution of the ratio of inner-jet gas partial pressure to total pressure, P_I / P, is shown in Fig. 15 for $V_B/V_{BAO} = 0.99$, 0.60, 0.41 and 0.21. The concentration profiles confirm the trend shown by the photographs (Fig. 14). For $V_B / V_{BAO} = 0.99$, the concentration profiles are cusped (highest concentration at

r_I / $r_0 \approx 0.4$) at $z = 0.75$ and 2.25 in., indicating a strong recirculation zone which extended to the inlet plane. This case is similar to the one shown in Fig. 10a. For V_B / $V_{BAO} = 0.60$, the concentration profile for $z = 0.75$ in. and $r/r_0 < 0.4$ indicates levels slightly greater than 1.0 which is not possible and reflects the accuracy of the data reduction procedure. For V_B / $V_{BAO} = 0.41$, the distribution of P_I / P indicates that a larger amount of inner-jet gas was in the chamber than in the two previous cases. For V_B / $V_{BAO} = 0.21$, the local inner-jet gas partial pressure ratio is less than 1.0 for all radius ratios; however, the cusp shown for $V_B/V_{BAO} = 0.99$ (Fig. 15a) does not appear, indicating a more general mixing occurred rather than a strong recirculation cell. Although all the local P_I / P ratios shown are estimated to be within 10 to 15 percent of their true values, the amount of inner-jet gas in the chamber determined by integration of these profiles is closer to the actual amount because the maximum errors built up in the data reduction procedure occur at inside radii where the density-area integral is small (Fig. 15a). The average densities calculated have any errors at the center compensated by smaller opposite errors at larger radii.

The axial distribution of area-averaged partial pressure ratio, P_I^* / P, for r_I / $r_0 = 0.5$ is shown in Fig. 16. P_I^* / P is the ratio of the average inner-jet gas partial pressure to the total pressure at each cross-section of the chamber (see Eq. (1)). For V_B / $V_{BAO} = 0.41$, the value of P_I^* / P is above 0.25, the value at the inlet plane, at three axial stations. This local increase may be due to the adverse pressure gradient that tends to decrease the inlet velocity and to cause recirculation. In Fig. 14, the photograph for V_B / $V_{BAO} = 0.42$ shows the inner-jet gas flaring out slightly behind the inlet.

The ratio of the average partial pressure of inner-jet gas to the total pressure in the chamber, $\bar{P}_I$ / P, is shown in Fig. 17 for the four flow conditions shown in Figs. 15 and 16. $\bar{P}_I$ / P is the integral of P_I^* / P from $z = 0$ to $z = L_C$, where L_C is the distance z where the exhaust nozzle cone would intersect the chamber wall (Fig. 2). The results show that there is a peak value of $\bar{P}_I$ / $P = 0.21$ at V_B / $V_{BAO} = 0.41$. At lower or higher velocity ratios $\bar{P}_I$ / P is lower; it decreases to approximately 0.10 at V_B / $V_{BAO} = 0.21$ and 1.0. The value of $\bar{P}_I$ / P for a cylinder of inner-jet gas having a radius r_I and length L_C is also shown in Fig. 17. Thus, the largest value of $\bar{P}_I$ / P obtained in this series of tests is about 85 percent of the value for the cylinder of inner-jet gas of volume $\pi r_I^2 L_C$.

Effects of V_B/V_{BAO} for r_I / $r_0 = 0.7$

Photographs showing the effects of the velocity ratio V_B/V_{BAO} on the containment of inner-jet gas for r_I / $r_0 = 0.7$ are presented in Fig. 18. For these tests, changes in the velocity ratio V_B / V_{BAO} do not appear to affect the containment. For a radius ratio of r_I / $r_0 = 0.6$, flow visualization studies showed that the effect of V_B / V_{BAO} was less than that for r_I / $r_0 = 0.5$, but still occurred. No concentration measurements were made for r_I / $r_0 = 0.6$.

The inner-jet gas distributions for $V_B/V_{BAO} = 0.65$ and 0.28 are shown in Fig. 19. For both of these cases some recirculation or mixing between the outer-stream and buffer-stream and the inner jet occurred close to the inlet. The effect of V_B/V_{BAO} on $\overline{P}_I/P$ is shown in Fig. 20; there was no effect of V_B/V_{BAO} on the containment characteristics for this inlet configuration, $r_I/r_O = 0.7$. Note that the maximum average partial pressure ratio is about 50 percent of the value for a cylinder of inner-jet gas having the volume $\pi r_I^2 L_C$, compared with about 85 percent for $r_I/r_O = 0.5$.

Effects of V_{BAO}/V_I

Photographs showing the effects of V_{BAO}/V_I on the containment of inner-jet gas are shown in Fig. 21. For this set of flow conditions, V_I was varied while V_O, V_B and V_{BAO} were held constant. For $V_{BAO}/V_I = 11$, no recirculation occurred. However, the size and strength of the recirculation cell increased with increasing V_{BAO}/V_I, so that for $V_{BAO}/V_I = 50$ and 90, the chamber does not appear to contain any inner-jet gas. For this set of photographs, as well as for the previous sets, the iodine concentration in the inner-jet gas at the inlet was the same for all flow conditions. The effect of V_{BAO}/V_I on P_I/P is shown in Fig. 22 for $V_{BAO}/V_I = 10$, 20, 36, and 52. For $V_{BAO}/V_I = 10$ (Fig. 22a), P_I/P is approximately 1.0 at $r = 0$ for all axial stations. Data from Fig. 15c for $V_{BAO}/V_I = 20$ is shown again in Fig. 22b for comparison. For $V_{BAO}/V_I = 36$ and 52 (Figs. 22c and 22d), a cusp appears at $r/r_O = 0.4$. This type of distribution would be expected on the basis of the inner-jet recirculation regions shown in Fig. 21. The axial distribution of area-averaged partial pressure ratio is shown in Fig. 23. For $V_{BAO}/V_I = 10$ and 20, P_I^*/P rises above 0.25 from $z = 0$ to about 4 in. For $V_{BAO}/V_I = 36$ and 52, the area-averaged partial pressure distribution shows the effect of the recirculation cells.

The effect of velocity ratio V_{BAO}/V_I on $\overline{P}_I/P$ is shown in Fig. 24. These data were obtained from the previous figure for $V_B/V_{BAO} = 0.4$ and from other tests at different values of V_B/V_{BAO}. The maximum values of $\overline{P}_I/P$ for each velocity ratio V_{BAO}/V_I were selected from Fig. 24 and replotted in Fig. 25 to show the variation of the ratio of maximum average partial pressure of inner-jet gas to total pressure $\left(\overline{P}_I/P\right)_{MAX}$ with V_{BAO}/V_I. Note that for velocity ratios above 20 where recirculation occurs, the variation of $\left(\overline{P}_I/P\right)_{MAX}$ with V_{BAO}/V_I is approximately proportional to $\left(V_{BAO}/V_I\right)^{-1}$. Data obtained from tests with $r_I/r_O = 0.7$ are shown on the same plot for comparison. Note that for the same velocity ratio, V_{BAO}/V_I, $\left(\overline{P}_I/P\right)_{MAX}$ is always greater for $r_I/r_O = 0.7$ than it is for $r_I/r_O = 0.5$.

Effects of Absolute Velocity Levels at Inlet

The effect of the absolute level of velocities V_{BAO} and V_I on $\overline{P_I}/P$ for fixed ratios of V_{BAO}/V_I and V_B/V_{BAO} is shown in Fig. 26. For all four sets of velocity levels, the variation of $\overline{P_I}/P$ with V_B/V_{BAO} has the same shape and approximately the same values. The maximum value of $\overline{P_I}/P$, obtained in all cases at $V_B/V_{BAO} \approx 0.4$, decreases very slightly with increasing ratio of V_{BAO}/V_I but does not vary with velocity level, considering the wide variations in V_{BAO} and V_I. The outer-stream and buffer-stream Reynolds number for these four cases varied from $Re_{BAO} = 36,000$ for $V_{BAO} = 35$ ft/sec to $Re_{BAO} = 276,000$ for $V_{BAO} = 205$ ft/sec. These Reynolds numbers include those presently estimated to be required for a full-scale rocket engine.

The effect of absolute values of V_{BAO} and V_I on the maximum values of $\overline{P_I}/P$ obtained from tests with $r_I/r_0 = 0.5$ and 0.7 are shown on Fig. 27. The data for $r_I/r_0 = 0.5$ (Fig. 27a) show excellent agreement between the tests at different absolute velocities. For $r_I/r_0 = 0.7$, the agreement between tests at 80 ft/sec and 35 to 40 ft/sec is good for $V_{BAO}/V_I = 20$ and is within 20 percent for $V_{BAO}/V_I = 36$. The conclusion is that no discernible effects of absolute velocity level on the average containment characteristics of the coaxial-flow jets occurred for the Reynolds numbers of these tests.

Effects of Inlet Gas Densities

Effects of ρ_I/ρ_{BAO}

$r_I/r_0 = 0.5$

Photographs showing the effects of density ratio ρ_I/ρ_{BAO} on the containment of inner-jet gas for $r_I/r_0 = 0.5$ are shown in Fig. 28. These tests were for velocity ratios $V_{BAO}/V_I = 20$ and $V_B/V_{BAO} = 0.41$, with air as the buffer-stream and outer-stream gas. The photograph with air as the inner-jet gas shows recirculation extending to the inlet plane. The test with Freon-11 as the inner-jet gas was at the standard flow condition with recirculation in the chamber just upstream of the exhaust nozzle. For FC-77 as the inner-jet gas, there was no recirculation in the chamber and the inner-jet core extended nearly to the exhaust nozzle. These flow patterns are similar to the flow patterns sketched in Fig. 10. Note that with FC-77 as the inner-jet gas, the inner-jet gas does not flare out downstream of the inlet as occurred with air and Freon-11 as the inner-jet gases.

18

The effects of density ratio ρ_I/ρ_{BAO} on $\overline{P}_I/P$ are shown in Fig. 29 for air and FC-77 as the inner-jet gases. The distribution for Freon-11 as the inner-jet gas may be obtained from Fig. 22b. Note that for air as the inner-jet gas (Fig. 29a), the highest partial pressures occurred at intermediate radii, $r/r_0 \approx 0.5$. This cusped shape again indicates the presence of the recirculation cells observed in the photographs (Fig. 28). For FC-77 as the inner-jet gas, the highest partial pressures occurred near $r = 0$. The effect of ρ_I/ρ_{BAO} on the axial distribution of P_I^*/P is shown in Fig. 30. The axial variation of P_I^*/P is approximately the same for Freon-11 and FC-77 as the inner-jet gases except at $z = 6.75$ in. where the flow with Freon-11 has recirculation. For air as the inner-jet gas, P_I^*/P was less than 0.25 at all values of z, and at $z = 6.75$ in. was approximately the same as with Freon-11 as the inner-jet gas. The effect of density ratio ρ_I/ρ_{BAO} on $\overline{P}_I/P$ is shown in Fig. 31. Data were obtained from Figs. 29 and 30 for $V_B/V_{BAO} = 0.41$ and from tests at other ratios of V_B/V_{BAO} with the same geometrical configuration. For all values of V_B/V_{BAO}, $\overline{P}_I/P$ for FC-77 as the inner-jet gas is greater than for air and Freon-11. The effect of ρ_I/ρ_{BAO} on the maximum value of $\overline{P}_I/P$ obtainable is shown in Fig. 32 for a range of velocity ratios, V_{BAO}/V_I, with air, Freon-11 and FC-77 as the inner-jet gases. For $\left(\overline{P}_I/P\right)_{MAX} > 0.2$, a large decrease in the velocity ratio V_{BAO}/V_I is required in order to obtain a moderate increase in $\left(\overline{P}_I/P\right)_{MAX}$.

$\underline{\quad r_I/r_0 \quad = 0.7}$

The effect of ρ_I/ρ_{BAO} on $\left(\overline{P}_I/P\right)_{MAX}$ for $r_I/r_0 = 0.7$ is summarized in Fig. 33. All of the data for Freon-11 and FC-77 as inner-jet gases with $V_{BAO} = 80$ ft/sec were obtained for flow conditions in which recirculation occurred. For air as inner-jet gas, $\left(\overline{P}_I/P\right)_{MAX} = 0.44$ was obtained at $V_{BAO}/V_I = 4.8$; this is 90 percent of the value for a cylinder of inner-jet gas having a volume of $\pi r_I^2 L_C$. The trends for the tests with $r_I/r_0 = 0.7$ were similar to those shown in Fig. 32 for $r_I/r_0 = 0.5$.

Effects of V_0/V_I, V_B/V_0 and ρ_B/ρ_0

$\underline{\quad r_I/r_0 \quad = 0.5}$

The effects of the velocity ratios V_0/V_I and V_B/V_0 on $\overline{P}_I/P$ with Freon-11 as the buffer and inner-jet gas are shown in Fig. 34. For $V_0/V_I = 18$, the velocity ratio V_B/V_0 has an appreciable effect; recirculation occurred for $V_B/V_0 = 0.49$ and did not occur for $V_B/V_0 = 0.21$. For $V_0/V_I = 32$ and 48, the effect of V_B/V_0 is less.

The effects of inner-jet gas density ratio ρ_I/ρ_0 on $\overline{P}_I/P$ with Freon-11 as the buffer gas are shown in Fig. 35. For these tests, the velocity ratio V_0/V_I was held approximately constant and the inner-jet gas was varied. The maximum values of $\overline{P}_I/P$ obtained from tests with air and Freon-11 as the buffer gases are compared in Fig. 36. The comparison was made for the variation of $\left(\overline{P}_I/P\right)_{MAX}$ with Q_{AIR}/Q_I;

$Q_{AIR} = Q_O$ for the tests with Freon-11 as the buffer-stream gas and $Q_{AIR} = Q_{BAO}$ for tests with air as the buffer-stream gas. For all tests with the same inner-jet gas, $(\bar{P}_I/P)_{MAX}$ at a given Q_{AIR}/Q_I is no greater with Freon-11 as the buffer-stream gas than it is with air as the buffer-stream gas. The important conclusion from these tests is that the use of Freon-11 instead of air as the buffer-stream gas does not increase $(\bar{P}_I/P)_{MAX}$.

$$r_I/r_O \doteq 0.7$$
-- -- -- -- -- --

The effects of V_O/V_I and V_B/V_O on $\bar{P}_I/P$ were approximately the same for tests with $r_I/r_O = 0.7$ as for tests with $r_I/r_O = 0.5$. A comparison of the maximum values of $\bar{P}_I/P$ obtained with air and Freon-11 as the buffer gases is shown in Fig. 37. Like the results from tests with $r_I/r_O = 0.5$, the values of $\bar{P}_I/P$ obtained for the same value of Q_{AIR}/Q_I are approximately the same for air and Freon-11 as the buffer-stream gas. Any improvement in $\bar{P}_I/P$ with increased buffer gas density at the same velocity ratio V_O/V_I was off-set by the decrease in airflow inlet area and, hence, in volume flow ratio, Q_{AIR}/Q_I.

Effects of Chamber Length and Exhaust Geometry

Effects of L_N/D

Photographs showing the effects of chamber L_N/D on the containment of inner-jet gas at the maximum values of V_{BAO}/V_I for which recirculation could be prevented by the proper choice buffer velocity are presented in Fig. 38. The two inner-jet gases used in these tests were Freon-11 and air. For $L_N/D = 0.75$, the maximum values of V_{BAO}/V_I which could be obtained without recirculation were 29.5 for Freon-11 and 13 for air. For $L_N/D = 1.25$, the maximum values of V_{BAO}/V_I were 14.4 and 6.5, respectively. These and additional results for the flow conditions of Fig. 38 are shown in Fig. 39. The optimum velocity ratio V_B/V_{BAO} required to prevent recirculation was independent of inner-jet gas and was dependent upon chamber L_N/D. The momentum flux ratios $\rho_{BAO}/V_{BAO}^2/\rho_I V_I^2$ obtained for a given geometry were approximately the same for air and Freon-11 as inner-jet gases. This result is in agreement with the data in Fig. 32 for the effect of density ratio on the maximum value of $\bar{P}_I/P$. The momentum flux ratios are approximately the same for $\bar{P}_I/P = 0.2$ which was a typical $\bar{P}_I/P$ for the flow conditions where recirculation began to occur. The variation of the maximum values of $\bar{P}_I/P$ with V_{BAO}/V_I obtained for $L_N/D = 1.00$ and 1.25 for inner-jet gases of air and Freon-11 and for $r_I/r_O = 0.5$ are shown in Fig. 40. The values of $(\bar{P}_I/P)_{MAX}$ for $L_N/D = 1.25$ are less than those obtained for $L_N/D = 1.00$ because, as shown in the previous figure, recirculation occurs at lower velocity ratios, V_{BAO}/V_I.

Effects of D_N/D

High-speed motion pictures of flow with the two-in. exhaust nozzle throat dia-meter, $D_N/D = 0.2$, without recirculation in the chamber indicated that the general flow structure was approximately the same as obtained in tests with $D_N/D = 0.6$. However, results from tests with recirculation in the chamber showed differences in the average and local distributions of the inner-jet gas partial pressure. The effect of D_N/D on P_I/P is shown in Fig. 41 for $r_I/r_0 = 0.7$. Although recirculation occurs for both $D_N/D = 0.2$ and 0.6, the cusped distribution of P_I/P begins to occur at $z = 2.25$ in. for $D_N/D = 0.2$ and at 5.25 in. for $D_N/D = 0.6$. The effects of exhaust nozzle diameter and V_B/V_{BAO} on $\overline{P_I}/P$ are shown in Fig. 42 for the same velocity ratio, V_{BAO}/V_I, as in Fig. 41. For $V_{BAO}/V_I = 19.8$, $\overline{P_I}/P$ was 30 percent less for tests with $D_N/D = 0.2$ than with $D_N/D = 0.6$. The effect of D_N/D on the maximum values of $\overline{P_I}/P$ obtainable for several values of V_{BAO}/V_I are shown in Fig. 43. The largest difference between test results with the two exhaust nozzles was obtained for $V_{BAO}/V_I \approx 20$ (see also Figs. 41 and 42). There was no effect on the containment characteristics for $V_{BAO}/V_I = 15$ where recirculation does not occur and the results for $D_N/D = 0.2$ approach those for $D_N/D = 0.6$ at $V_{BAO}/V_I \approx 36$.

SUMMARY OF CONTAINMENT CHARACTERISTICS

Flow Patterns

Sketches of the three typical flow patterns observed are shown in Fig. 44 (typical for $V_{BAO}/V_I = 18$, $r_I/r_O = 0.5$ and $L_N/D = 1$). The inner-jet gas and the level of buffer-stream velocity ratio, V_B/V_{BAO}, for which the flow pattern occurs are noted above each of the three sketches. In Fig. 44a, where the recirculation zone is directly behind the inlet plane, values of the average inner-jet gas partial pressure ratio, $\bar{P}_I/P$, obtained from light absorption measurements were less than 0.10. In Fig. 44b, where the recirculation zone occurs upstream of the exhaust nozzle but does not extend up to the inlet manifold, the values of $\bar{P}_I/P$ ranged from approximately 0.10 to 0.20. In Fig. 44c, where the core of the inner-gas jet extends nearly to the exhaust nozzle, the values of $\bar{P}_I/P$ were above 0.20.

Containment Data

Data from Figs. 32 and 33 for $r_I/r_O = 0.5$ and 0.7 are summarized in Figs. 45, 46 and 47. The effects of the volume flow rate ratio Q_{BAO}/Q_I on the maximum values of $\bar{P}_I/P$ obtained in the tests at each value of Q_{BAO}/Q_I are shown in Fig. 45 for each combination of inlet geometry and inner-jet gas. For all three inner-jet gases and for values of $(\bar{P}_I/P)_{MAX} < 0.2$, a greater value of Q_{BAO}/Q_I was obtained for tests with $r_I/r_O = 0.5$ than for $r_I/r_O = 0.7$. For values of $(\bar{P}_I/P)_{MAX} > 0.2$, this trend with r_I/r_O is reversed. Also, for a given combination of inlet geometry and volume flow rate ratio Q_{BAO}/Q_I, increasing the density of the inner-jet gas increased the value of $(\bar{P}_I/P)_{MAX}$. The effect of weight flow rate ratio, W_{BAO}/W_I, on $(\bar{P}_I/P)_{MAX}$ at each value of W_{BAO}/W_I is summarized in Fig. 46 for each combination of inlet geometry and inner-jet gas. Note that for a given W_{BAO}/W_I and inlet geometry, increasing the inner-jet gas density decreased the value of $(\bar{P}_I/P)_{MAX}$. The effect of W_{BAO}/W_I on the maximum value of $\bar{\rho}_I/\rho_{BAO}$ at each value of W_{BAO}/W_I is summarized in Fig. 47 for each combination of inlet geometry and inner-jet gas. For a given inlet geometry and W_{BAO}/W_I, increasing the inner-jet gas density increased $(\bar{\rho}_I/\rho_{BAO})_{MAX}$.

The information provided in Figs. 45 through 47 allows the containment characteristics for different density gases and geometric configurations to be compared. In this form, the data should also be useful for comparisons of the performance of coaxial-flow gaseous-core nuclear rocket engines with the performance of other open-cycle engine concepts.

REFERENCES

1. Clark, J. W., B. V. Johnson, J. S. Kendall, A. E. Mensing and A. Travers: Summary of Gaseous Nuclear Rocket Fluid Mechanics Research Conducted Under Contract NASw-847. United Aircraft Research Laboratories Report F-910091-13, prepared under Contract NASw-847, May 1967. Also AIAA Paper No. 67-500, presented at AIAA 3rd Propulsion Joint Specialist Conference, Washington, D. C., July 17-21, 1967.

2. Ragsdale, R. G. and F. E. Rom: Gas-Core Reactor Work at NASA/Lewis. AIAA Paper No. 67-499, presented at AIAA 3rd Propulsion Joint Specialist Conference, Washington, D. C., July 17-21, 1967.

3. Weinstein, H. and R. G. Ragsdale: A Coaxial Flow Reactor - A Gaseous Nuclear Rocket Concept. ARS Preprint 1518-60, presented at the ARS 15th Annual Meeting, Washington, D. C., December 1960.

4. Rom, F. E. and R. G. Ragsdale: Advanced Concepts for Nuclear Rocket Propulsion. Nuclear Rocket Propulsion, NASA SP-20, December 1962, pp. 3-15.

5. Ragsdale, R. G., H. Weinstein, and C. D. Lanzo: Correlation of a Turbulent Air-Bromine Coaxial-Flow Experiment. NASA Technical Note D-2121, February 1964.

6. Ragsdale, R. G. and O. J. Edwards: Data Comparisons and Photographic Observations of Coaxial Mixing of Dissimilar Gases at Nearly Equal Stream Velocities. NASA Technical Note D-3131, December 1965.

7. Baker, R. L. and H. Weinstein: Experimental Investigation of the Mixing of Two Parallel Streams of Dissimilar Fluids. NASA Contractor Report CR-957, January 1968.

8. Zawacki, T. S. and H. Weinstein: Experimental Investigation of Turbulence in the Mixing Region Between Coaxial Streams. NASA Contractor Report CR-959, February 1968.

9. D'Souza, G. J., A. Montealegre, and H. Weinstein: Measurement of Turbulent Correlations in a Coaxial Flow of Dissimilar Fluids. NASA Contractor Report CR-960, January 1968.

10. Montealegre, A., G. J. D'Souza, and H. Weinstein: Evaluation of Turbulence Correlations in a Coaxial Flow of Dissimilar Fluids. NASA Contractor Report CR-961, January 1968.

11. Weinstein, H. and C. A. Todd: A Numerical Solution of the Problem of Mixing of Laminar Coaxial Streams of Greatly Different Densities - Isothermal Case. NASA Technical Note D-1534, February 1963.

12. Weinstein, H. and C. A. Todd: Analysis of Mixing of Coaxial Streams of Dissimilar Fluids Including Energy-Generation Terms. NASA Technical Note D-2123, March 1964.

13. Ragsdale, R. G.: Effects of a Momentum Buffer Region on the Coaxial Flow of Dissimilar Gases. NASA Technical Note D-3138, December 1965.

14. Donovan, L. F. and C. A. Todd: Computer Program for Calculating Isothermal, Turbulent Jet Mixing of Two Gases. NASA Technical Note D-4378, March 1968.

15. Agarwal, U. and T. P. Torda: Numerical Investigation of Unsteady Laminar Incompressible Co-Axial Boundary Layer Flows. NASA Contractor Report CR-908, October 1967.

16. Baker, R. L. and H. Weinstein: Analytical Investigation of the Mixing of Two Parallel Streams of Dissimilar Fluids. NASA Contractor Report CR-956, January 1968.

17. Baker, R. L., T. Rozenman and H. Weinstein: Stability of Shear Flow With Density Gradient and Viscosity. NASA Contractor Report CR-958, February 1968.

18. Kendall, J. S., A. E. Mensing and B. V. Johnson: Containment Measurements in Vortex Tubes with Radial Outflow and Large Superimposed Axial Flows. United Aircraft Research Laboratories Report F-910091-12, prepared under Contract NASw-847, May 1967. Also issued as NASA Contractor Report CR-993, March 1968.

19. Nestor, O. H. and N. H. Olsen: Numerical Methods for Reducing Line and Surface Probe Data. SIAM Review, Vol. 2, No. 3, July 1960.

20. Cremers, C. J. and R. C. Birkebak: Application of the Abel Integral Equation to Spectrographic Data. Applied Optics, Vol. 5, June 1966, p. 1057.

21. Mensing, A. E. and J. S. Kendall: Experimental Investigation of Containment of a Heavy Gas in a Light-Gas Vortex. United Aircraft Research Laboratories Report D-910091-4, prepared under Contract NASw-847, March 1965. To be issued as NASA CR report.

LIST OF SYMBOLS

D — Diameter of coaxial-flow chamber, in. or ft

D_N — Diameter of exhaust nozzle, in. or ft

I — Intensity of light beam after passing through an absorbing media of thickness x, candles

I_0 — Intensity of incident light beam, candles

L — Length in chamber, in. or ft

L_C — Length of chamber from inlet plane to beginning of nozzle, in. or ft

L_N — Length of chamber from inlet plane to nozzle throat, in. or ft

P — Total pressure, lb/ft^2 or atm

P_I — Local partial pressure of inner-jet gas, lb/ft^2

P_I^* — Area-average of inner-jet gas partial pressure, $P_I^* = 2 \int_0^{r_o} P_I \, r \, dr / r_0^2$, lb/ft^2

$\bar{P}_I$ — Average partial pressure of inner-jet gas, $\bar{P}_I = 2 \int_0^{L_C} \int_0^{r_o} P_I \, r \, dr \, dz / r_0^2 L_C$, lb/ft^2

$(\bar{P}_I / P)_{MAX}$ — Maximum average partial pressure ratio of inner-jet gas

P_{REF} — Wall pressure at inlet, lb/ft^2

Q_{AIR} — Air volume flow rate used for comparison of tests with air or Freon-11 as buffer-stream gas, ft^3/sec

Q_{BAO} — Outer-stream and buffer-stream air volume flow rate, ft^3/sec

Q_I — Inner-jet gas volume flow rate, ft^3/sec

Q_0 — Outer-stream volume flow rate, ft^3/sec

Re_{BAO} — Outer-stream and buffer-stream Reynolds number, $Re_{BAO} = 2 V_{BAO}(r_0 - r_I) \rho_{BAO} / \mu$, dimensionless

Re_I — Inner-jet Reynolds number, $Re_I = 2 V_I r_I \rho_I / \mu$, dimensionless

r — Local radius from center of chamber, in. or ft

r_B Buffer-stream radius at inlet, in. or ft

r_I Inner-jet radius at inlet, in. or ft

r_0 Peripheral-wall radius, in. or ft

T Temperature, deg R (except as noted)

V Local velocity, ft/sec

V_B Inlet velocity of buffer stream, ft/sec

V_{BAO} Average inlet velocity of combined outer stream and buffer stream, $V_{BAO} = W_{BAO}/\rho_{BAO}\, \pi\,(r_0{}^2 - r_I{}^2)$, ft/sec

V_I Inlet velocity of inner jet, ft/sec

V_0 Inlet velocity of outer stream, ft/sec

W_{BAO} Combined weight flow rate of outer-stream and buffer-stream gases, lb/sec

W_I Weight flow rate of inner-jet gas, lb/sec

x Thickness of absorbing media, ft (Appendix)

y Perpendicular distance from a chord to the centerline of the chamber, ft

z Axial distance downstream from inlet plane, in. or ft

η_C Containment parameter, $\eta_C = 2 \int_0^L \int_0^{r_0} (P_I\,/\,P)\, r\, dr\, dz\, /\, L\, r_I{}^2$

λ Wave length of light used for light absorbtion measurement, $\overset{\circ}{A}$

ρ_B Buffer-stream gas density at inlet, lb/ft^3

ρ_{BAO} Average density of combined outer-stream and buffer-stream gases at inlet, $\rho_{BAO} = (\rho_B + \rho_0)/2$, lb/ft^3

ρ_I Inner-jet gas density at inlet, lb/ft^3

ρ_{I_2} Density of iodine vapor, lb/ft^3

ρ_o Outer-stream gas density at inlet, lb/ft^3

$\rho_{I_2}{}^*$ Effective density of iodine vapor absorbing light, $\rho_{I_2}{}^* = \rho_{I_2}\left(1 - e^{-553/T}\right)$, lb/ft^3

$\bar{\rho}_I$ Average density of inner-jet gas contained in chamber, $\bar{\rho}_I = 2\int_0^{L_c}\int_0^{r_o}\rho_I\, r\,dr\,dz/r_o^2 L_c$, lb/ft^3

$(\bar{\rho}_I/\rho_{BAO})_{MAX}$ Maximum average density ratio of inner-jet gas

APPENDIX

THEORY OF CHORDAL ABSORPTOMETER

This theoretical analysis illustrating the principle of the chordal absorptometer is adapted for the present report from Ref. 21.

The radial distribution of the density of one component of a two-component gas mixture in an axisymmetric flow field can be determined by measuring the light absorbed by this component along several chords. The wavelength of light to be absorbed must be chosen so that absorption will occur only by the component of interest. This light absorption technique permits measurements to be made without inserting a probe into the chamber; hence, there is no disturbance to the flow field. The principle of operation is illustrated in Sketch 1.
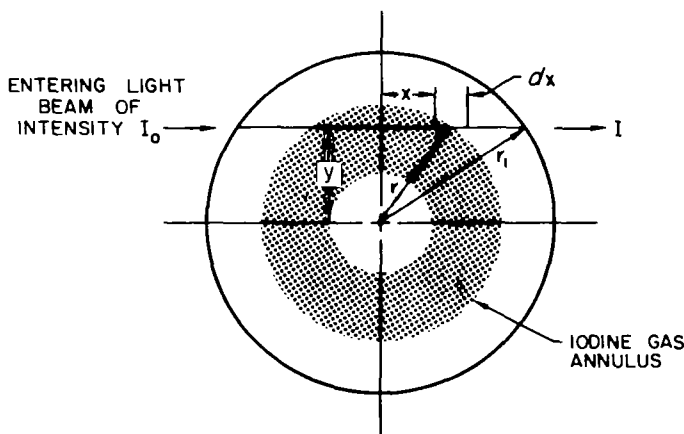
Sketch 1

The relationship for light absorbed by the iodine in the distance dx is

$$d I(\lambda) = - I(\lambda)\, \alpha(\lambda)\, \rho_{I_2}^{*}\, dx \qquad (A-1)$$

where $I(\lambda)$ is the spectral intensity of light entering the volume, $dI(\lambda)$ is the amount of light absorbed, $\alpha(\lambda)$ is the spectral absorption coefficient, and $\rho_{I_2}^{*}$ is

the effective density of gas absorbing light at wavelength λ. The local iodine density ρ_{I_2} is related approximately to the effective density of iodine $\rho_{I_2}^*$ by the equation

$$\rho_{I_2}^* = \rho_{I_2} \left(1 - e^{-553/T} \right) \tag{A-2}$$

where T is in deg R. The absorption coefficient $\alpha(\lambda)$ was measured using an interference filter with $\lambda = 5250$ Å and a half-width of 50 Å, and was found to be 5170 ft^2/lb. Therefore, the light transmitted through a chord of length $2x$ can be determined by the following equation:

$$\ln(I/I_0) = -2\,\alpha(\lambda)\left(1 - e^{-553/T} \right) \int_0^x \rho_{I_2} dx \tag{A-3}$$

where ρ_{I_2} is a function of x, and I and I_0 are understood for this discussion to be spectral light intensities. By reference to Sketch 1, it may be seen that the semi-chordlength, x, can be expressed as $x = \sqrt{r^2 - y^2}$. Thus,

$$dx = \frac{r\,dr}{\sqrt{r^2 - y^2}} \tag{A-4}$$

Combining Eqs. (A-3) and (A-4) yields

$$\ln(I/I_0) = -2\,\alpha(\lambda)\left(1 - e^{-553/T} \right) \int_y^{r_1} \frac{r\,\rho_{I_2}(r)\,dr}{\sqrt{r^2 - y^2}} \tag{A-5}$$

For simplification, let

$$K = 2\,\alpha(\lambda)\left(1 - e^{-553/T} \right) \tag{A-6}$$

To find the density distribution, $\rho_{I_2}(r)$, it is necessary to invert the integral equation, Eq. (A-5). If both sides of Eq. (A-5) are multiplied by $y \cdot dy \sqrt{y^2 - u^2}$ and integrated from u to r_1 (u is a dummy variable), then, by changing the order of integration, Eq. (A-5) becomes

$$\int_u^{r_1} \frac{y \ln(I/I_0)\,dy}{\sqrt{y^2 - u^2}} = -K \int_u^{r_1} r\,\rho_{I_2}(r)\,dr \int_u^r \frac{y\,dy}{\sqrt{y^2 - u^2}\,\sqrt{r^2 - y^2}} \tag{A-7}$$

The second integral on the right of Eq. (A-7) has a value of $\pi/2$. Therefore, Eq. (A-7) becomes

$$\int_u^{r_1} \frac{y \ln(I/I_0)\, dy}{\sqrt{y^2 - u^2}} = -\frac{\pi}{2} K \int_u^{r_1} r\, \rho_{I_2}(r)\, dr \tag{A-8}$$

Differentiating Eq. (A-8) with respect to u, letting $\rho_{I_2}(r_1) = 0$, and replacing u by r yields

$$\rho_{I_2}(r) = \frac{2}{\pi K} \frac{d}{dr} \int_r^{r_1} \frac{y \ln(I/I_0)\, dy}{\sqrt{y^2 - r^2}} \tag{A-9}$$

Integration of Eq. (A-9) by parts, again using $\rho_{I_2}(r_1) = 0$, and substitution for K gives

$$\rho_{I_2}(r) = \frac{1}{\pi} \left(\frac{1}{1 - e^{-553/T}} \right) \frac{1}{\alpha(\lambda)} \int_r^{r_1} \frac{d/dy\,[\ln(I/I_0)]\, dy}{\sqrt{y^2 - r^2}} \tag{A-10}$$

Thus, from the chordal measurements of light transmission, the radial density distribution of iodine can be calculated from Eq. (A-10). However, since the measured values of I/I_0 normally cannot be readily described analytically, Eq. (A-10) must be integrated numerically. The numerical integration technique employed herein is given in Refs. 19 and 20 and consists of dividing the integral in Eq. (A-10) into N subintegrals and assuming that $\ln(I/I_0)$ is linear throughout each subintegral. By integrating the subintegrals and summing the coefficients, the following equation results (see Ref. 19):

$$\rho_{I_2{(r = r_k)}} = -\frac{2N}{\pi r_0} \left(\frac{1}{1 - e^{-553/T}} \right) \frac{1}{\alpha(\lambda)} \left[\frac{\ln(I/I_0)\big|_{y = y_k}}{\sqrt{2K+1}} + \sum_{n = k+1}^{N} \left\{ \frac{\sqrt{(n+1)^2 - k^2}}{2n + 1} \right. \right. \tag{A-11}$$

$$\left. \left. + \frac{\sqrt{(n-1)^2 - k^2}}{2n - 1} - \frac{4n\sqrt{n^2 - k^2}}{4n^2 - 1} \right\} \ln(I/I_0)\big|_{y = y_n} \right]$$

Table I

SUMMARY OF GEOMETRIC CONFIGURATIONS INVESTIGATED

See Fig. 2 for Schematic of Coaxial-Flow Test Apparatus

a. <u>Inlet Manifold</u>

Designation	r_I, in.	r_B, in.	r_O, in.	r_I / r_O	r_B / r_O
$r_I / r_O = 0.5$	2.5	3.25	5.0	0.50	0.65
$r_I / r_O = 0.6$	3.0	3.63	5.0	0.60	0.725
$r_I / r_O = 0.7$	3.5	4.00	5.0	0.70	0.80

b. <u>Chambers</u>

Designation	L_N, in.	L_C, in.	L_N / D	L_C / D
$L_N / D = 0.75$	7.5	5.0	0.75	0.50
$L_N / D = 1.00$	10.0	7.5	1.00	0.75
$L_N / D = 1.25$	12.5	10.0	1.25	1.00

c. <u>Nozzles</u>

Designation	D_N, in.	D_N / D
$D_N / D = 0.2$	2.0	0.2
$D_N / D = 0.4$	4.0	0.4
$D_N / D = 0.6$	6.0	0.6

Table II

SUMMARY OF FLOW CONDITIONS INVESTIGATED

Outer-stream gas - air for all tests   Velocities listed are approximate

| Geometric Configuration | | | | Gases | | V_{BAO} | Primary | Secondary | Flow Visualization, | Details of Concentration Measurements, | Summary of Concentration Measurements, |
r_I/r_O	r_B/r_O	D_N/D	L_N/D	Buffer-Stream	Inner-Jet	ft/sec	Variable	Variable	See Figure	See Figure	See Figure
0.5	0.65	0.6	1.00	Air	Freon-11	80	V_B/V_{BAO}	-	14	15,16	17
0.6	0.725							-	See Text	-	-
0.7	0.80						↓	-	18	19	20
0.5	0.65						↓	V_{BAO}/V_I	V_B/V_{BAO}	21	22,23	24,25
0.7	0.80						↓	↓	↓	See Text	See Text	25
0.5	0.65					40, 80, 154, 205	V_{BAO}	V_B/V_{BAO}, V_{BAO}/V_I			26,27
0.7	0.80					40, 80	↓	↓	↓	↓	27
0.5	0.65				Air, Freon-11, FC-77	-	Inner-Jet Gas Density, ρ_I/ρ_{BAO}		28	29,30	31,32
0.7	0.80				↓	-	↓		See Text	See Text	33
0.5	0.65			Freon-11	Freon-11	-	V_B/V_O	V_O/V_I			34,36
0.5	0.65				Air, Freon-11, FC-77	-	Inner-Jet Gas Density ρ_I/ρ_O	V_B/V_O, V_O/V_I			35,36
0.7	0.80		↓	↓	↓	-	↓	↓	↓	See Text	37
0.5	0.65		0.75, 1.00, 1.25	Air	Freon-11	80	L_N/D	V_B/V_{BAO}, V_{BAO}/V_I	38		39,40
0.7	0.80	0.2	1.00	↓	↓	57	D_N/D	↓	See Text	41	42,43

32

SKETCH OF COAXIAL-FLOW GASEOUS-CORE NUCLEAR REACTOR

SUPPLEMENTARY PROPELLANT INJECTION

NOZZLE

PRIMARY PROPELLANT INJECTION

FUEL INJECTION PORTS

FUEL-CONTAINMENT REGION

BUFFER PROPELLANT INJECTION

MODERATOR-REFLECTOR

COAXIAL-FLOW REGION
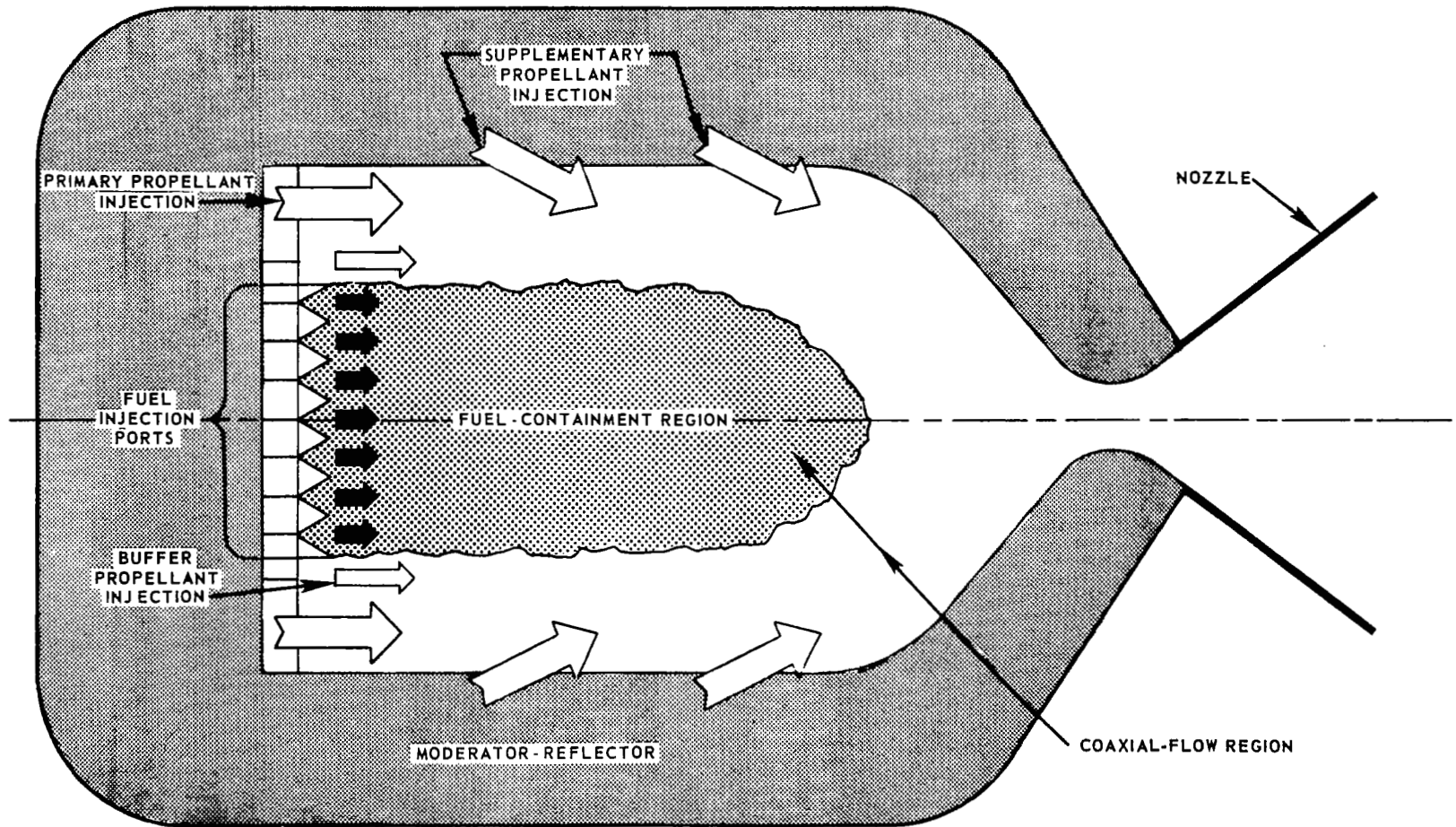
33

FIG. 1

FIG. 2

SCHEMATIC OF COAXIAL–FLOW TEST APPARATUS

SEE TABLE I FOR SUMMARY OF GEOMETRIC CONFIGURATIONS TESTED
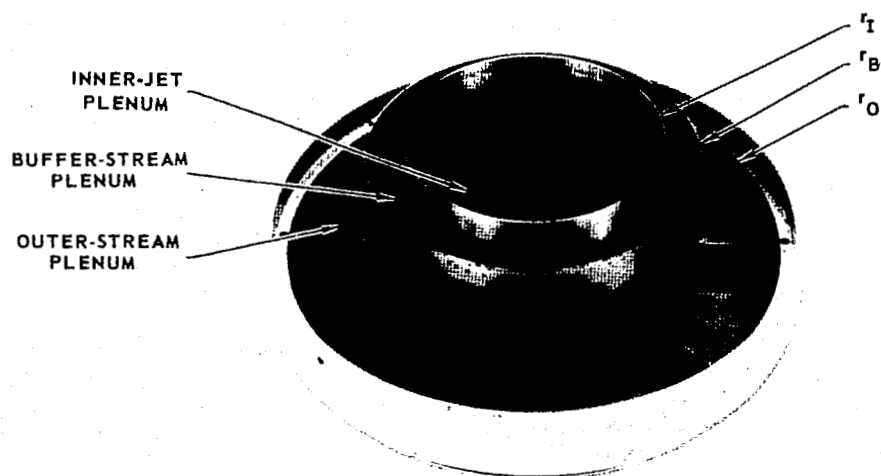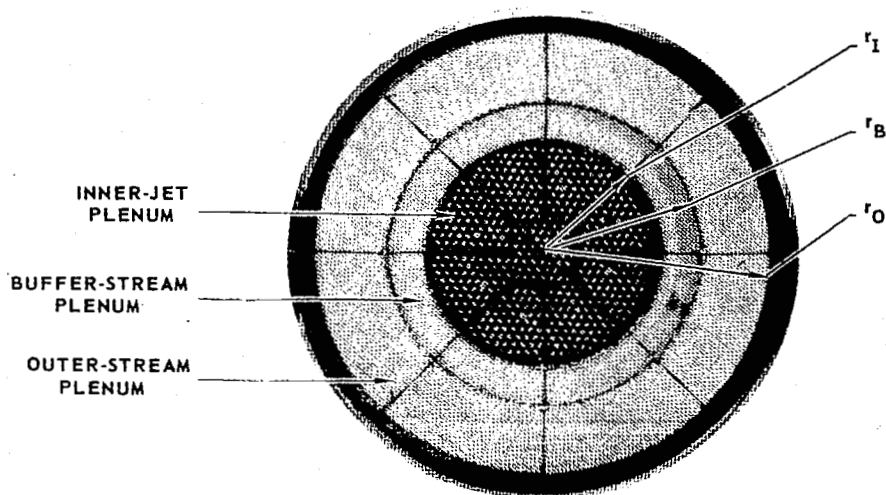## CHAMBER DIAMETER, D = $2r_o$ = 10 IN. FOR ALL TESTS

INNER-JET INLET
(SIMULATED–FUEL, AIR, FREON–11, OR FC–77)

BUFFER–STREAM INLET
(SIMULATED–BUFFER, AIR OR FREON - 11)

OUTER-STREAM INLET
(SIMULATED–PROPELLANT, AIR)

OUTER-STREAM PLENUM

INLET MANIFOLD

POROUS PLATE

FLOW STRAIGHTENERS

POROUS PLATE

SCREEN (CHAMBER INJECTION PLANE)

LIGHT ABSORPTION CHORDAL TRAVERSE STATIONS (z = 0.75, 2.25, 3.75, 5.25, 6.75 AND 8.25 IN.)

CHAMBER

r_I

r_B

r_O

z

L_N

L_C

SPACER FOR VARIABLE L_N /D

EXHAUST NOZZLE DIAMETER, D_N

TO EXHAUST

34

FIG. 3

INLET MANIFOLD

CHAMBER DIAMETER, $D = 2r_O = 10$ IN.

SEE TABLE I FOR OTHER DIMENSIONS

a) TOP VIEW

r_I
r_B
r_O

INNER-JET
PLENUM

BUFFER-STREAM
PLENUM

OUTER-STREAM
PLENUM

b) BOTTOM VIEW

r_I

r_B

r_O

INNER-JET
PLENUM

BUFFER-STREAM
PLENUM

OUTER-STREAM
PLENUM

35

CHAMBERS

LUCITE CHAMBER USED FOR FLOW-VISUALIZATION PHOTOGRAPHY
STEEL CHAMBER USED FOR CONTAINMENT MEASUREMENTS

SEE TABLE I FOR DIMENSIONS

a) LUCITE CHAMBER WITH INLET MANIFOLD
AND EXHAUST NOZZLE
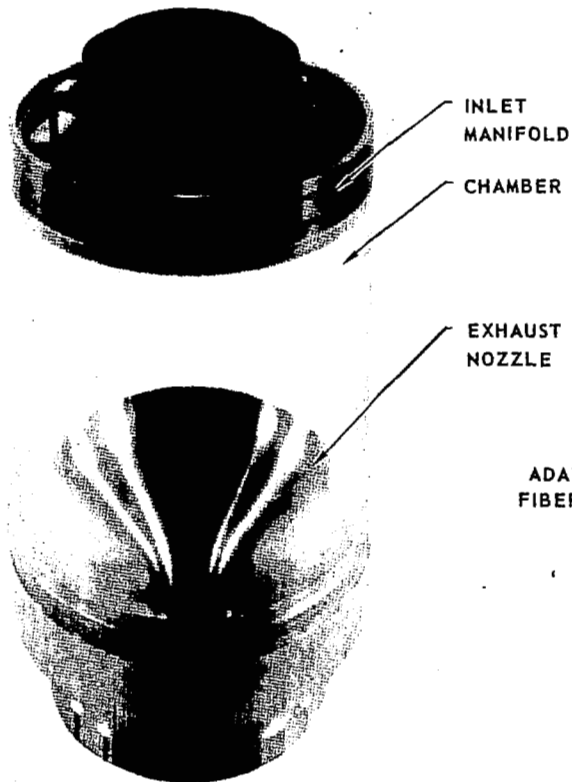
b) STEEL CHAMBER WITH TRANSMISSION SECTOR
AND PICKUP INSERT

INLET
MANIFOLD

CHAMBER

EXHAUST
NOZZLE

SLOTS (6) FOR
TRANSMISSION
SECTORS

HOLES (6) FOR
PICKUP INSERTS

TRANSMISSION
SECTOR

ADAPTER FOR
FIBER OPTIC

0.002-IN.-THICK
GLASS STRIP
COVERING HOLES

INSERT TO HOLD
FIBER OPTIC PICKUP

36

FIG. 4

FIG. 5
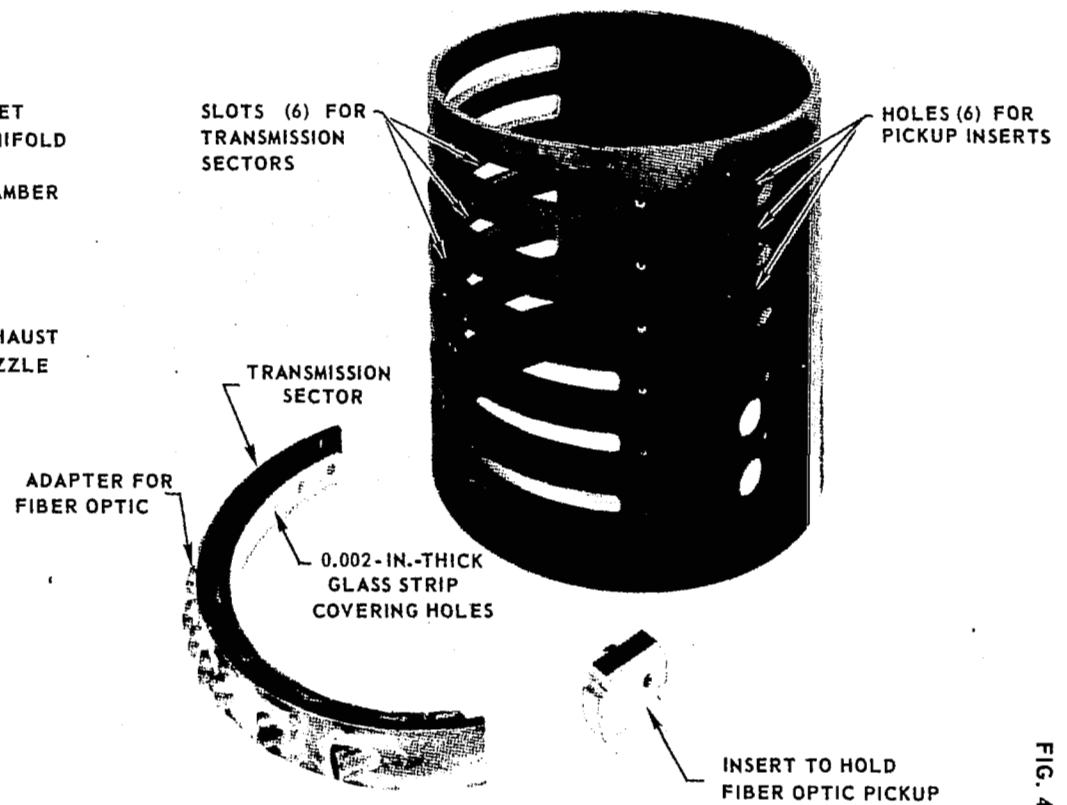
PHOTOGRAPH OF COAXIAL-FLOW FACILITY SHOWING FLOW SYSTEM

NOZZLE FOR MEASURING BUFFER-STREAM AND OUTER-STREAM AIR FLOW RATE

AND HEAT EXCHANGERS NOT SHOWN IN PHOTOGRAPH

37
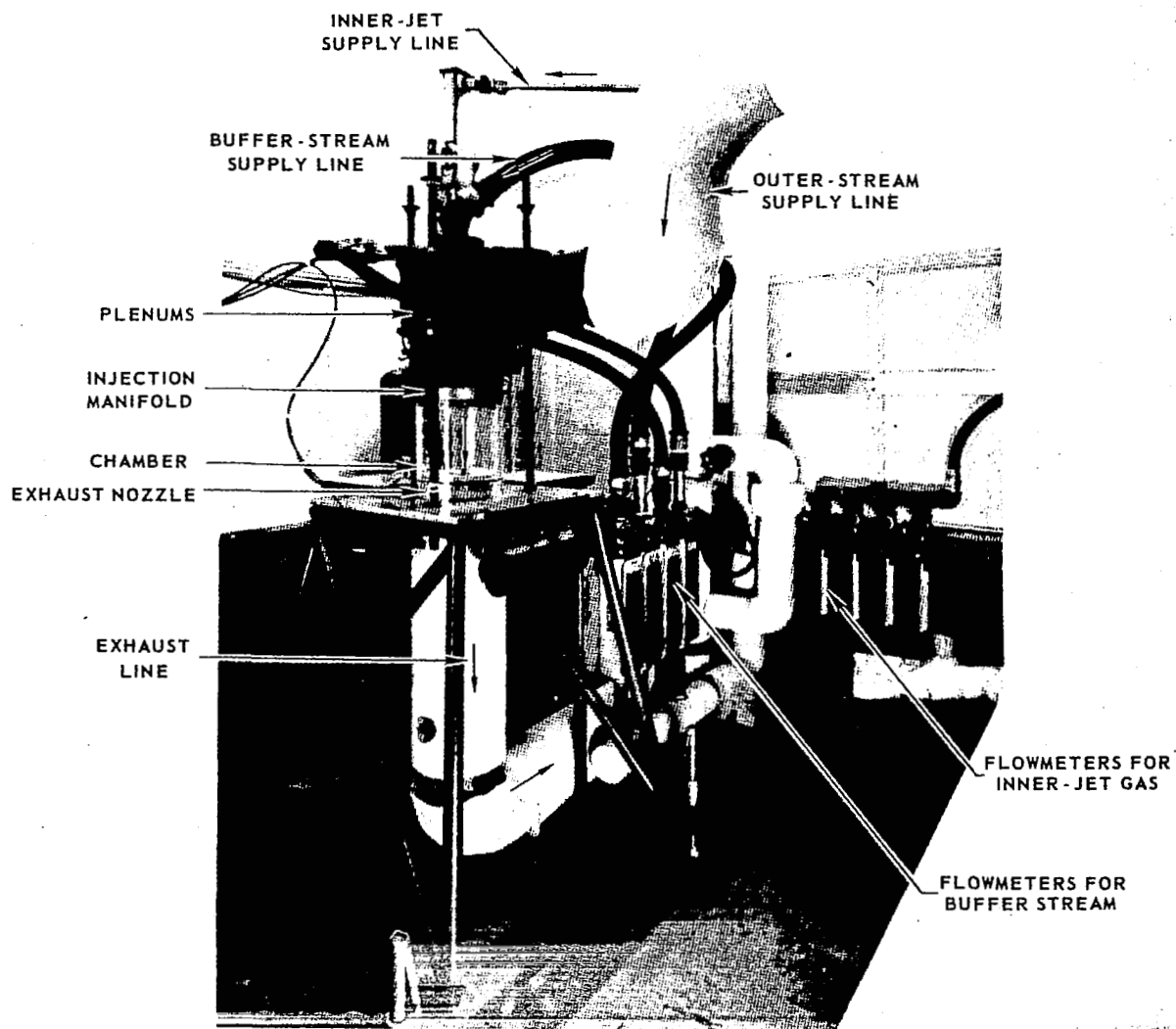
TYPICAL INLET VELOCITY PROFILES

$r_I/r_O = 0.5$ $L_N/D = 1.25$ $D_N/D = 0.6$

INNER, BUFFER AND OUTER GASES - AIR, AIR,AIR; $\rho_I/\rho_{BAO} = 1.0$

$V_I = 6.7$ FT/SEC, $V_B = 70$ FT/SEC, $V_o \approx 66$ FT/SEC (BASED ON NOMINAL INLET DIMENSIONS)

VELOCITY CALCULATED USING LOCAL TOTAL PRESSURE AND WALL STATIC PRESSURE

a) z = 3/8 IN.   b) z = 2 3/8 IN.   b) CONTINUED

SYMBOL	o	□	◊	△
θ	22.5	112.5	202.5	292.5

SYMBOL	o	□	◊	◁	x	▽	D	△
θ	22.5	67.5	112.5	157.5	202.5	247.5	292.5	337.5

SYMBOL	o	□	◆	▲
θ	0	180	11.2	191.2

FIG. 6

38

FIG. 7
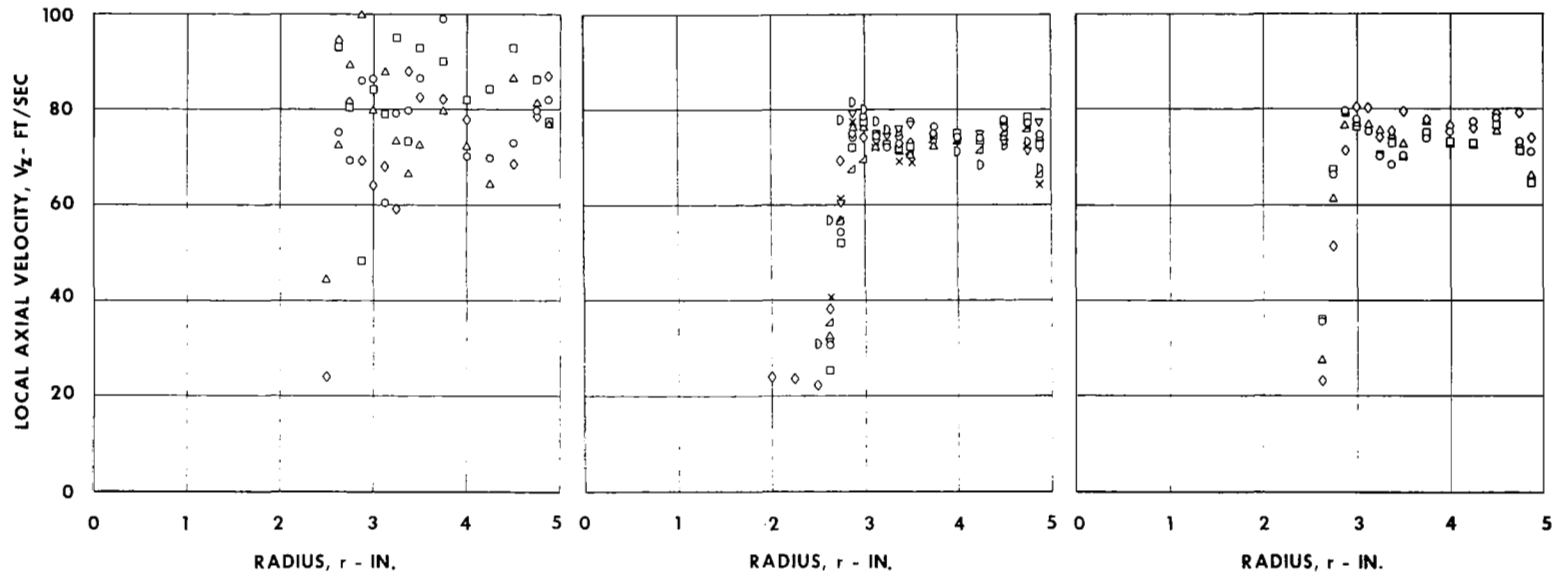
SCHEMATIC OF OPTICAL SYSTEM FOR FLOW VISUALIZATION PHOTOGRAPHY

TOP VIEW

QUARTZ-IODINE LAMPS

FROSTED GLASS

FROSTED GLASS
OR OPAL GLASS

CROSS-SECTION
OF CHAMBER
(FLOW INTO THE PAGE)

CAMERA
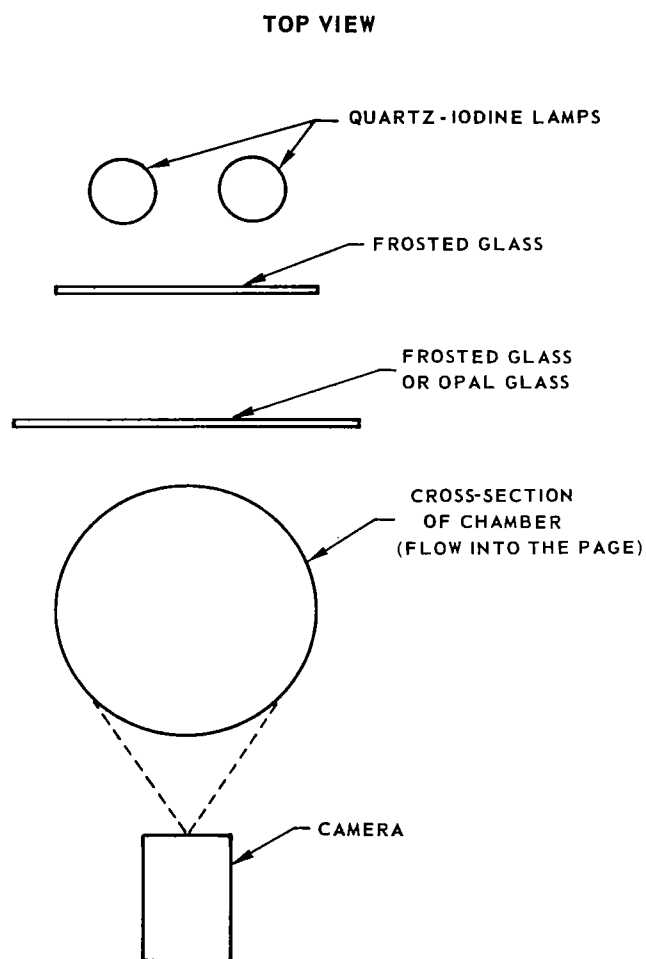
SCHEMATIC OF CHORDAL LIGHT ABSORPTION SYSTEM

TO PHOTOMULTIPLIER TUBE

SEE DETAIL "A"

FIBER OPTIC HOLDER

CHOPPER WHEEL

FIBER OPTICS

COLLIMATING LENS

TUNGSTEN RIBBON LAMP

FIBER OPTIC (RECEIVER)

10-IN. ID

CHAMBER

47

DETAIL "A"   (HALF SIZE)

FOCUSING LENS

NEUTRAL DENSITY FILTER

FIBER OPTIC

CHAMBER WALL

SEAL

0.002-IN. — THICK GLASS STRIP

SLIDING ADJUSTMENT
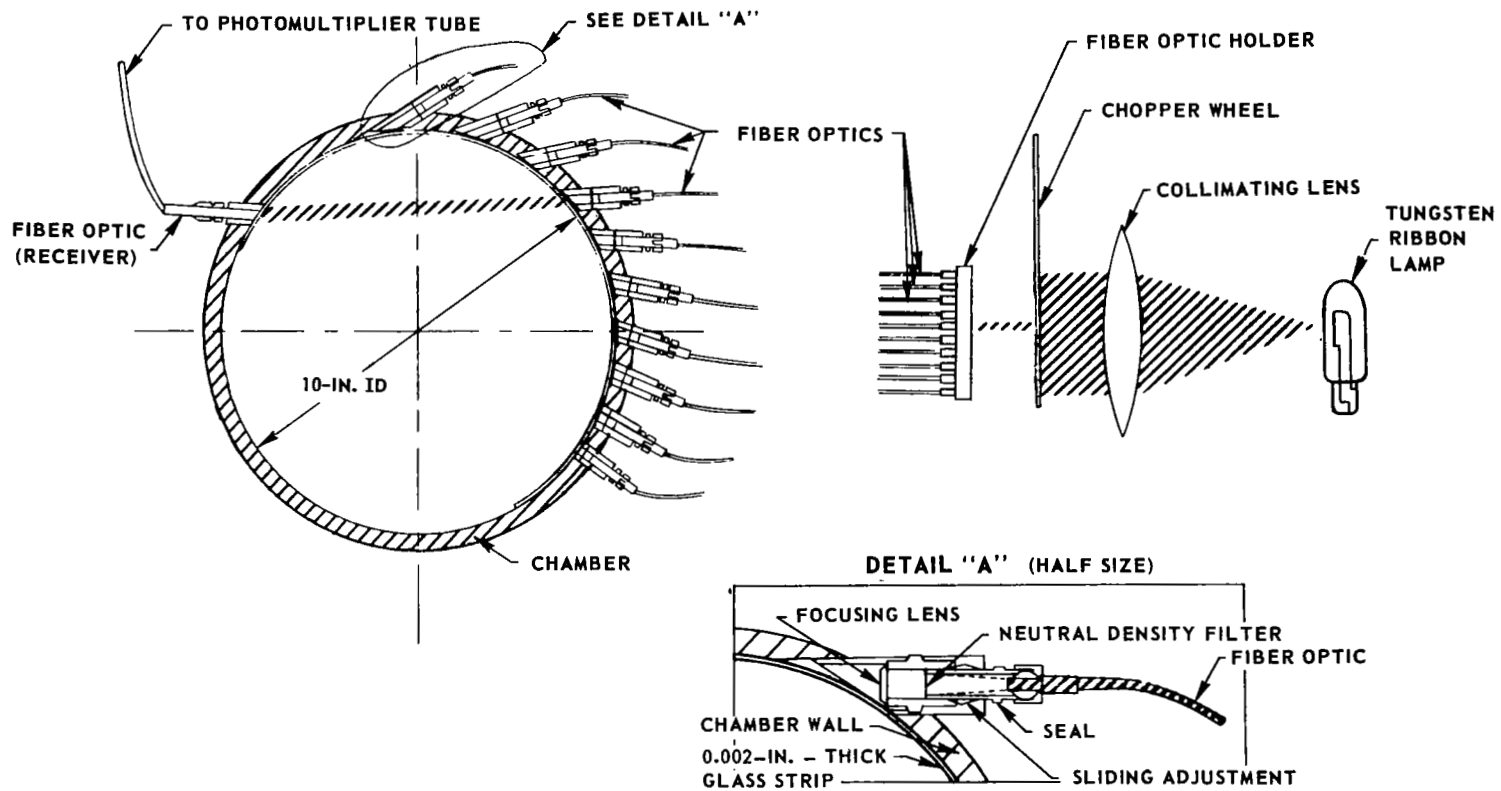
FIG. 8

PHOTOGRAPH OF CHORDAL ABSORPTOMETER

FIBER OPTICS (AMERICAN OPTICAL TYPE LGM-3)

CO AXIAL - FLOW CHAMBER

CHOPPER WHEEL

COLLIMATING LENSES AND LENS HOLDERS

PHOTOMULTIPLIER TUBE (6655A)

TUNGSTEN RIBBON LAMP

INTERFERENCE FILTER(5250 Å WITH 50 Å HALF-WIDTH)

47
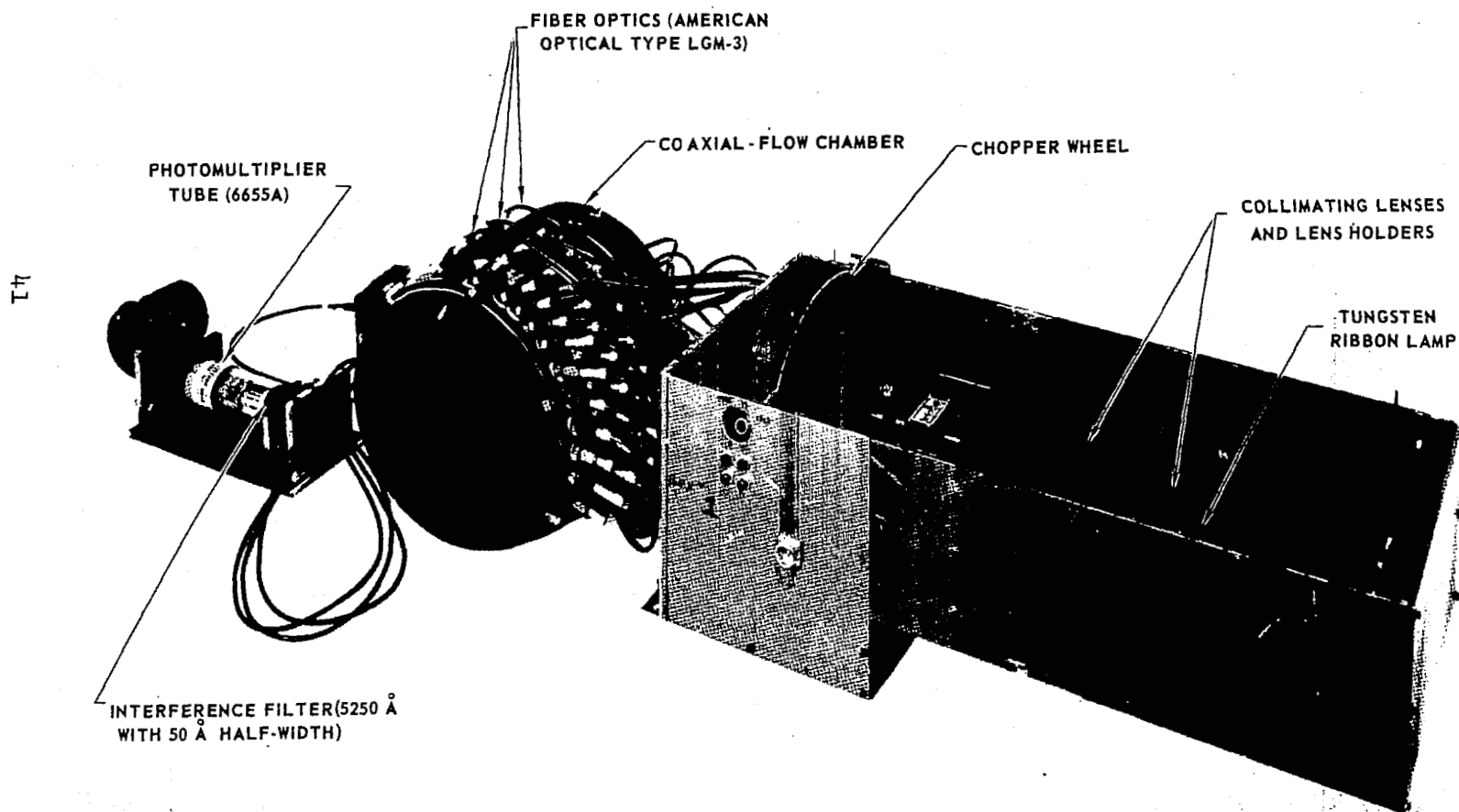
FIG. 9

SKETCHES OF FLOW PATTERNS IN COAXIAL – FLOW JETS

a) RECIRCULATION ZONE DIRECTLY
   BEHIND INLET (HIGH V_{BAO}/V_I)
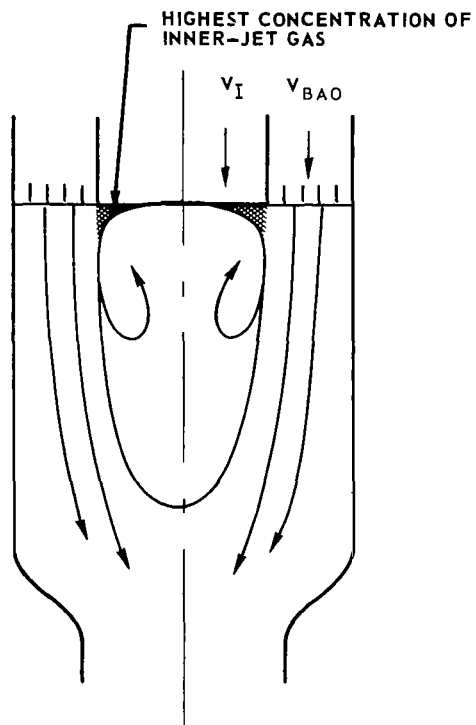
b) RECIRCULATION ZONE FORMS
   DOWNSTREAM OF INLET
   (INTERMEDIATE V_{BAO}/V_I)
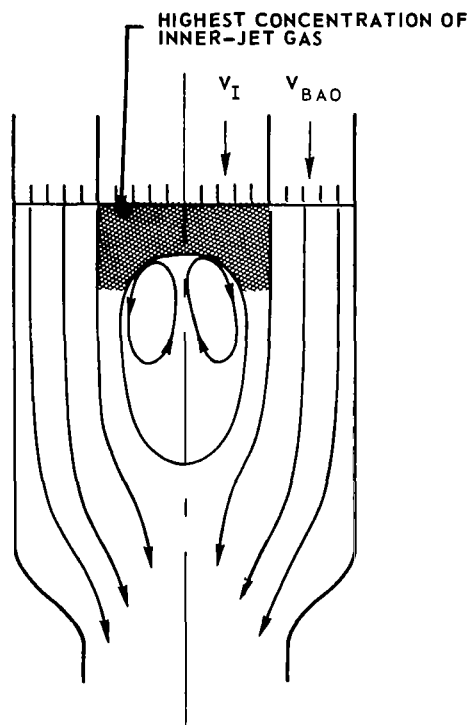
c) TURBULENT MIXING BETWEEN STREAMS
   WITHOUT RECIRCULATION ZONE
   (LOW V_{BAO}/V_I, BUT GREATER THAN ONE)

HIGHEST CONCENTRATION OF
INNER–JET GAS

V_I V_{BAO}

HIGHEST CONCENTRATION OF
INNER–JET GAS

V_I V_{BAO}

HIGHEST CONCENTRATION OF
INNER–JET GAS

V_I V_{BAO}

PLANE
OF INLET
MANIFOLD

42
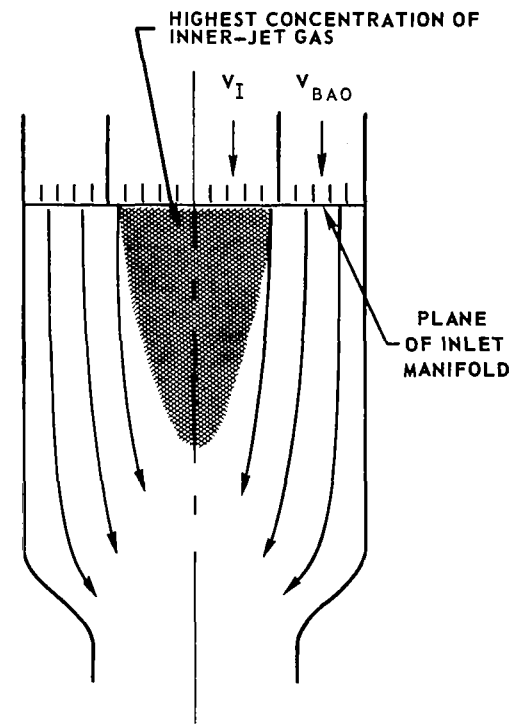
FIG. 10

FIG. 11

EFFECT OF VELOCITY RATIO V_{BAO}/V_I ON AXIAL DISTRIBUTIONS OF WALL AND CENTERLINE PRESSURES

V_I VARIED; V_B, V_O AND V_{BAO} HELD CONSTANT

$r_I/r_O = 0.5$ $L_N/D = 1.0$ $D_N/D = 0.6$

INNER, BUFFER AND OUTER GASES — AIR, AIR, AIR; $\rho_I/\rho_{BAO} = 1.0$

$V_B \approx 33$ FT/SEC, $V_O \approx 97$ FT/SEC, $V_{BAO} \approx 80$ FT/SEC; $V_B/V_{BAO} \approx 0.41$

P_{REF} IS WALL PRESSURE AT INLET, $P_{REF} = 1555$ LB/FT^2

SYMBOL		V_{BAO}/V_I	V_B/V_I
O	●	40.0	16.4
□	■	20.1	8.44
△	▲	9.5	3.99
◇	◆	4.8	2.06
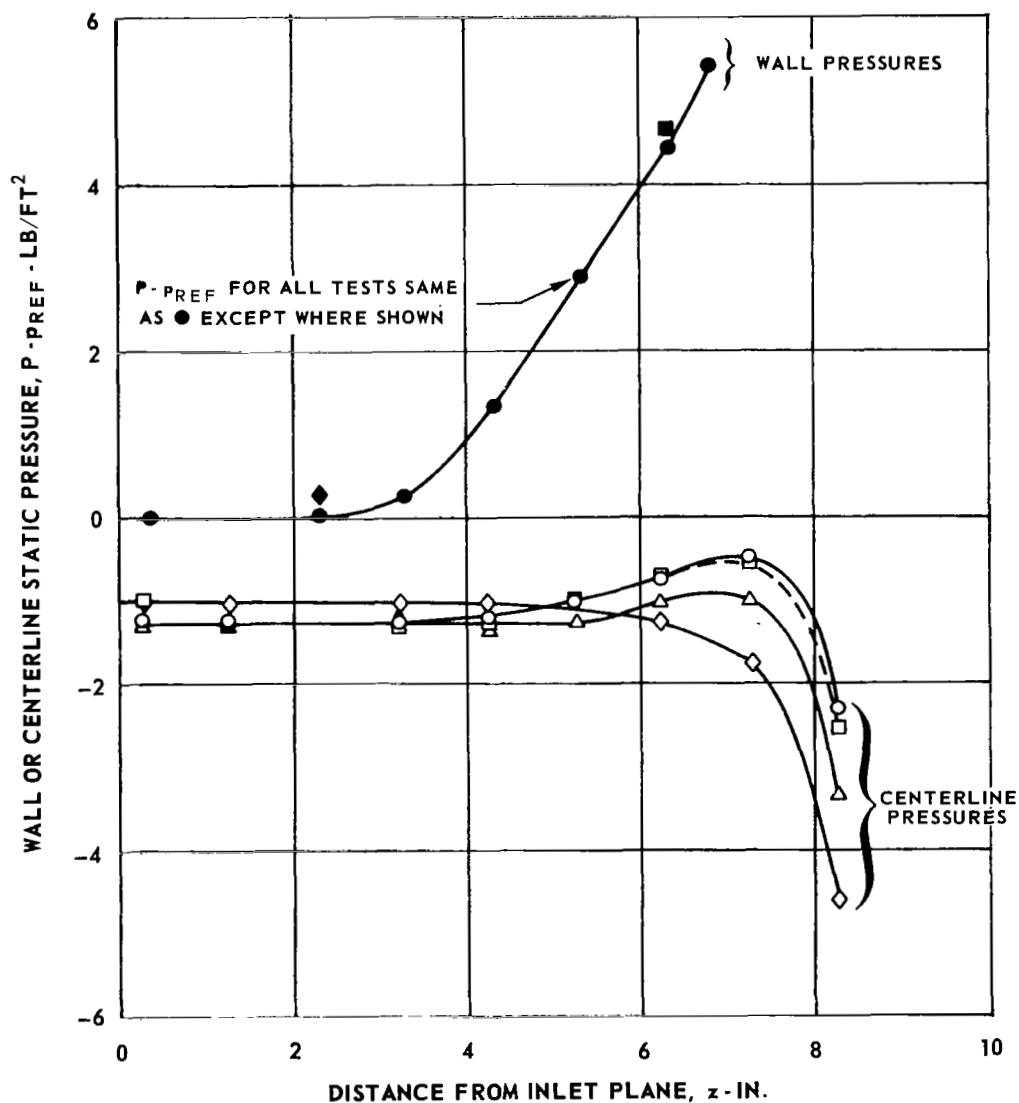
FIG. 12

HIGH-SPEED MOTION PICTURE FRAMES SHOWING FLUCTUATIONS IN FLOW

V_B AND V_O VARIED; V_I AND V_{BAO} HELD CONSTANT

$r_I/r_O = 0.5$ $L_N/D = 1.25$ $D_N/D = 0.6$

INNER, BUFFER AND OUTER GASES- FREON - 11, AIR, AIR; $\rho_I/\rho_{BAO} = 4.7$

$V_{BAO} \approx 87$ FT/SEC, $V_I = 4.5$ FT/SEC; $V_{BAO}/V_I = 19.5$
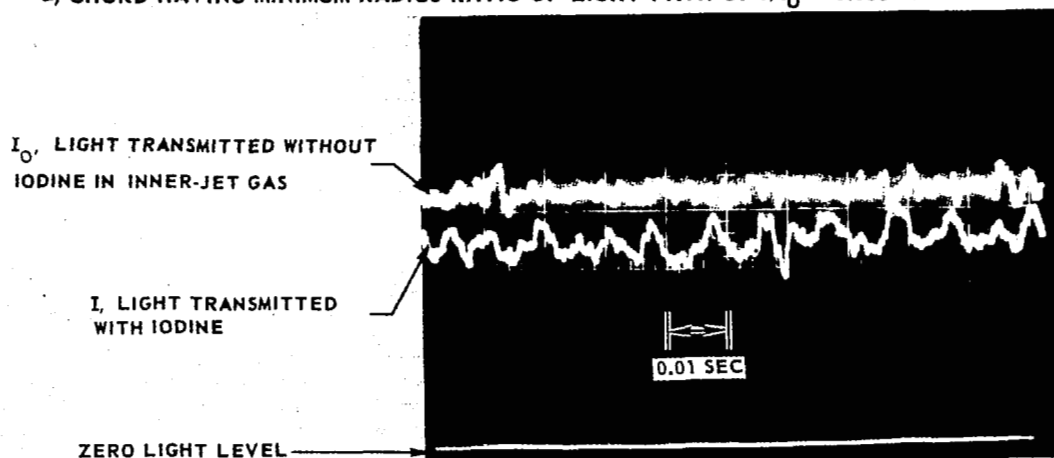
a) HIGH BUFFER VELOCITY
($V_B/V_{BAO} = 0.89$)
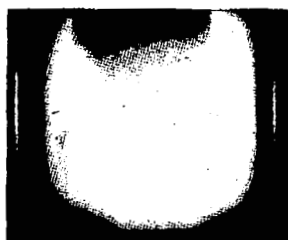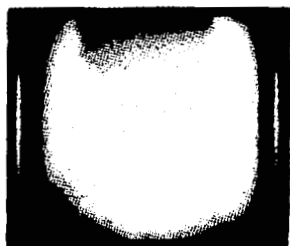
b) MODERATE BUFFER VELOCITY
($V_B/V_{BAO} = 0.45$)

t = 0.000 SEC

0.003 SEC

0.006 SEC

FIG. 13
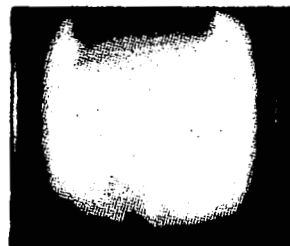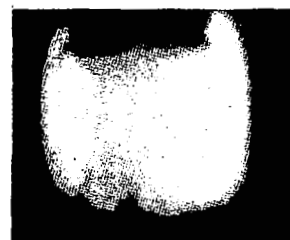
PHOTOGRAPHS OF OSCILLOSCOPE TRACES SHOWING TIME VARIATION OF LIGHT TRANSMITTED THROUGH CHAMBER

$r_I/r_O = 0.5$ $L_N/D = 1.0$ $D_N/D = 0.6$

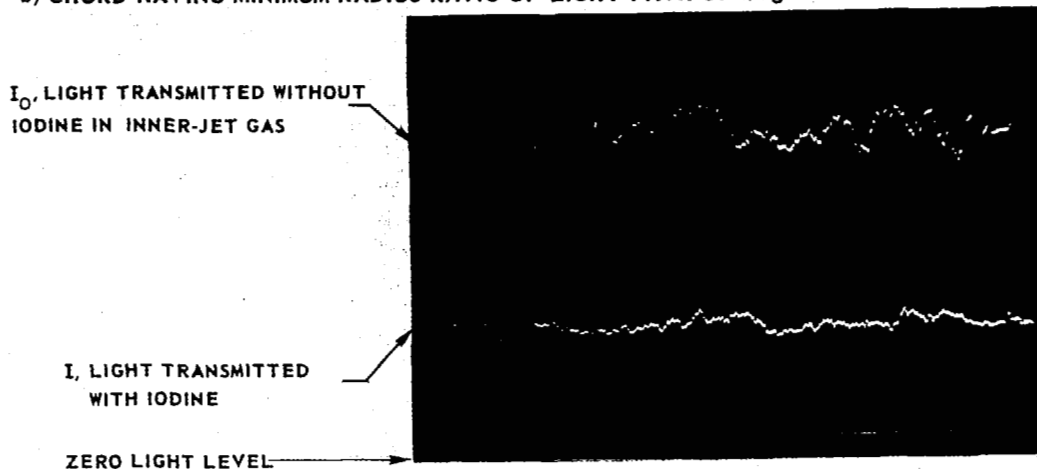INNER, BUFFER AND OUTER GASES - FREON-11, AIR, AIR; $\rho_I/\rho_{BAO} = 4.7$

$V_{BAO} \approx 80$ FT/SEC, $V_O \approx 97$ FT/SEC, $V_B \approx 33$ FT/SEC, $V_I \approx 4$ FT/SEC; $V_{BAO}/V_I = 20$

TRACES SHOW PHOTOMULTIPLIER OUTPUT (SEE FIG. 8) FOR TWO DIFFERENT CHORDS AT $z = 3.75$ IN.

a) CHORD HAVING MINIMUM RADIUS RATIO OF LIGHT PATH OF $r/r_O = 0.566$

I_O, LIGHT TRANSMITTED WITHOUT IODINE IN INNER-JET GAS

I, LIGHT TRANSMITTED WITH IODINE

0.01 SEC

ZERO LIGHT LEVEL

b) CHORD HAVING MINIMUM RADIUS RATIO OF LIGHT PATH OF $r/r_O = 0.400$

I_O, LIGHT TRANSMITTED WITHOUT IODINE IN INNER-JET GAS

I, LIGHT TRANSMITTED WITH IODINE

ZERO LIGHT LEVEL

45

FIG. 14

PHOTOGRAPHS SHOWING EFFECTS OF VELOCITY RATIO V_B/V_{BAO} ON CONTAINMENT OF INNER-JET GAS FOR $r_I/r_O = 0.5$

V_B AND V_O VARIED; V_{BAO} AND V_I HELD CONSTANT
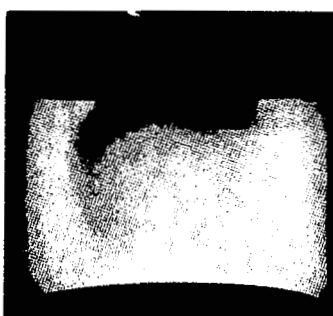
$L_N/D = 1.0$ $D_N/D = 0.6$

INNER, BUFFER AND OUTER GASES - FREON-11, AIR, AIR; $\rho_I/\rho_{BAO} = 4.7$

$V_{BAO} \approx 80$ FT/SEC, $V_I \approx 4$ FT/SEC; $V_{BAO}/V_I = 20$
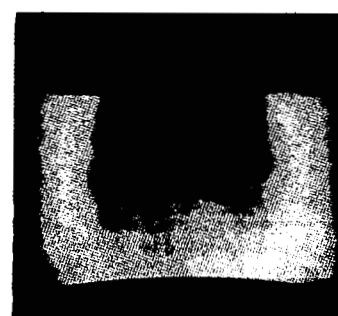
IODINE CONCENTRATION IN INNER-JET GAS AT INLET SAME IN ALL PHOTOGRAPHS
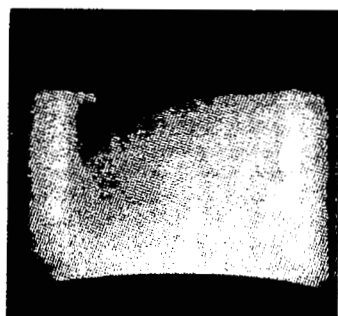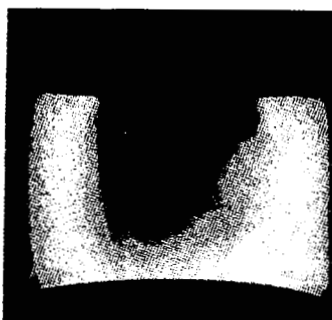
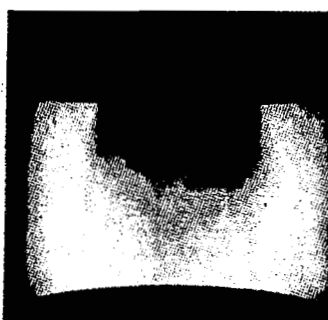

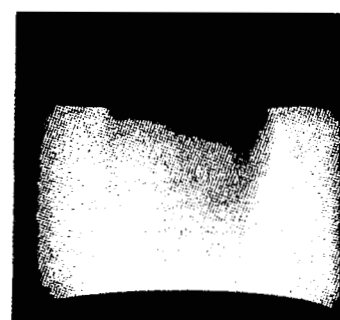$V_B/V_{BAO} = 0$ $V_B/V_{BAO} = 0.21$ $V_B/V_{BAO} = 0.42$

$V_B/V_{BAO} = 0.50$ $V_B/V_{BAO} = 0.62$ $V_B/V_{BAO} = 1.04$

EFFECT OF VELOCITY RATIO V_B/V_{BAO} ON RADIAL DISTRIBUTION
OF INNER-JET GAS PARTIAL PRESSURE FOR $r_I/r_O = 0.5$

V_B AND V_O VARIED; V_{BAO} AND V_I HELD CONSTANT

$L_N/D = 1.0$ $D_N/D = 0.6$

INNER, BUFFER AND OUTER GASES - FREON-11, AIR, AIR; $\rho_I/\rho_{BAO} = 4.7$

CASE	V_I - FT/SEC	V_B - FT/SEC	V_O - FT/SEC	V_{BAO} - FT/SEC	V_{BAO}/V_I	V_B/V_I	V_O/V_I	V_B/V_{BAO}
258	3.85	78.3	80.7	78.9	20.5	20.3	21.0	0.99
259	3.96	48.0	91.1	79.8	20.1	12.1	23.0	0.60

AXIAL STATION, z - IN.	0.75	2.25	3.75	5.25	6.75
SYMBOL	○	△	□	◇	▷

FIG. 15a,b

(CONTINUED)

EFFECT OF VELOCITY RATIO V_B/V_{BAO} ON RADIAL DISTRIBUTION OF INNER - JET GAS PARTIAL PRESSURE FOR $r_I/r_O = 0.5$
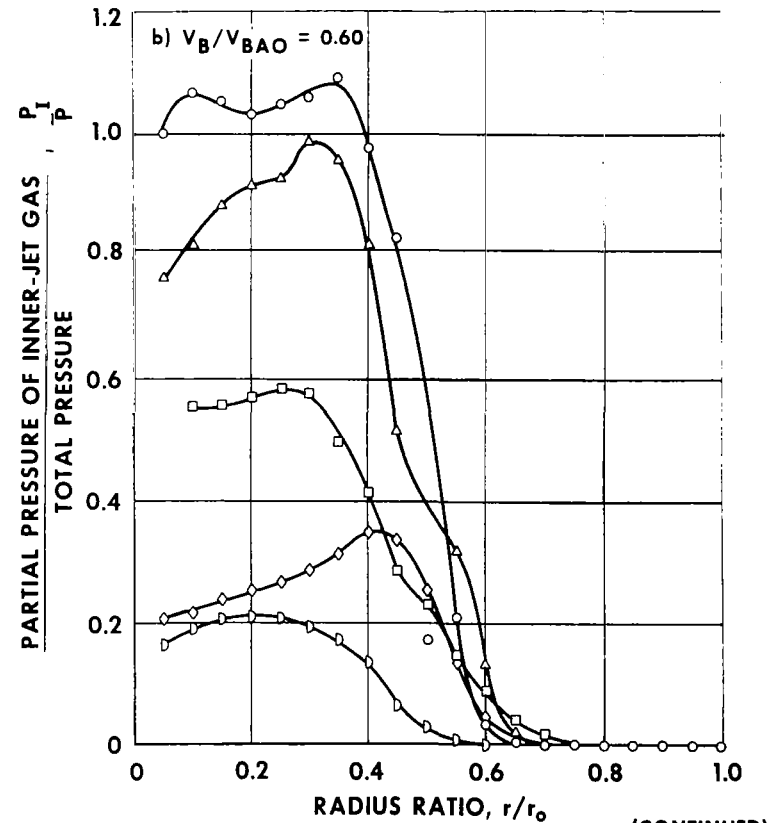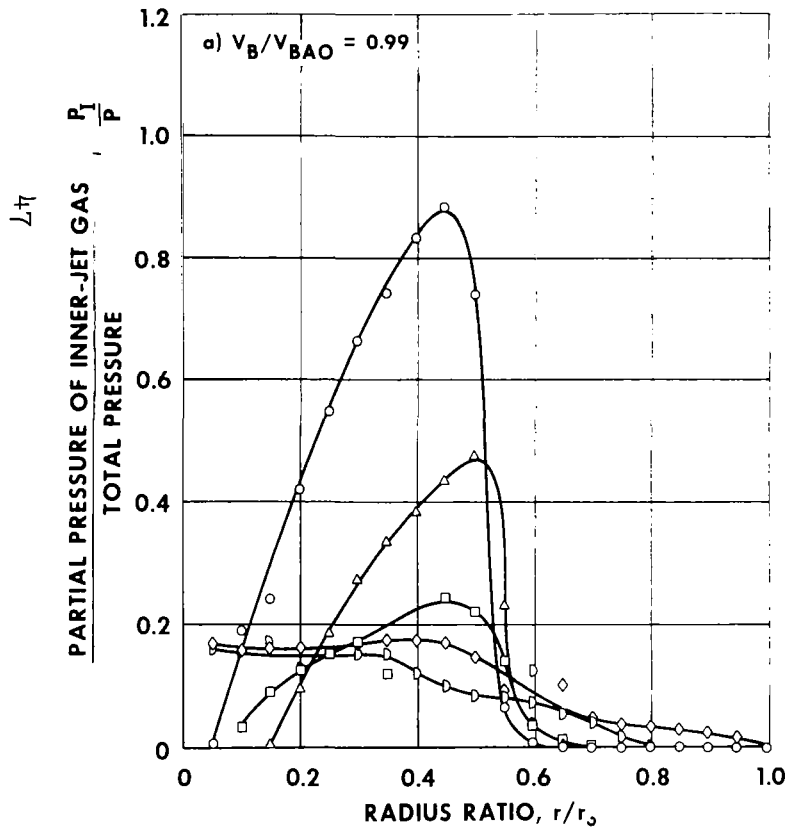
V_B AND V_O VARIED; V_{BAO} AND V_I HELD CONSTANT

$L_N/D = 1.0$ $D_N/D = 0.6$

INNER, BUFFER AND OUTER GASES - FREON-11, AIR, AIR ; $\rho_I/\rho_{BAO} = 4.7$

CASE	V_I - FT/SEC	V_B - FT/SEC	V_O- FT/SEC	V_{BAO}- FT/SEC	V_{BAO}/V_I	V_B/V_I	V_O/V_I	V_B/V_{BAO}
260	3.99	32.6	96.6	80.0	20.1	8.2	24.2	0.41
261	3.98	16.3	100.7	79.5	20.0	4.1	25.3	0.21

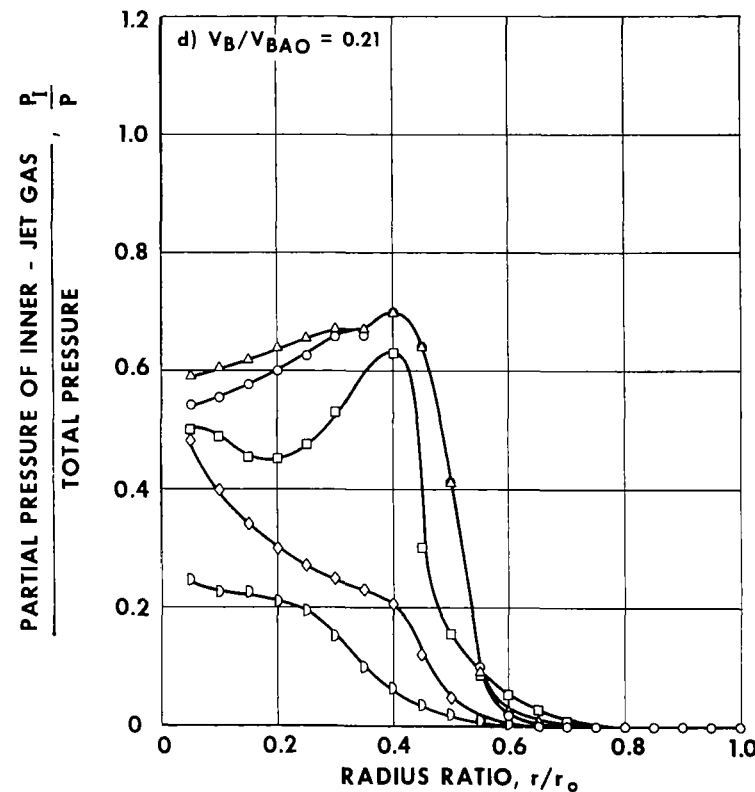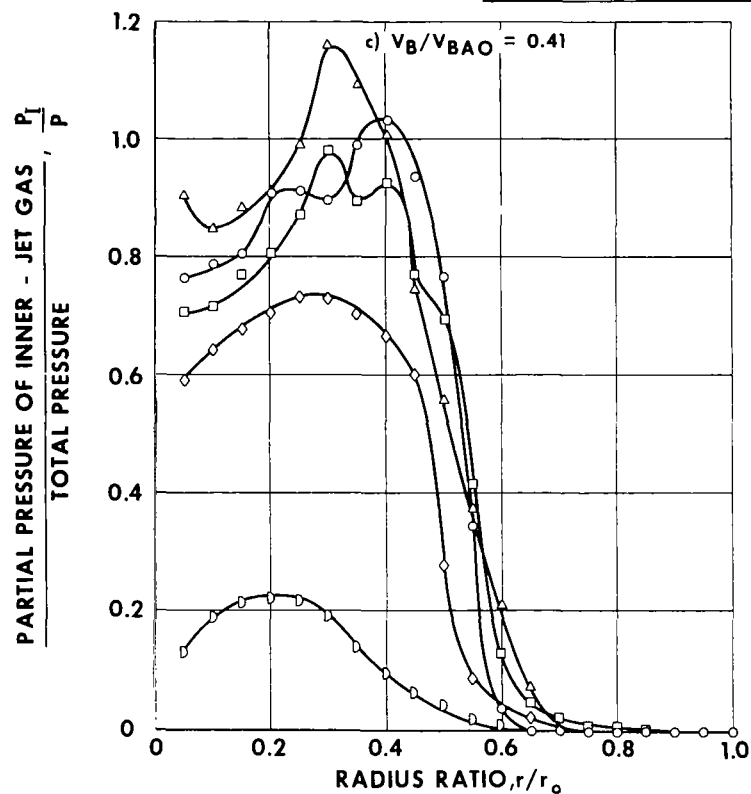| AXIAL STATION, z - IN.	0.75	2.25	3.75	5.25	6.75
SYMBOL	o	△	□	◇	▷

FIG. 15c, d

FIG. 16

EFFECT OF VELOCITY RATIO V_B/V_{BAO} ON AXIAL DISTRIBUTION OF AREA-AVERAGE PARTIAL PRESSURE RATIO P_I^*/P FOR $r_I/r_O = 0.5$

V_B AND V_O VARIED; V_{BAO} AND V_I HELD CONSTANT

$V_{BAO} \approx 80$ FT/SEC, $V_O \approx 97$ FT/SEC, $V_B \approx 33$ FT/SEC, $V_I \approx 4$ FT/SEC

P_I^*/P DERIVED FROM DATA IN FIG. 15

$$P_I^*/P = 2\int_0^{r_O}(P_I/P)\,r\,dr\,/\,r_O^2$$

CASE	SYMBOL	V_{BAO}/V_I	V_B/V_I	V_B/V_{BAO}
261	△─ ─△	20.0	4.1	0.21
260	○──○	20.1	8.2	0.41
259	□─ ─□	20.1	12.1	0.60
258	◇─ ─◇	20.5	20.3	0.99

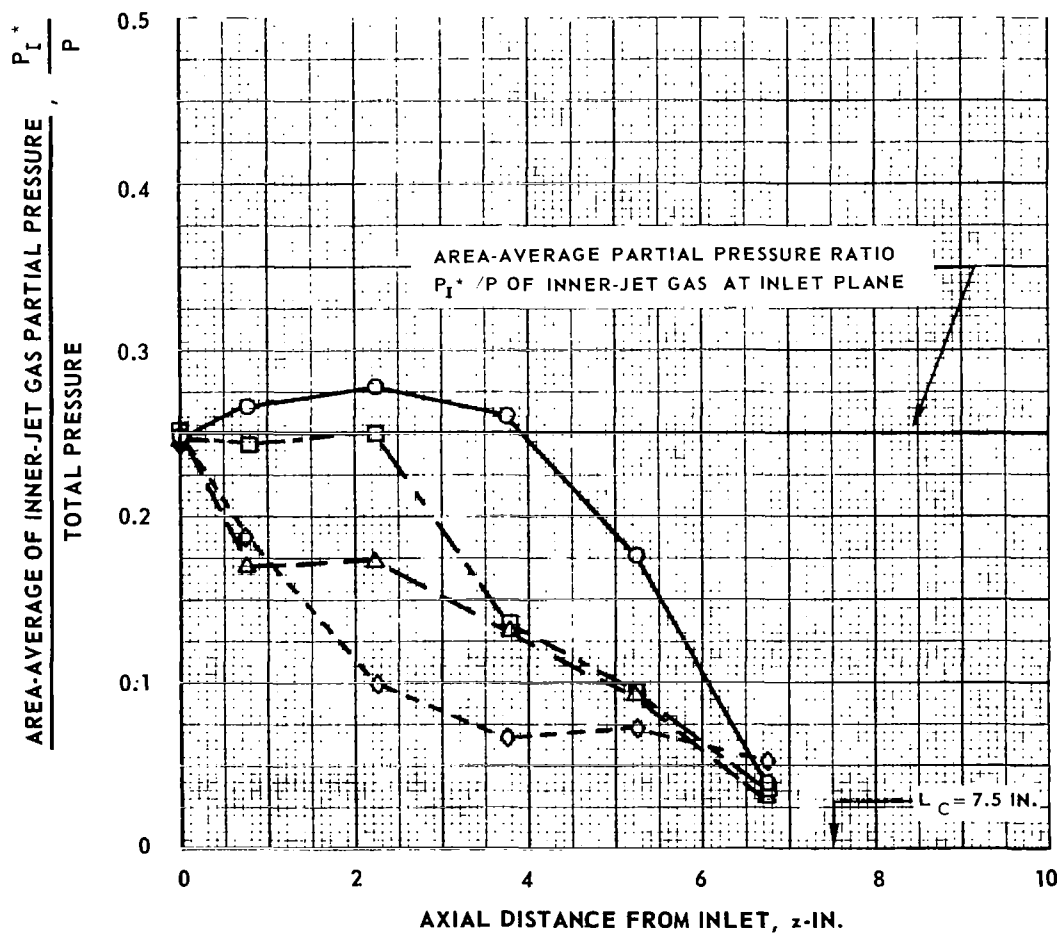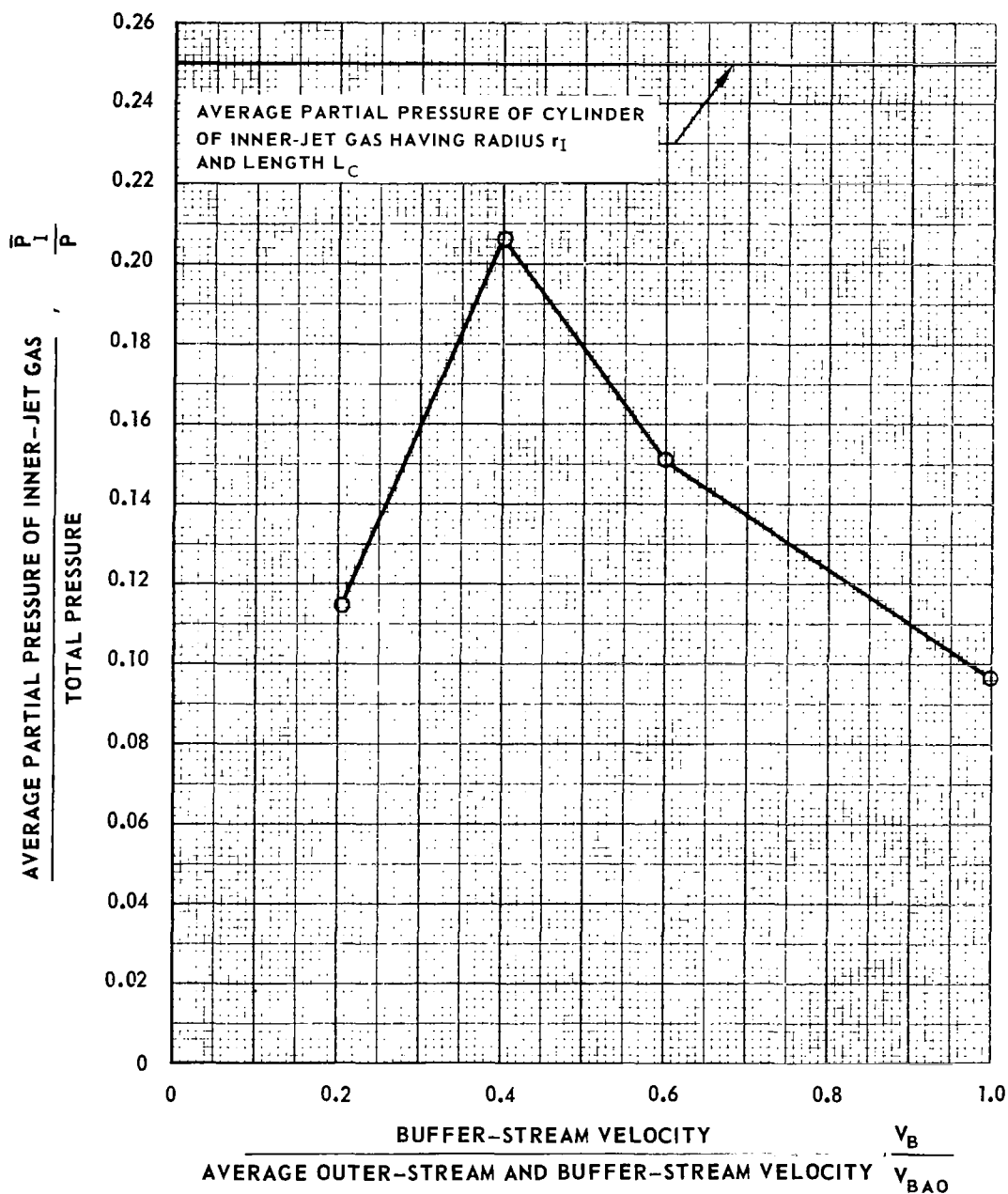
AXIAL DISTANCE FROM INLET, z-IN.

49

FIG. 17

EFFECT OF VELOCITY RATIO V_B/V_{BAO} ON AVERAGE PARTIAL PRESSURE OF INNER–JET GAS IN CHAMBER FOR $r_I/r_O = 0.5$

V_B AND V_O VARIED; V_{BAO} AND V_I HELD CONSTANT

$\overline{P}_I/P$ DERIVED FROM DATA IN FIGS. 15 AND 16

$$\overline{P}_I/P = \frac{2}{L_C r_O^2} \int_0^{L_C} \int_0^{r_O} \left(P_I/P\right) r \; dr \; dz$$

AVERAGE PARTIAL PRESSURE OF CYLINDER OF INNER-JET GAS HAVING RADIUS r_I AND LENGTH L_C

y-axis: $\dfrac{\overline{P}_I}{P}$, AVERAGE PARTIAL PRESSURE OF INNER–JET GAS / TOTAL PRESSURE

x-axis: BUFFER–STREAM VELOCITY / AVERAGE OUTER–STREAM AND BUFFER–STREAM VELOCITY, $\dfrac{V_B}{V_{BAO}}$

FIG. 18

PHOTOGRAPHS SHOWING EFFECTS OF VELOCITY RATIO V_B/V_{BAO}
ON CONTAINMENT OF INNER-JET GAS FOR $r_I/r_O = 0.7$

V_B AND V_O VARIED; V_{BAO} AND V_I HELD CONSTANT

$L_N/D = 1.0$ $D_N/D = 0.6$

INNER, BUFFER AND OUTER GASES – FREON-11, AIR, AIR; $\rho_I/\rho_{BAO} = 4.7$

$V_{BAO} \approx 80$ FT/SEC, $V_I \approx 4$ FT/SEC; $V_{BAO}/V_I = 20$

IODINE CONCENTRATION IN INNER-JET GAS AT INLET SAME IN ALL PHOTOGRAPHS

$V_B/V_{BAO} = 0.24$

$V_B/V_{BAO} = 0.48$

$V_B/V_{BAO} = 0.71$

$V_B/V_{BAO} = 1.18$

EFFECT OF VELOCITY RATIO V_B/V_{BAO} ON RADIAL DISTRIBUTION
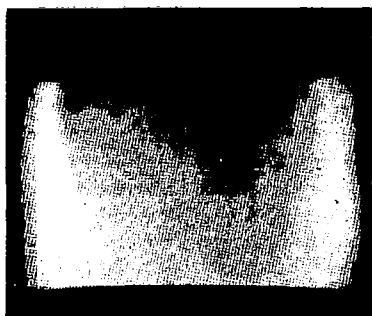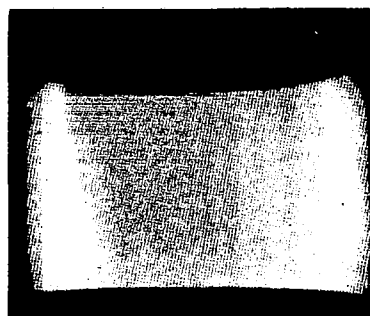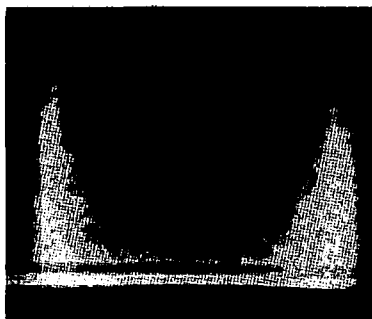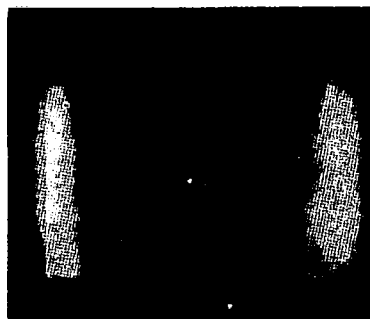## OF INNER - JET GAS PARTIAL PRESSURE FOR $r_I/r_O = 0.7$

V_B AND V_O VARIED; V_{BAO} AND V_I HELD CONSTANT

$L_N/D = 1.0$ $D_N/D = 0.6$

INNER, BUFFER AND OUTER GASES - FREON-11, AIR, AIR; $\rho_I/\rho_{BAO} = 4.7$

CASE	V_I - FT/SEC	V_B -FT/SEC	V_O -FT/SEC	V_{BAO} - FT/SEC	V_{BAO}/V_I	V_B/V_I	V_O/V_I	V_B/V_{BAO}
148	3.7	52.3	93.6	80.6	22.0	14.3	25.6	0.65
150	4.4	23.8	107.8	86.0	19.6	5.4	24.6	0.28

AXIAL STATION, z - IN.	0.75	2.25	3.75	5.25	6.75
SYMBOL	○	△	□	◇	D

a) $V_B/V_{BAO} = 0.65$

b) $V_B/V_{BAO} = 0.28$

PARTIAL PRESSURE OF INNER-JET GAS, $\dfrac{P_I}{P}$ TOTAL PRESSURE
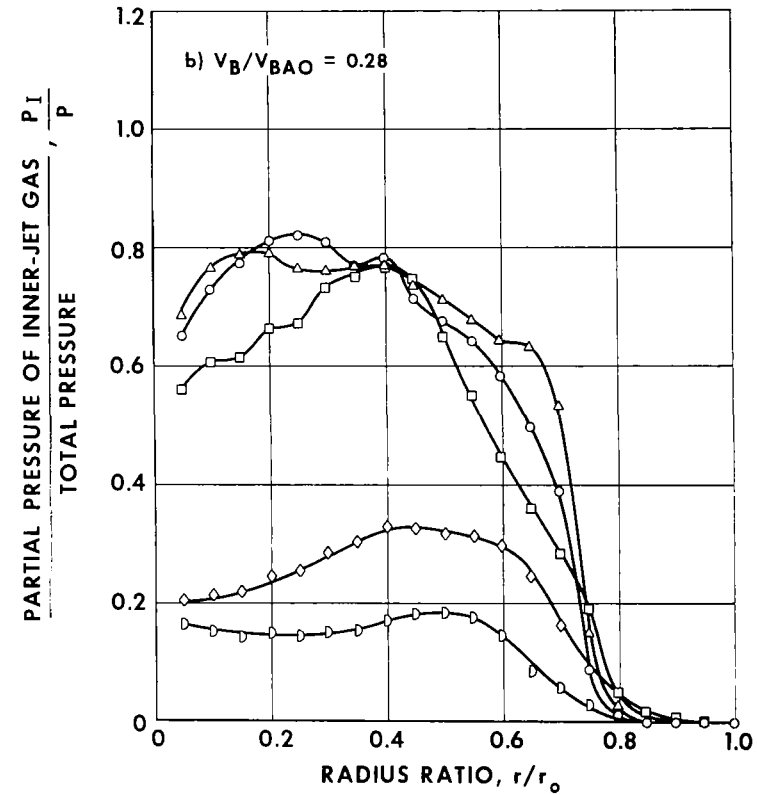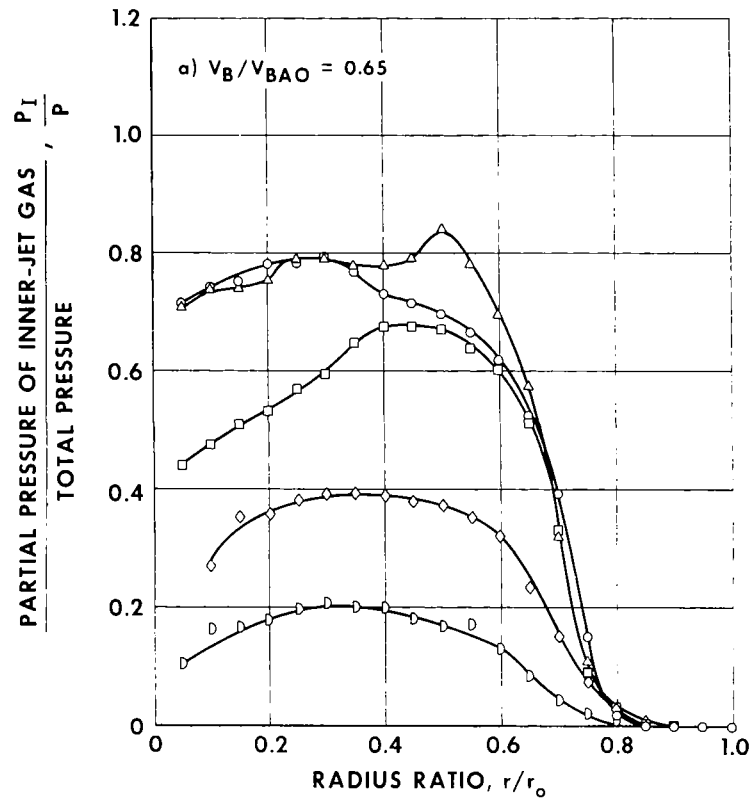
RADIUS RATIO, r/r_o

FIG. 19

FIG. 20

EFFECT OF VELOCITY RATIO V_B/V_{BAO} ON AVERAGE PARTIAL PRESSURE OF INNER-JET GAS IN CHAMBER FOR $r_I/r_0 = 0.7$

V_B AND V_0 VARIED; V_{BAO} AND V_I HELD CONSTANT

$L_N/D = 1.0$ $D_N/D = 0.6$

INNER, BUFFER AND OUTER GASES - FREON-11, AIR, AIR; $\rho_I/\rho_{BAO} = 4.7$

$V_{BAO} \approx 80$ FT/SEC , V_I = FT/SEC

$$(\bar{P}_I/P) = \frac{2}{L_C\, r_0^2} \int_0^{L_C} \int_0^{r_0} (P_I/P)\, r\, dr\, dz$$

SYMBOL	r_I/r_0	r_B/r_0
O———O	0.5	0.65
△— — —△	0.7	0.80

AVERAGE PARTIAL PRESSURE OF INNER-JET GAS $\dfrac{\bar{P}_I}{P}$, $\dfrac{}{\text{TOTAL PRESSURE}}$

$r_I/r_0 = 0.7$

AVERAGE PARTIAL PRESSURE OF CYLINDER OF INNER-JET GAS HAVING VOLUME $\pi r_I^2\, L_C$

$r_I/r_0 = 0.5$

$r_I/r_0 = 0.5$; FROM FIG. 17

BUFFER-STREAM VELOCITY

AVERAGE OUTER-STREAM AND BUFFER-STREAM VELOCITY , $\dfrac{V_B}{V_{BAO}}$

53

PHOTOGRAPHS SHOWING EFFECTS OF VELOCITY RATIO V_{BAO}/V_I
ON CONTAINMENT OF INNER-JET GAS FOR $r_I/r_O = 0.5$

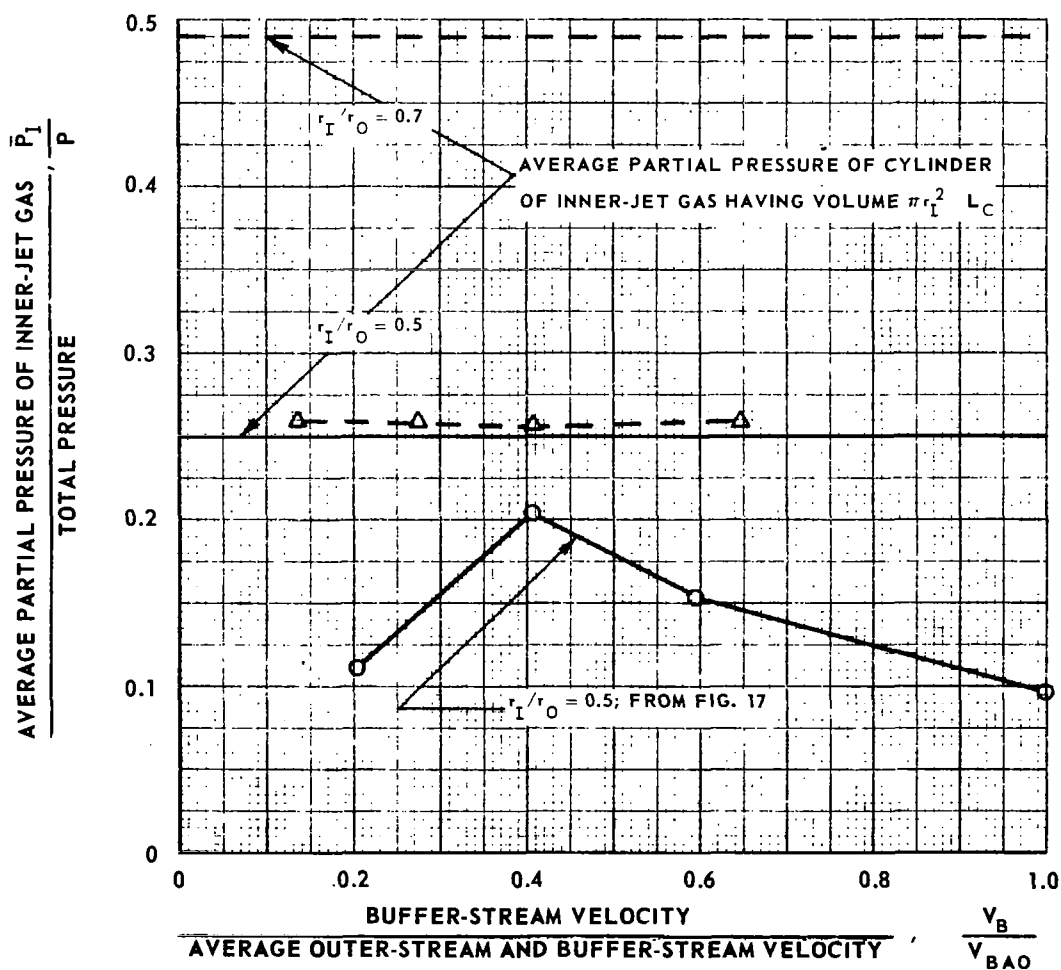FIG. 21

V_I VARIED; V_B, V_O AND V_{BAO} HELD CONSTANT

$L_N/D = 1.0$ $\qquad$ $D_N/D = 0.6$
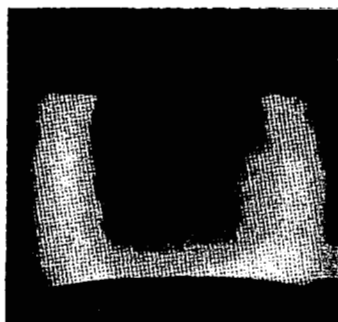
INNER, BUFFER AND OUTER GASES - FREON-11, AIR, AIR; $\rho_I/\rho_{BAO} = 4.7$

$V_{BAO} \approx 80$ FT/SEC, $V_B \approx 33$ FT/SEC; $V_B/V_{BAO} = 0.41$

IODINE CONCENTRATION IN INNER-JET GAS AT INLET SAME IN ALL PHOTOGRAPHS

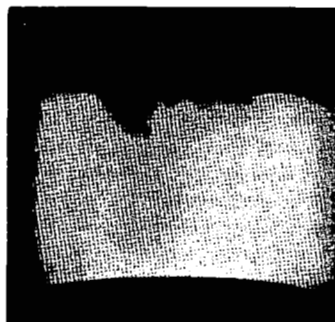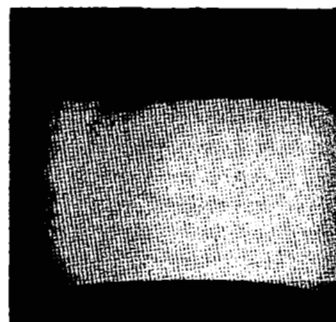$V_{BAO}/V_I = 11$ $\qquad\qquad$ $V_{BAO}/V_I = 20$ $\qquad\qquad$ $V_{BAO}/V_I = 35$

$V_{BAO}/V_I = 50$ $\qquad\qquad\qquad$ $V_{BAO}/V_I = 90$

EFFECT OF VELOCITY RATIO V_{BAO}/V_I ON RADIAL DISTRIBUTION OF INNER - JET GAS PARTIAL PRESSURE FOR $r_I/r_o = 0.5$

V_I VARIED; V_B, V_O AND V_{BAO} HELD CONSTANT

$L_N/D = 1.0$ $D_N/D = 0.6$

INNER, BUFFER AND OUTER GASES-FREON-11, AIR, AIR; $\rho_I/\rho_{BAO} = 4.7$

CASE	V_I-FT/SEC	V_B-FT/SEC	V_O-FT/SEC	V_{BAO}-FT/SEC	V_{BAO}/V_I	V_B/V_I	V_O/V_I	V_B/V_{BAO}
264	7.87	33.1	96.6	80.6	10.2	4.2	12.3	0.41
260	3.99	32.6	96.6	80.0	20.1	8.2	24.2	0.41

AXIAL STATION, z - IN.	0.75	2.25	3.75	5.25	6.75
SYMBOL	○	△	□	◇	⬭
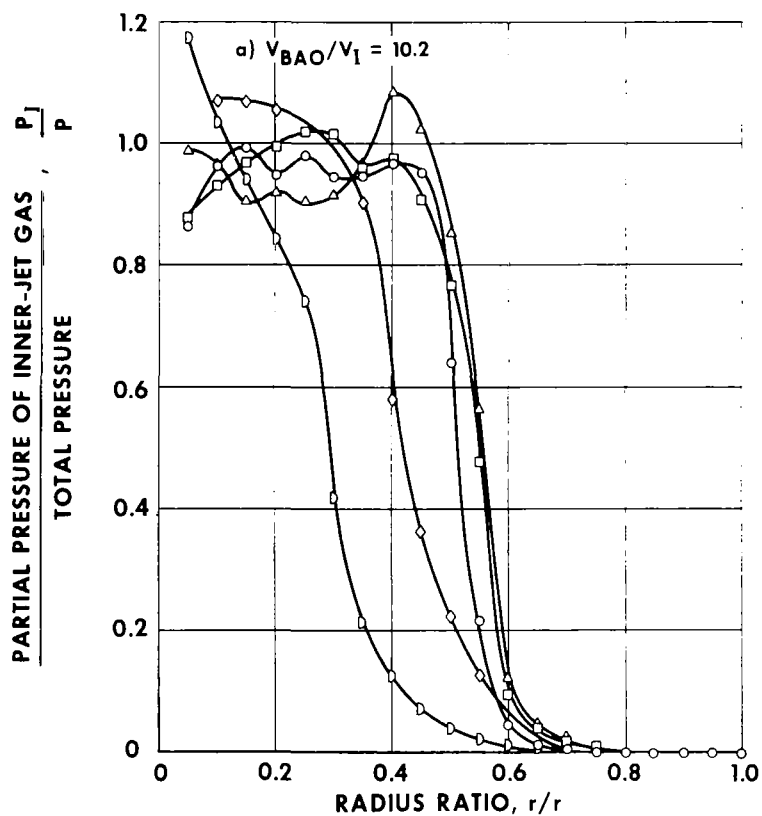
a) $V_{BAO}/V_I = 10.2$

b) $V_{BAO}/V_I = 20.1$

PARTIAL PRESSURE OF INNER-JET GAS, $\dfrac{P_I}{P}$ TOTAL PRESSURE

RADIUS RATIO, r/r

PARTIAL PRESSURE OF INNER - JET GAS, $\dfrac{P_I}{P}$ TOTAL PRESSURE
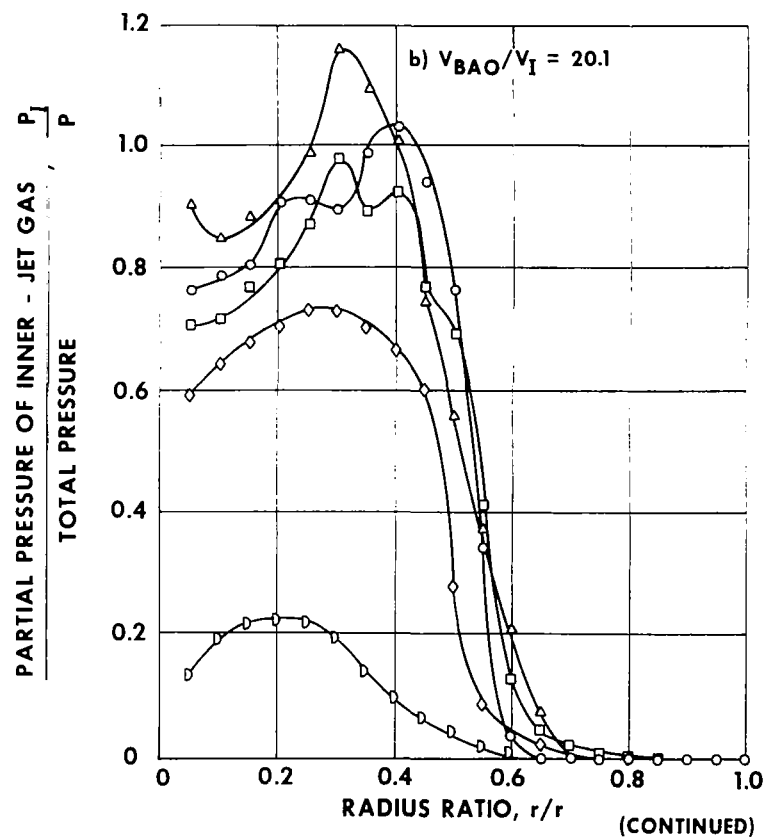
RADIUS RATIO, r/r

(CONTINUED)

EFFECT OF VELOCITY RATIO V_{BAO}/V_I ON RADIAL DISTRIBUTION OF INNER - JET GAS PARTIAL PRESSURE FOR $r_o/r_o = 0.5$

V_I VARIED; V_B, V_O AND V_{BAO} HELD CONSTANT $L_N/D = 1.0$ $D_N/D = 0.6$ INNER, BUFFER AND OUTER GASES - FREON-11, AIR, AIR; $\rho_I/\rho_{BAO} = 4.7$

CASE	V_I-FT/SEC	V_B-FT/SEC	V_O-FT/SEC	V_{BAO}-FT/SEC	V_{BAO}/V_I	V_B/V_I	V_O/V_I	V_B/V_{BAO}
256	2.17	32.3	94.6	78.4	36.2	14.9	43.7	0.41
252	1.49	32.0	93.1	77.9	52.2	21.5	62.4	0.41

AXIAL STATION, z - IN.	0.75	2.25	3.75	5.25	6.75
SYMBOL	o	△	□	◇	D
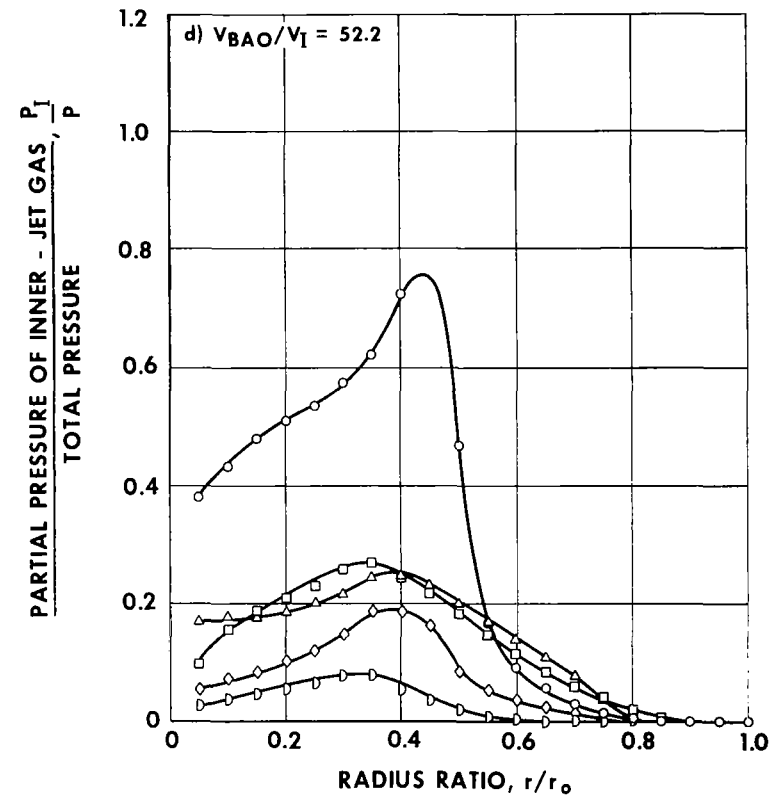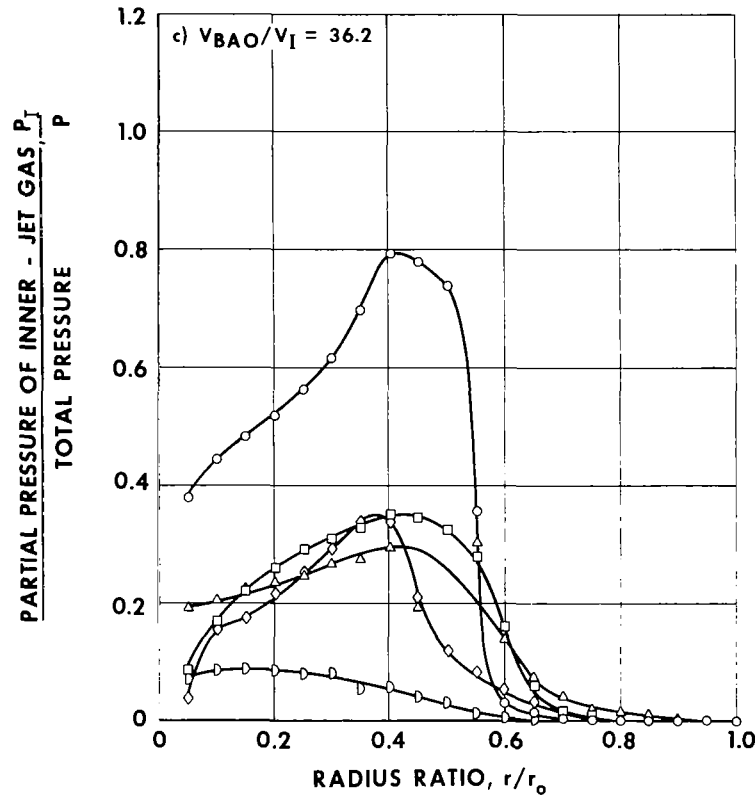
c) $V_{BAO}/V_I = 36.2$

d) $V_{BAO}/V_I = 52.2$

FIG. 23

EFFECT OF VELOCITY RATIO V_{BAO}/V_I ON AXIAL DISTRIBUTION OF AREA-AVERAGE PARTIAL PRESSURE RATIO P_I*/P FOR $r_I/r_O = 0.5$

V_I VARIED; V_B, V_O AND V_{BAO} HELD CONSTANT

P_I*/P DERIVED FROM DATA IN FIG. 22

$$P_I*/P = 2 \int_0^{r_O} (P_I/P) \, r \, dr / r_O^2 .$$

CASE	SYMBOL	V_{BAO}/V_I	V_B/V_{BAO}
264	△ — — △	10	0.41
260	◯——◯	20	0.41
256	▢ — — ▢	36	0.41
252	◇ · · · · ◇	52	0.41

AREA-AVERAGE PARTIAL PRESSURE RATIO P_I*/P OF INNER-JET GAS AT INLET PLANE

L_C = 7.5 IN.

AXIAL DISTANCE FROM INLET, z - IN.

$\frac{P_I*}{P}$, AREA-AVERAGE OF INNER-JET GAS PARTIAL PRESSURE / TOTAL PRESSURE
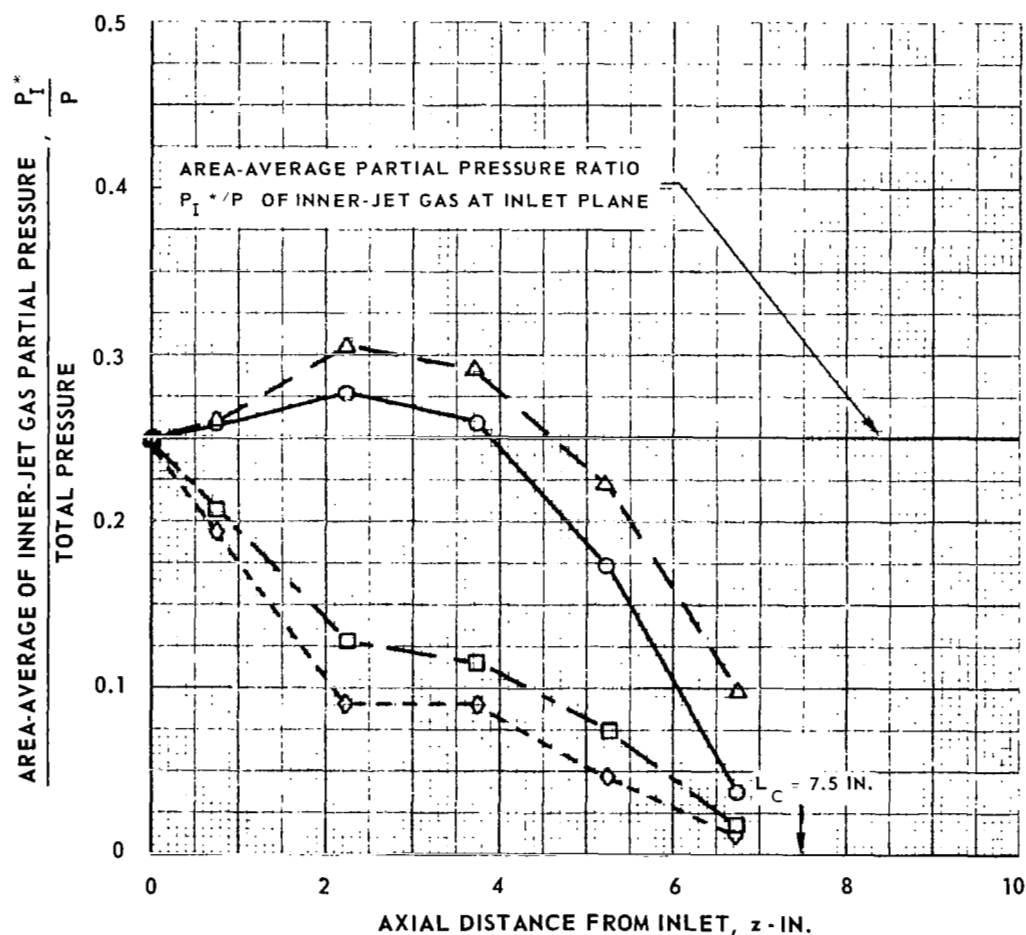
FIG. 24

EFFECT OF VELOCITY RATIO V_{BAO}/V_I ON AVERAGE PARTIAL PRESSURE
OF INNER-JET GAS IN CHAMBER FOR $r_I/r_O = 0.5$

$\overline{P}_I/P$ DERIVED FROM DATA IN FIGS. 22 AND 23 AND OTHER TESTS OF SAME GEOMETRIC CONFIGURATION

$$\overline{P}_I/P = \frac{2}{L_C r_O^2} \int_0^{L_C} \int_0^{r_O} (P_I/P)\ r\ dr\ dz$$

SYMBOL	V_{BAO}/V_I
△——△	10
○——○	20
□— -□	36
◇- - -◇	52

MAXIMUM VALUES OF $\overline{P}_I/P$ FOR VELOCITY RATIO V_{BAO}/V_I

AVERAGE PARTIAL PRESSURE OF CYLINDER OF INNER-JET GAS HAVING VOLUME $\pi r_I^2 L_C$

$\overline{P}_I/P$ — AVERAGE PARTIAL PRESSURE OF INNER-JET GAS / TOTAL PRESSURE

BUFFER-STREAM VELOCITY / AVERAGE OUTER-STREAM AND BUFFER-STREAM VELOCITY , V_B/V_{BAO}

58

FIG. 25

EFFECT OF VELOCITY RATIO V_{BAO}/V_I ON MAXIMUM VALUES OF $\bar{P}_I/P$

FOR $r_I/r_O = 0.5$ AND 0.7

$L_N/D = 1.0 \quad D_N/D = 0.6$

INNER, BUFFER AND OUTER GASES - FREON-11, AIR, AIR; $\rho_I/\rho_{BAO} = 4.7$

$V_{BAO} \approx 80$ FT/SEC

MAXIMUM VALUES OF $\bar{P}_I/P$ OBTAINED FOR EACH VELOCITY RATIO, V_{BAO}/V_I

SEE FIG. 24 FOR DATA FOR $r_I/r_O = 0.5$
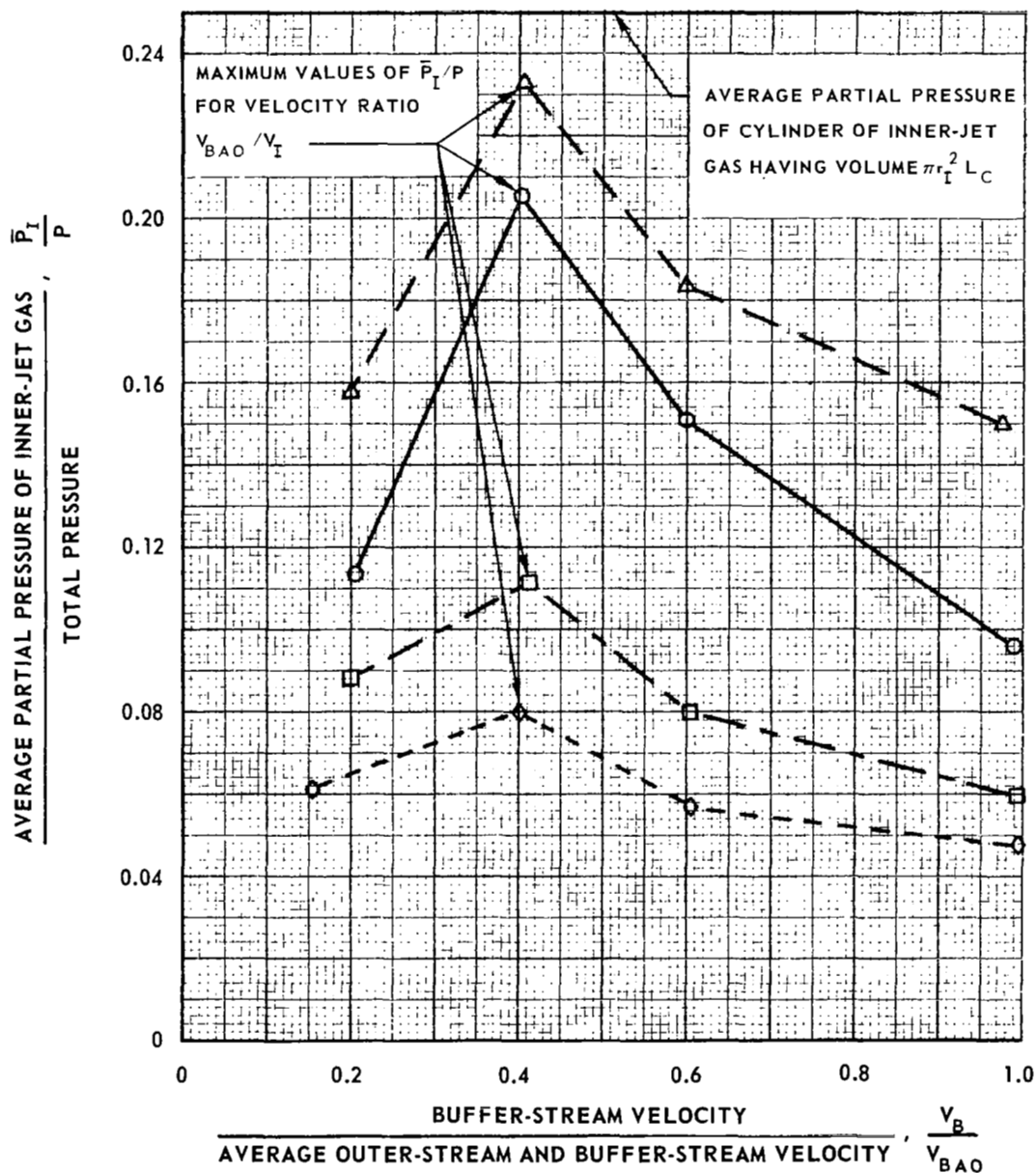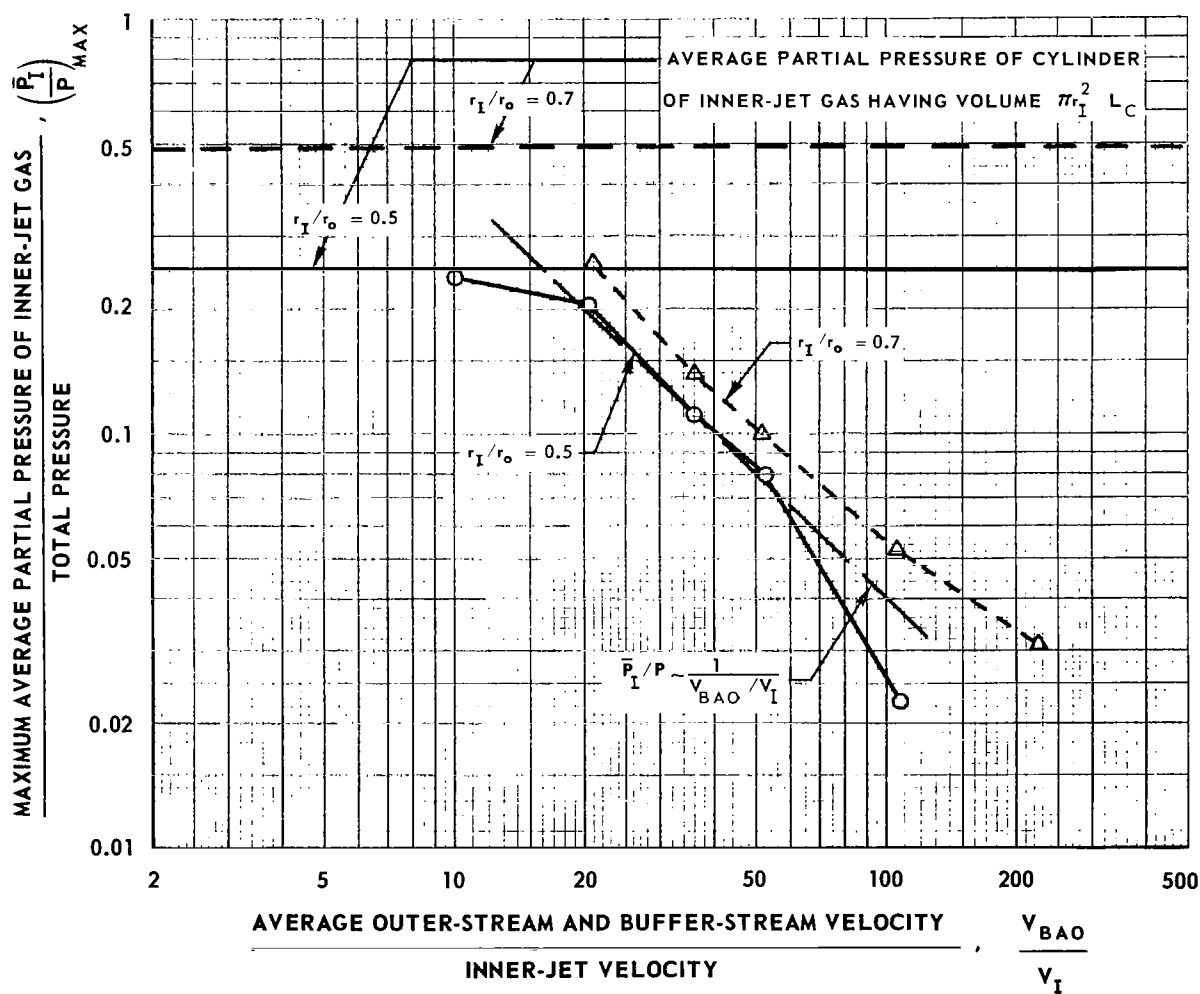
FIG. 26

EFFECT OF ABSOLUTE VALUES OF V_{BAO} AND V_I ON AVERAGE PARTIAL PRESSURE OF INNER-JET GAS IN CHAMBER FOR $r_I/r_O = 0.5$

$L_N/D = 1.0$ $D_N/D = 0.6$

INNER, BUFFER AND OUTER GASES- FREON-11, AIR, AIR; $\rho_I/\rho_{BAO} = 4.7$

SYMBOL	V_{BAO}- FT/SEC	V_I -FT/SEC	V_{BAO}/V_I	W_{BAO}- LB/SEC
△——△	35	1.9	18.3	0.59
○——○	80	4.0	20.1	1.30
□——□	154	7.9	19.5	2.82
◇——◇	205	9.1	22.5	3.80

AVERAGE PARTIAL PRESSURE OF CYLINDER OF INNER-JET GAS HAVING VOLUME $\pi r_I^2 L_C$

AVERAGE PARTIAL PRESSURE OF INNER-JET GAS $\frac{\bar{P}_I}{P}$, TOTAL PRESSURE

BUFFER-STREAM VELOCITY

AVERAGE OUTER-STREAM AND BUFFER-STREAM VELOCITY $, \frac{V_B}{V_{BAO}}$

60
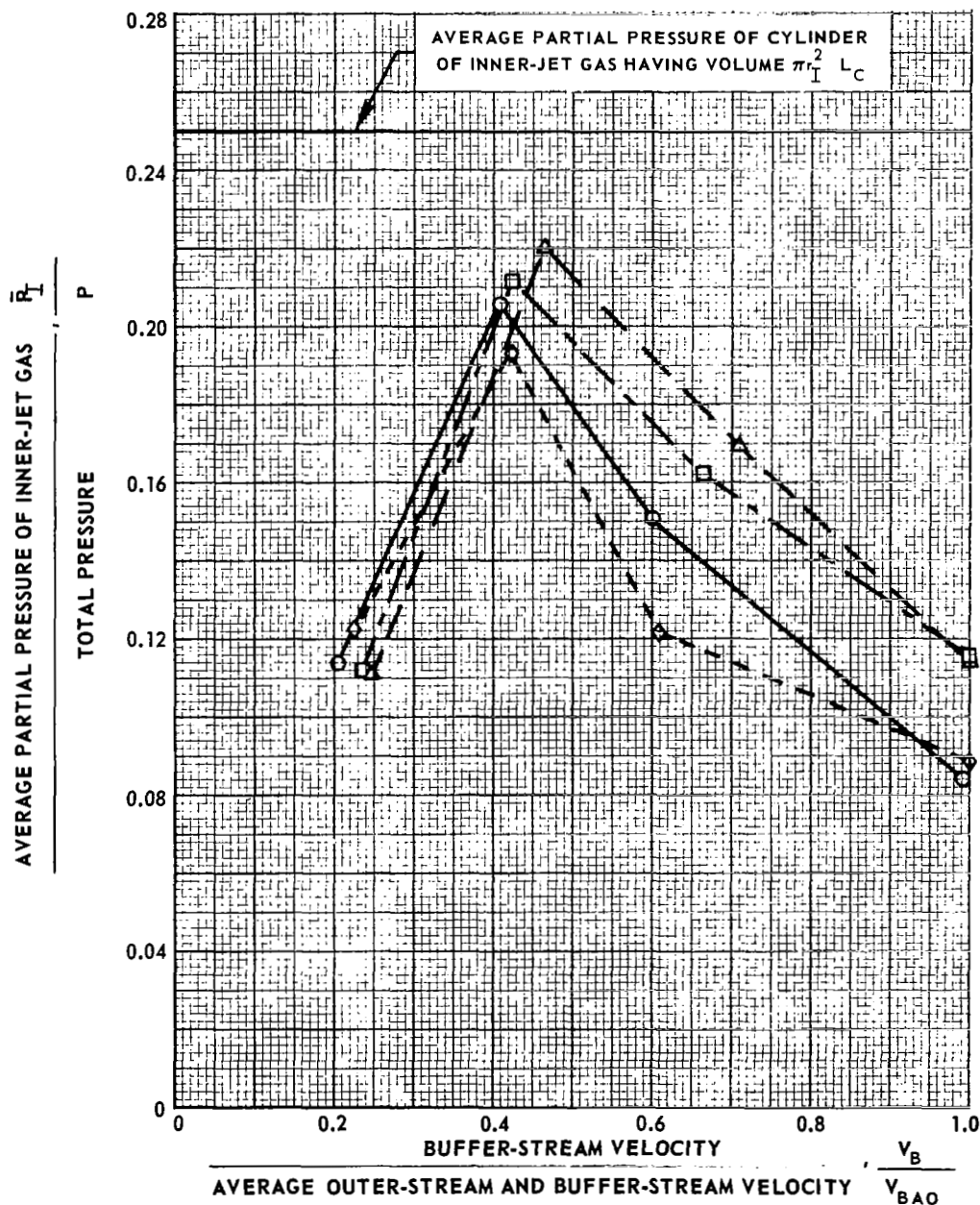
EFFECT OF ABSOLUTE VALUES OF V_{BAO} AND V_I AND VELOCITY RATIO V_{BAO}/V_I
ON MAXIMUM VALUES OF $\bar{P}_I/P$ FOR $r_I/r_O = 0.5$ AND 0.7

$L_N/D = 1.00$ $D_N/D = 0.6$

INNER, BUFFER AND OUTER GASES - FREON-11, AIR, AIR

MAXIMUM VALUES OF $\bar{P}_I/P$ OBTAINED FOR EACH VELOCITY RATIO, V_{BAO}/V_I

SYMBOL	△ ▲	○ ●	□	◇
V_{BAO} - FT/SEC	35–40	80	150	205
W_{BAO} –LB/SEC	0.59	1.30	2.82	3.80

a) $r_I/r_O = 0.5$

AVERAGE PARTIAL PRESSURE OF CYLINDER OF INNER-JET GAS HAVING VOLUME $\pi r_I^2 L_C$

b) $r_I/r_O = 0.7$

AVERAGE PARTIAL PRESSURE OF CYLINDER OF INNER-JET GAS HAVING VOLUME $\pi r_I^2 L_C$

MAXIMUM AVERAGE PARTIAL PRESSURE OF INNER-JET GAS, $\left(\dfrac{\bar{P}_I}{P}\right)_{MAX}$ / TOTAL PRESSURE

OUTER-STREAM AND BUFFER-STREAM VELOCITY , $\dfrac{V_{BAO}}{V_I}$
INNER-JET VELOCITY

OUTER-STREAM AND BUFFER STREAM VELOCITY , $\dfrac{V_{BAO}}{V_I}$
INNER-JET VELOCITY

61

FIG. 27

FIG. 28

PHOTOGRAPHS SHOWING EFFECTS OF DENSITY RATIO ρ_I/ρ_{BAO} ON CONTAINMENT OF INNER-JET GAS FOR $r_I/r_O = 0.5$

ρ_I VARIED; ρ_B, ρ_O AND ρ_{BAO} HELD CONSTANT

$L_N/D = 1.0$ $D_N/D = 0.6$

BUFFER AND OUTER GAS - AIR

$V_{BAO} \approx 80$ FT/SEC, $V_O \approx 97$ FT/SEC $V_B \approx 33$ FT/SEC, $V_I \approx 4$ FT/SEC

$V_{BAO}/V_I = 20$, $V_B/V_{BAO} = 0.41$
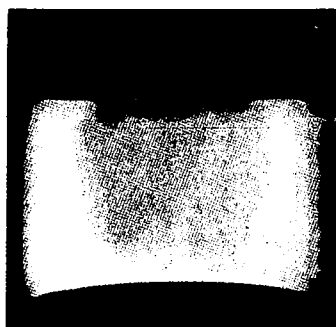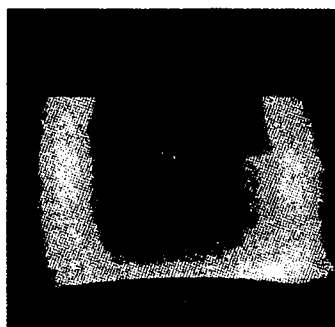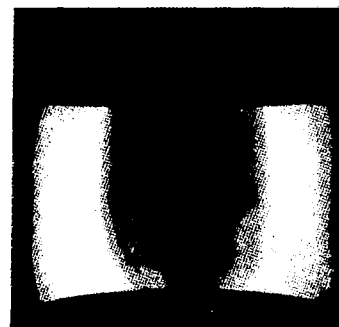
INNER-JET GAS - AIR	FREON-11	FC-77
$\rho_I/\rho_{BAO} = 1.0$	$\rho_I/\rho_{BAO} = 4.7$	$\rho_I/\rho_{BAO} = 14.0$

EFFECT OF DENSITY RATIO ρ_I/ρ_{BAO} ON RADIAL DISTRIBUTION OF INNER - JET GAS PARTIAL PRESSURE FOR $r_I/r_O = 0.5$

ρ_I VARIED; ρ_B, ρ_O AND ρ_{BAO} HELD CONSTANT

$L_N/D = 1.0$ $D_N/D = 0.6$

BUFFER-STREAM AND OUTER-STREAM GAS - AIR

SEE FIG. 22b FOR RADIAL DISTRIBUTION WITH FREON-11 AS INNER-JET GAS

CASE	INNER-JET GAS	ρ_I/ρ_{BAO}	V_I-FT/SEC	V_B-FT/SEC	V_O-FT/SEC	V_{BAO}-FT/SEC	V_{BAO}/V_I	V_B/V_I	V_O/V_I	V_B/V_{BAO}
278	AIR	1.0	4.42	33.2	96.5	80.6	18.2	7.5	21.9	0.41
316	FC-77	14.0	4.12	33.1	97.1	81.2	19.7	8.0	23.6	0.41

AXIAL STATION, z - IN.	0.75	2.25	3.75	5.25	6.75
SYMBOL	o	△	□	◇	D

a) AIR AS INNER-JET GAS

b) FC-77 AS INNER-JET GAS

PARTIAL PRESSURE OF INNER-JET GAS / TOTAL PRESSURE, $\frac{P_I}{P}$
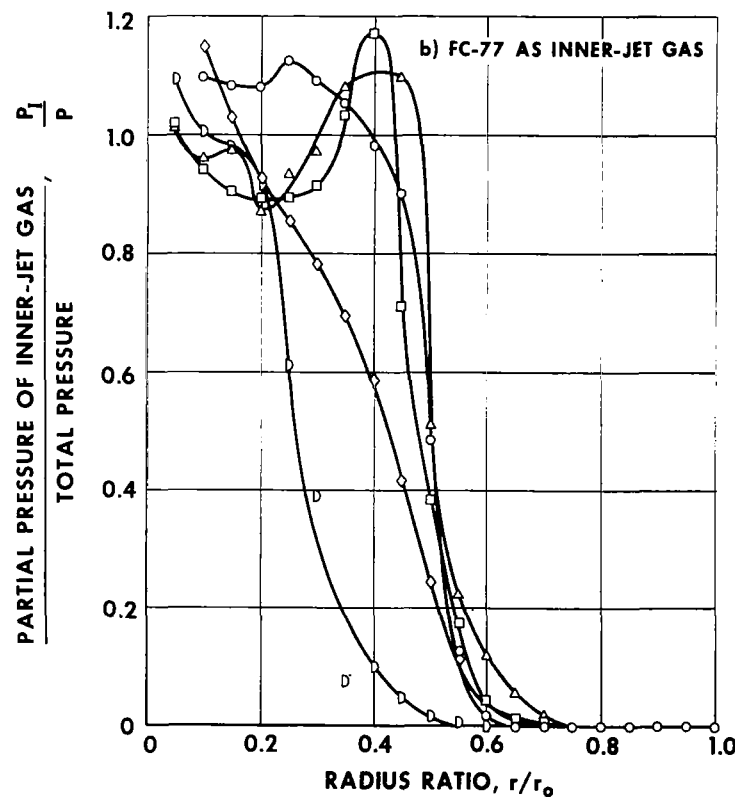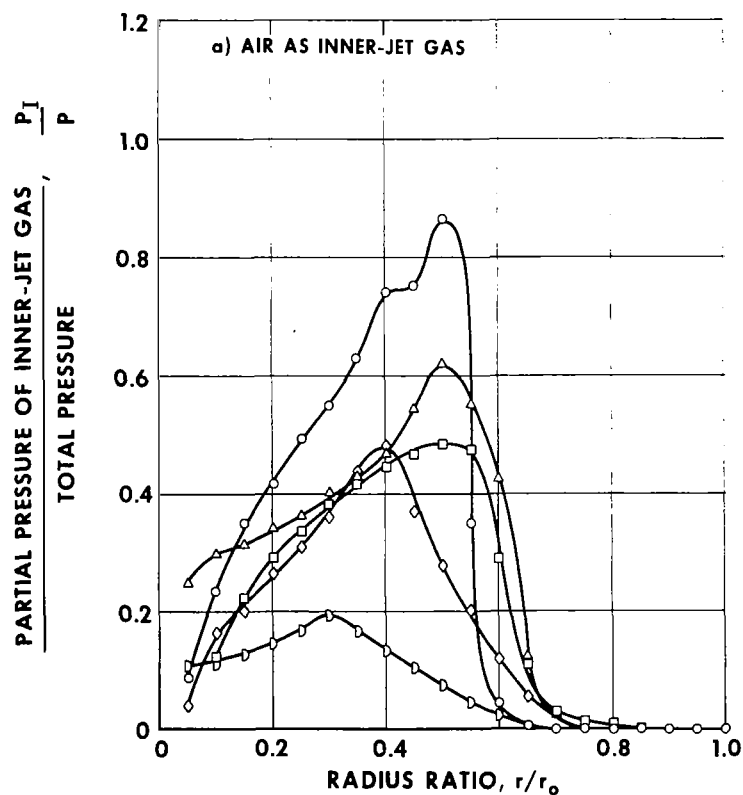
RADIUS RATIO, r/r_o

FIG. 29

FIG. 30

EFFECT OF DENSITY RATIO ρ_I/ρ_{BAO} ON AXIAL DISTRIBUTION

OF AREA-AVERAGE PARTIAL PRESSURE RATIO P_I*/P FOR $r_I/r_O = 0.5$

ρ_I VARIED; ρ_B, ρ_O AND ρ_{BAO} HELD CONSTANT

P_I*/P DERIVED FROM DATA IN FIGS. 22b AND 29

$$P_I*/P = 2\int_0^{r_O}(P_I/P)\, r\, dr/r_O^2$$

CASE	SYMBOL	INNER-JET GAS	ρ_I/ρ_{BAO}	V_{BAO}/V_I	V_B/V_{BAO}
278	△— — —△	AIR	1.0	18	0.41
260	○———○	FREON-11	4.7	20	0.41
316	□— ——□	FC-77	14.0	20	0.41

AREA-AVERAGE PARTIAL PRESSURE RATIO, P_I*/P, OF INNER-JET GAS AT INLET PLANE

$L_C = 7.5$ IN.

AREA-AVERAGE OF INNER-JET GAS PARTIAL PRESSURE, $\dfrac{P_I*}{P}$
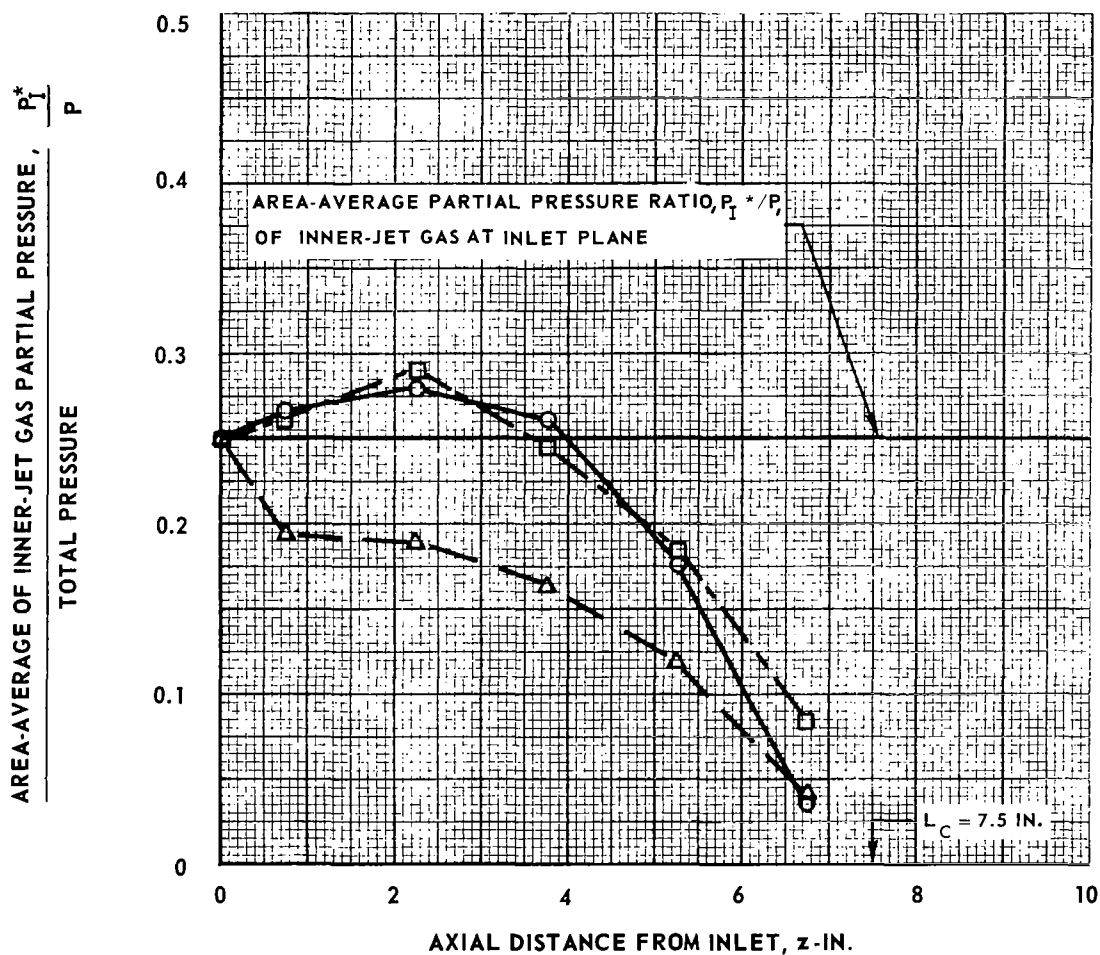
TOTAL PRESSURE

AXIAL DISTANCE FROM INLET, z-IN.

FIG. 31

EFFECT OF DENSITY RATIO ρ_I/ρ_{BAO} ON AVERAGE PARTIAL PRESSURE OF INNER-JET GAS IN CHAMBER FOR $r_I/r_O = 0.5$

ρ_I VARIED; ρ_B, ρ_O AND ρ_{BAO} HELD CONSTANT

$\overline{P}_I/P$ DERIVED FROM DATA IN FIGS. 29 AND 30 AND

OTHER TESTS OF SAME GEOMETRIC CONFIGURATION

SYMBOL	INNER-JET GAS	ρ_I/ρ_{BAO}	V_{BAO}/V_I
△— — —△	AIR	1.0	18
○———○	FREON-11	4.7	20
□— · —□	FC-77	14.0	20

NOTE:
AVERAGE PARTIAL PRESSURE OF CYLINDER OF
INNER-JET GAS HAVING VOLUME $\pi r_I^2 L_C$
IS $\overline{P}_I/P = 0.25$

0.24

0.20

0.16

0.12

0.08

0.04

0

AVERAGE PARTIAL PRESSURE OF INNER-JET GAS $\dfrac{\overline{P}_I}{P}$, $\dfrac{}{\text{TOTAL PRESSURE}}$

$$\overline{P}_I/P = \frac{2}{L_C r_O^2} \int_0^{L_C} \int_0^{r_O} (P_I/P)\, r\, dr\, dz$$

0   0.2   0.4   0.6   0.8   1.0

BUFFER-STREAM VELOCITY
——————————————————————————— , $\dfrac{V_B}{V_{BAO}}$
AVERAGE OUTER-STREAM AND BUFFER-STREAM VELOCITY

FIG. 32

EFFECT OF DENSITY RATIO ρ_I/ρ_{BAO} ON MAXIMUM VALUES OF $\bar{P}_I/P$ FOR $r_I/r_o = 0.5$

ρ_I VARIED; ρ_B, ρ_O AND ρ_{BAO} HELD CONSTANT

$L_N/D = 1.0$ $D_N/D = 0.6$

BUFFER AND OUTER GAS - AIR

$V_{BAO} = 80$ FT/SEC

MAXIMUM VALUES OF $\bar{P}_I/P$ OBTAINED FOR EACH VELOCITY RATIO, V_{BAO}/V_I

SYMBOL	INNER-JET GAS	ρ_I/ρ_{BAO}
△-----△	AIR	1.0
O———O	FREON-11	4.7
□---□	FC-77	14.0

FIG. 33

EFFECT OF DENSITY RATIO ρ_I/ρ_{BAO} ON MAXIMUM VALUES OF $\bar{P}_I/P$ FOR $r_I/r_O = 0.7$

ρ_I VARIED; ρ_B, ρ_0 AND ρ_{BAO} HELD CONSTANT

$L_N/D = 1.0$ $D_N/D = 0.6$

BUFFER AND OUTER GAS - AIR

$V_{BAO} \approx 80$ FT/SEC

MAXIMUM VALUES OF $\bar{P}_I/P$ OBTAINED FOR EACH VELOCITY RATIO, V_{BAO}/V_I

SYMBOL	INNER-JET GAS	ρ_I / ρ_{BAO}
△— — —△	AIR	1.0
⊙——⊙	FREON-11	4.7
□— — —□	FC-77	14.0

AVERAGE PARTIAL PRESSURE OF CYLINDER OF INNER-JET GAS HAVING VOLUME, $\pi r_I^2 L_C$

y-axis: MAXIMUM AVERAGE PARTIAL PRESSURE OF INNER-JET GAS / TOTAL PRESSURE, $\left(\dfrac{\bar{P}_I}{P}\right)_{MAX}$

x-axis: AVERAGE OUTER-STREAM AND BUFFER-STREAM VELOCITY / INNER-JET VELOCITY, $\dfrac{V_{BAO}}{V_I}$
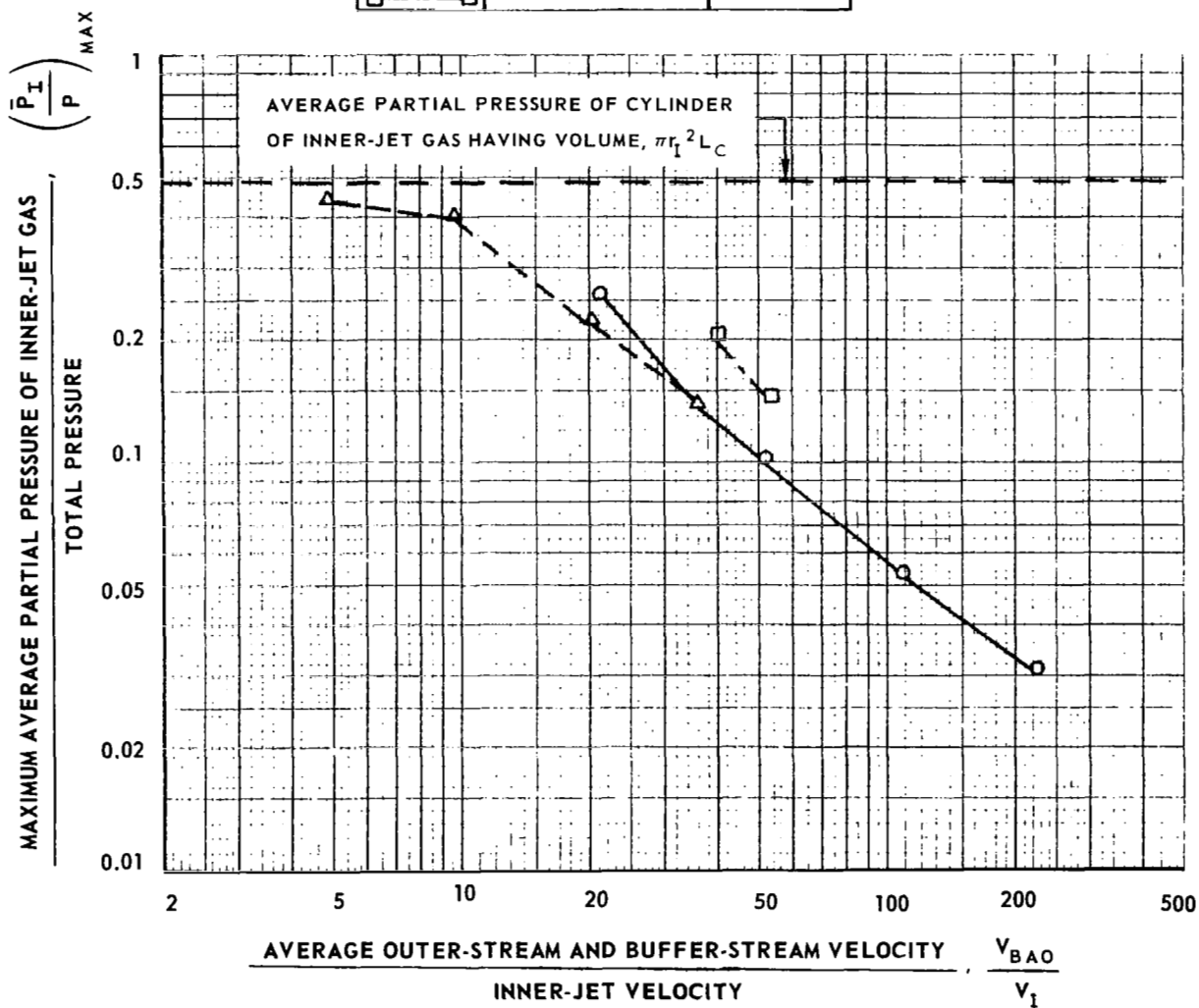
67

FIG. 34

EFFECT OF VELOCITY RATIOS V_O/V_I AND V_B/V_O ON AVERAGE PARTIAL PRESSURE OF INNER-JET GAS IN CHAMBER WITH FREON-11 AS BUFFER GAS
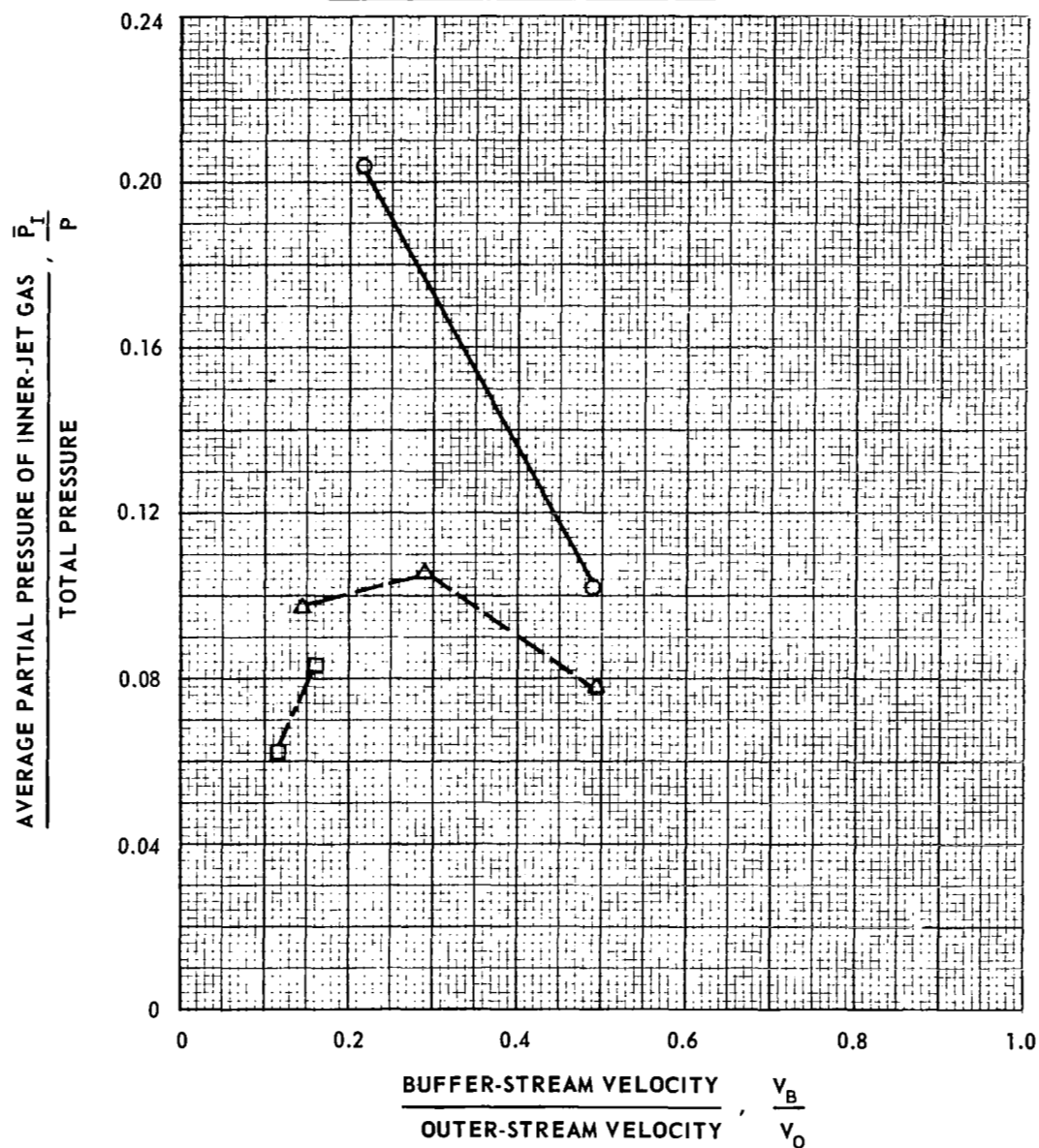
$r_I/r_O = 0.5$

V_I AND V_B VARIED; V_O HELD CONSTANT

$L_N/D = 1.0$ $D_N/D = 0.6$

INNER AND OUTER GASES - FREON-11, AIR; $\rho_I/\rho_O = 4.7$, $\rho_B/\rho_O = 4.7$

$V_O \approx 57$ FT/SEC

SYMBOL	V_O/V_I	Q_O/Q_I
O———O	18.0	41.6
△———△	32.0	74.0
□———□	48.0	111.0

Y-axis: AVERAGE PARTIAL PRESSURE OF INNER-JET GAS / TOTAL PRESSURE , $\dfrac{\bar{P}_I}{P}$

X-axis: $\dfrac{\text{BUFFER-STREAM VELOCITY}}{\text{OUTER-STREAM VELOCITY}}$, $\dfrac{V_B}{V_O}$

68

FIG. 35

EFFECT OF DENSITY RATIO ρ_I / ρ_0 ON AVERAGE PARTIAL PRESSURE OF INNER-JET

GAS IN CHAMBER WITH FREON-11 AS BUFFER GAS

V_B AND ρ_I VARIED; V_I, V_0, ρ_B AND ρ_0 HELD CONSTANT

$r_I / r_0 = 0.5$ $L_N/D = 1.0$ $D_N/D = 0.6$

OUTER GAS - AIR; $\rho_B/\rho_0 = 4.7$

$V_0 \approx 57$ FT/SEC, $V_I \approx 1.7$ FT/SEC; $V_0/V_I = 33$

SYMBOL	INNER-JET GAS	Q_0/Q_I	ρ_I/ρ_0
O——————O	AIR	74	1.0
△— —△	FREON-11	74	4.7
□— - —□	FC-77	76	14.0
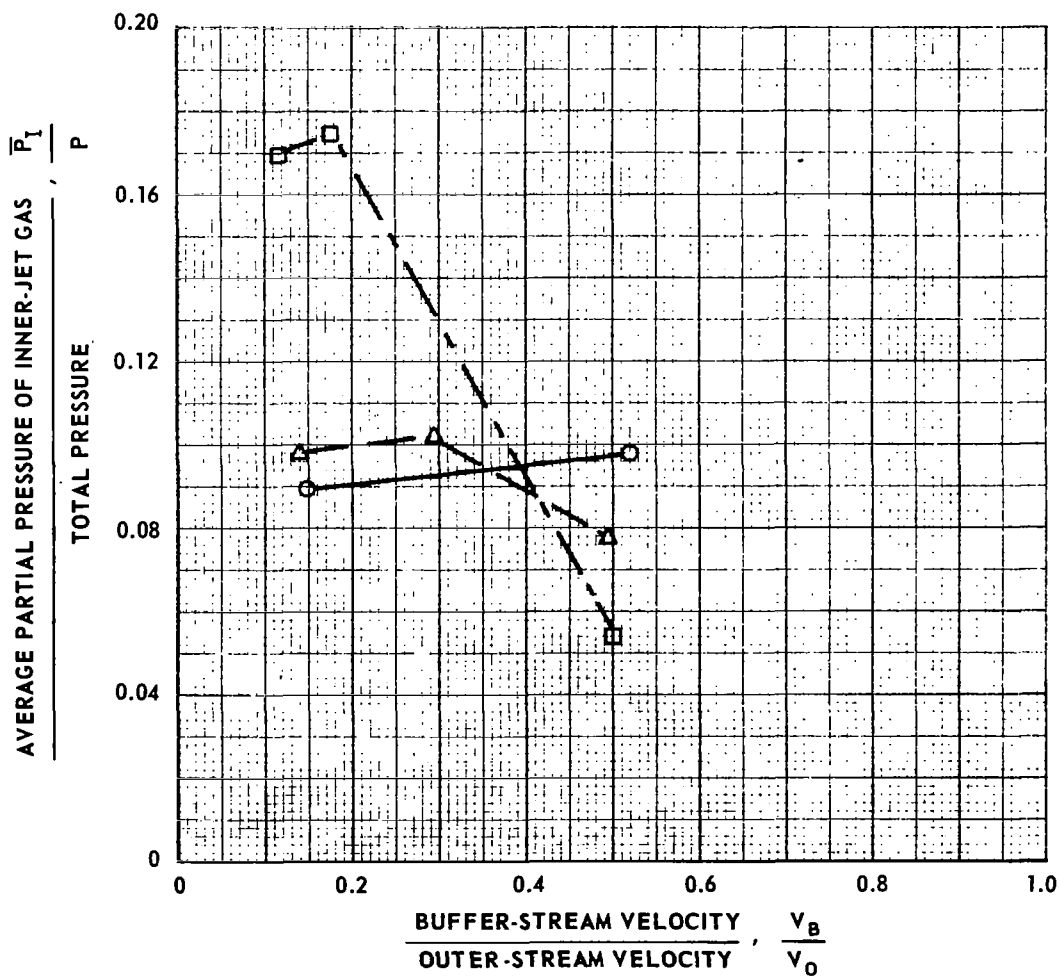
Y-axis: AVERAGE PARTIAL PRESSURE OF INNER-JET GAS / TOTAL PRESSURE , $\dfrac{\overline{P}_I}{P}$

X-axis: BUFFER-STREAM VELOCITY / OUTER-STREAM VELOCITY , $\dfrac{V_B}{V_0}$

FIG. 36

COMPARISON OF MAXIMUM VALUES OF $\overline{P}_I/P$ FOR TESTS WITH AIR AND FREON-11 AS BUFFER GASES AND $r_I/r_O = 0.5$

$L_N/D = 1.0$ $\qquad$ $D_N/D = 0.6$

OUTER GAS - AIR

MAXIMUM VALUES OF $\overline{P}_I/P$ OBTAINED FOR EACH FLOW RATE RATIO, Q_{AIR}/Q_I

SYMBOL	INNER-JET GAS	ρ_I/ρ_{BAO}	BUFFER-STREAM GAS	ρ_B/ρ_O	ρ_B/ρ_I
△———△	AIR	1.0	AIR	1.0	1.0
○———○	FREON-11	4.7			0.21
□———□	FC-77	14.0	↓	↓	0.07
▲———▲	AIR	1.0	FREON-11	4.7	4.7
●———●	FREON-11	4.7			1.0
■———■	FC-77	14.0	↓	↓	0.34

AVERAGE PARTIAL PRESSURE OF CYLINDER OF INNER-JET GAS HAVING VOLUME $\pi r_I^2 L_C$

MAXIMUM AVERAGE PARTIAL PRESSURE OF INNER-JET GAS $\dfrac{\left(\overline{P}_I\right)}{P}_{MAX}$, TOTAL PRESSURE

$\dfrac{\text{OUTER-STREAM AND BUFFER-STREAM AIR VOLUME FLOW RATE}}{\text{INNER-JET GAS VOLUME FLOW RATE}}$, $\dfrac{Q_{AIR}}{Q_I}$
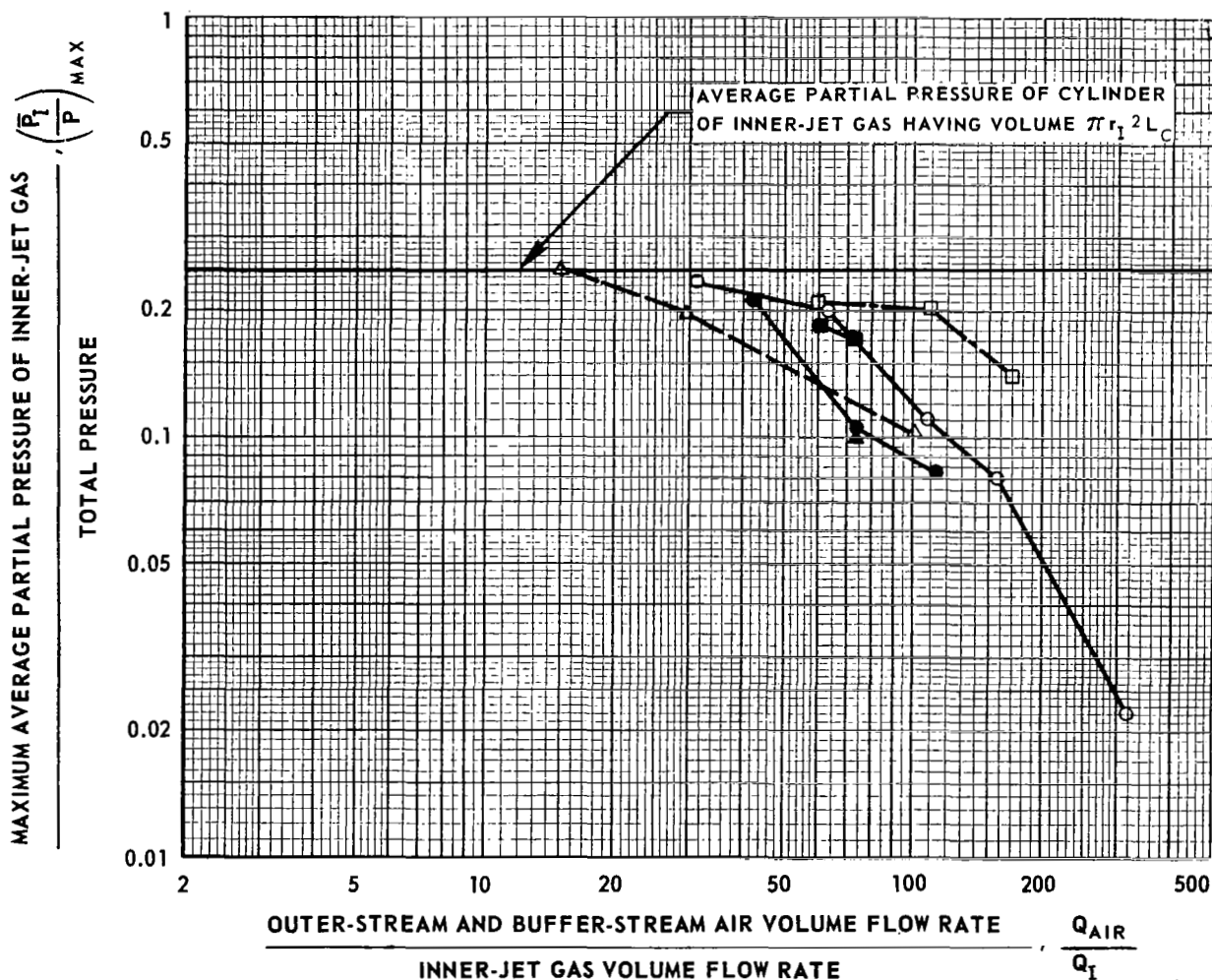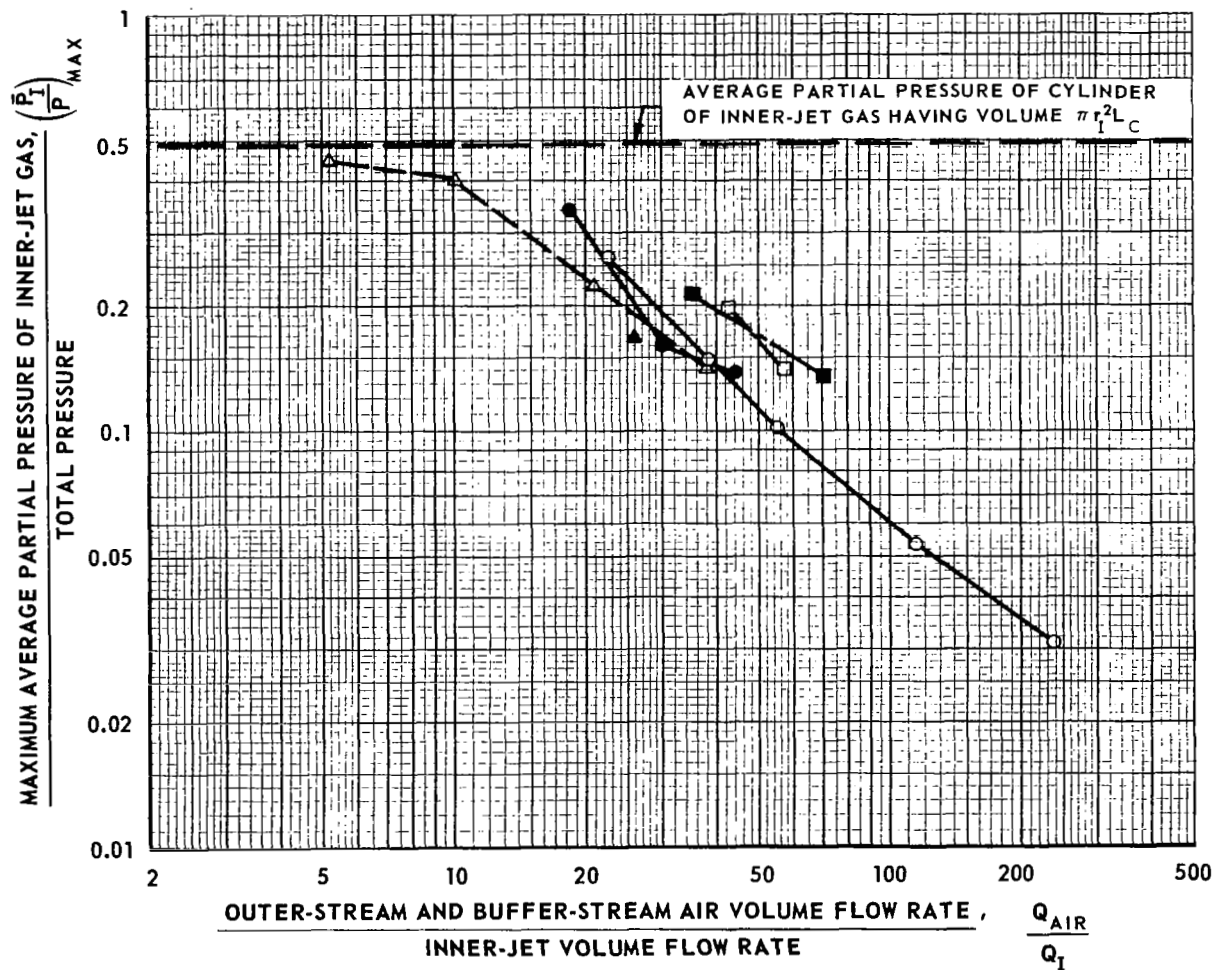
FIG. 37

COMPARISON OF MAXIMUM VALUES OF $\bar{P}_I/P$ FOR TESTS WITH AIR AND FREON-11 AS BUFFER GASES AND $r_I/r_O = 0.7$

$L_N/D = 1.0 \quad D_N/D = 0.6$

OUTER GAS - AIR

MAXIMUM VALUES OF $\bar{P}_I/P$ OBTAINED FOR EACH FLOW RATE RATIO, Q_{AIR}/Q_I

SYMBOL	INNER-JET GAS	ρ_I/ρ_O	BUFFER-STREAM GAS	ρ_B/ρ_O	ρ_B/ρ_I
△———△	AIR	1.0	AIR	1.0	1.0
○———○	FREON-11	4.7	↓	↓	0.21
□—·—□	FC-77	14.0	↓	↓	0.07
▲———▲	AIR	1.0	FREON-11	4.7	4.7
●———●	FREON-11	4.7	↓	↓	1.0
■—·—■	FC-77	14.0	↓	↓	0.34

MAXIMUM AVERAGE PARTIAL PRESSURE OF INNER-JET GAS, $\left(\dfrac{\bar{P}_I}{P}\right)_{MAX}$ — $\dfrac{\text{(inner-jet gas)}}{\text{TOTAL PRESSURE}}$

AVERAGE PARTIAL PRESSURE OF CYLINDER OF INNER-JET GAS HAVING VOLUME $\pi r_I^2 L_C$

OUTER-STREAM AND BUFFER-STREAM AIR VOLUME FLOW RATE , $\dfrac{Q_{AIR}}{Q_I}$
INNER-JET VOLUME FLOW RATE

PHOTOGRAPHS SHOWING EFFECTS OF CHAMBER L_N/D ON CONTAINMENT OF INNER-JET GAS AT MAXIMUM VALUES OF V_{BAO}/V_I FOR WHICH RECIRCULATION COULD BE PREVENTED BY PROPER CHOICE OF BUFFER VELOCITY
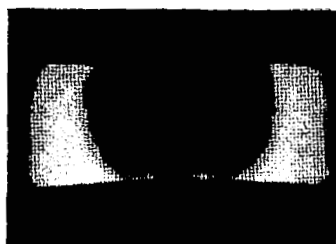
L_N VARIED

$r_I/r_O = 0.5$ $D_N/D = 0.6$

OUTER AND BUFFER GAS - AIR
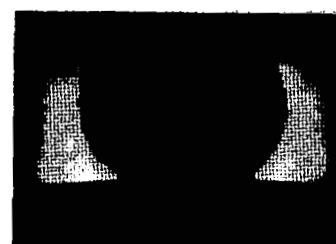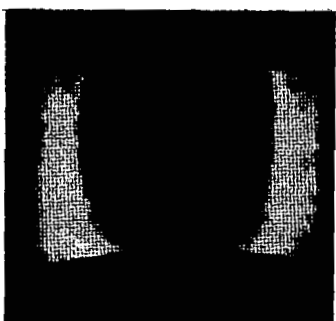
$V_{BAO} \approx 80$ FT/SEC
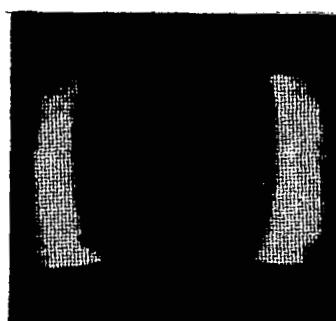
a) INNER-JET GAS - FREON-11

b) INNER-JET GAS - AIR

$L_N/D = 0.75$
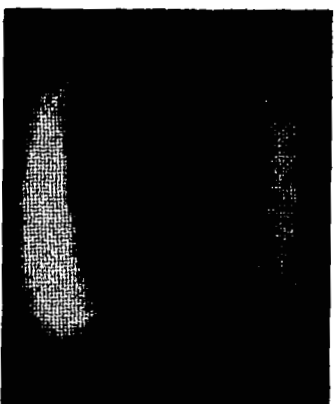
$V_{BAO}/V_I = 29.5$

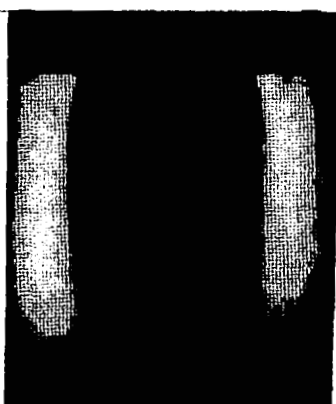$V_{BAO}/V_I = 13.0$

$L_N/D = 1.00$

$V_{BAO}/V_I = 18.4$

$V_{BAO}/V_I = 8.2$

$L_N/D = 1.25$

$V_{BAO}/V_I = 14.4$

$V_{BAO}/V_I = 6.5$

72

EFFECT OF CHAMBER L_N/D ON MAXIMUM VALUE OF V_{BAO}/V_I FOR WHICH RECIRCULATION COULD BE PREVENTED BY PROPER CHOICE OF BUFFER VELOCITY

L_N VARIED

$r_I/r_O = 0.5$ $\qquad\qquad\qquad$ $D_N/D = 0.6$

BUFFER AND OUTER GAS - AIR; $V_{BAO} \approx 80$ FT/SEC

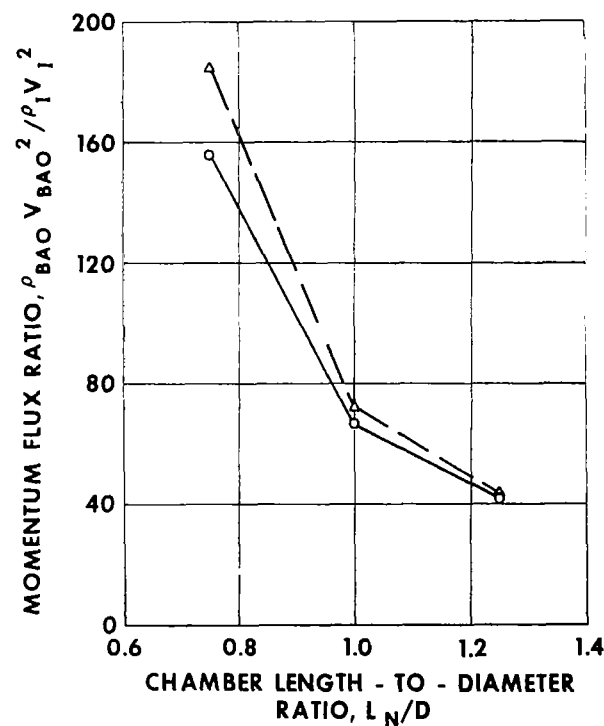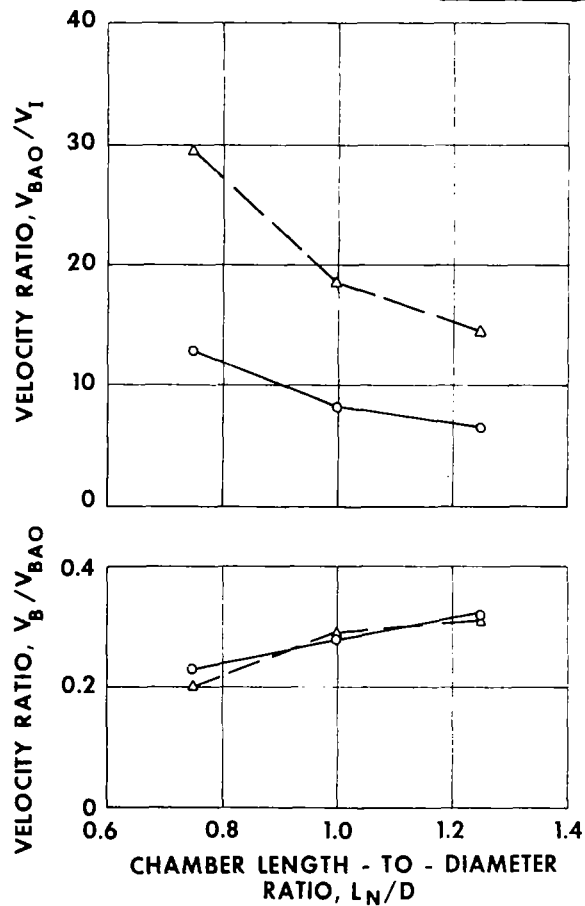| SYMBOL	INNER - JET GAS	ρ_I/ρ_{BAO}
o——o	AIR	1.0
△——△	FREON - 11	4.7

FIG. 39

FIG. 40

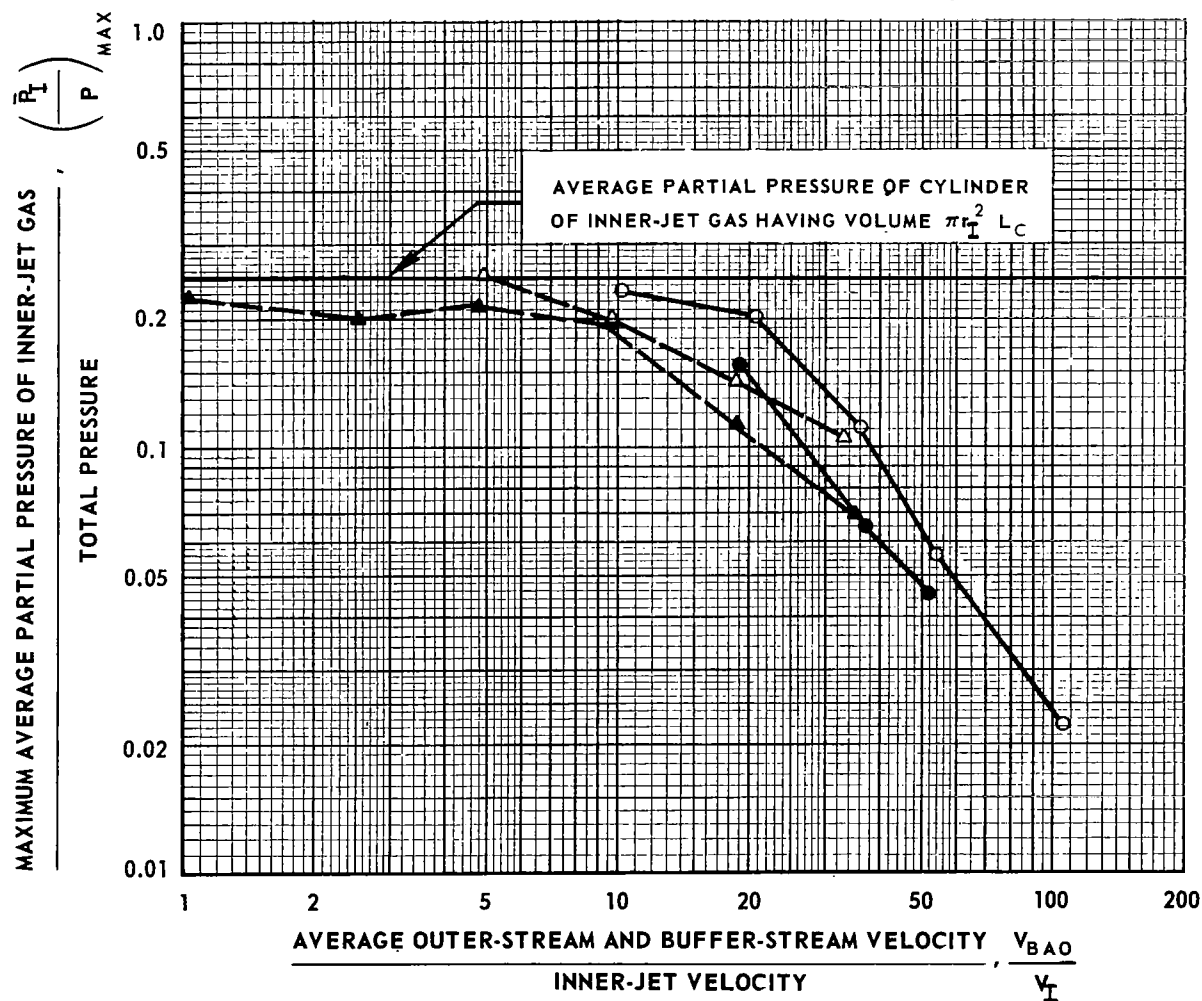# EFFECT OF CHAMBER L_N/D ON MAXIMUM VALUES OF $\bar{P}_I/P$ FOR $r_I/r_O = 0.5$

L_N VARIED

$D_N/D = 0.6$

BUFFER AND OUTER GAS - AIR

$V_{BAO} \approx 80$ FT/SEC

MAXIMUM VALUE OF $\bar{P}_I/P$ OBTAINED FOR EACH VELOCITY RATIO, V_{BAO}/V_I

SYMBOL	L_N/D	L_C/D	INNER-JET GAS	ρ_I/ρ_{BAO}
△ — — △	1.00	0.75	AIR	1.0
▲ — — ▲	1.25	1.00	AIR	1.0
○——○	1.00	0.75	FREON-11	4.7
●——●	1.25	1.00	FREON-11	4.7

AVERAGE PARTIAL PRESSURE OF CYLINDER OF INNER-JET GAS HAVING VOLUME $\pi r_I^2 L_C$

Y-axis: MAXIMUM AVERAGE PARTIAL PRESSURE OF INNER-JET GAS, $\left(\dfrac{\bar{P}_I}{P}\right)_{MAX}$, TOTAL PRESSURE

X-axis: AVERAGE OUTER-STREAM AND BUFFER-STREAM VELOCITY / INNER-JET VELOCITY, $\dfrac{V_{BAO}}{V_I}$

EFFECT OF EXHAUST NOZZLE DIAMETER RATIO D_N/D ON RADIAL
DISTRIBUTION OF INNER - JET GAS PARTIAL PRESSURE
D_N VARIED

$r_I/r_O \approx 0.7$ $\qquad$ $L_N/D \boxdot 1.0$

INNER , BUFFER AND OUTER GASES - FREON-11, AIR, AIR; $\rho_I/\rho_{BAO} = 4.7$

CASE	D_N IN.	D_N/D	V_I - FT/SEC	V_B - FT/SEC	V_O - FT/SEC	V_{BAO} - FT/SEC	V_{BAO}/V_I	V_B/V_I	V_O/V_I	V_B/V_{BAO}
183	6.0	0.6	2.02	16.5	50.7	40.2	19.9	8.2	25.1	0.41
232	2.0	0.2	2.56	22.8	63.0	50.6	19.8	8.9	24.7	0.45

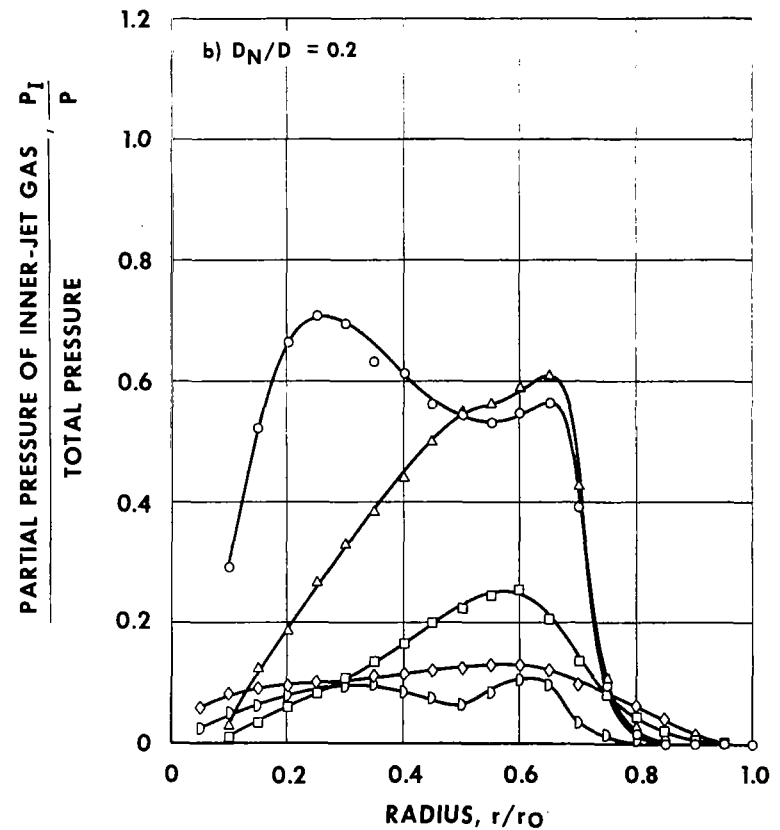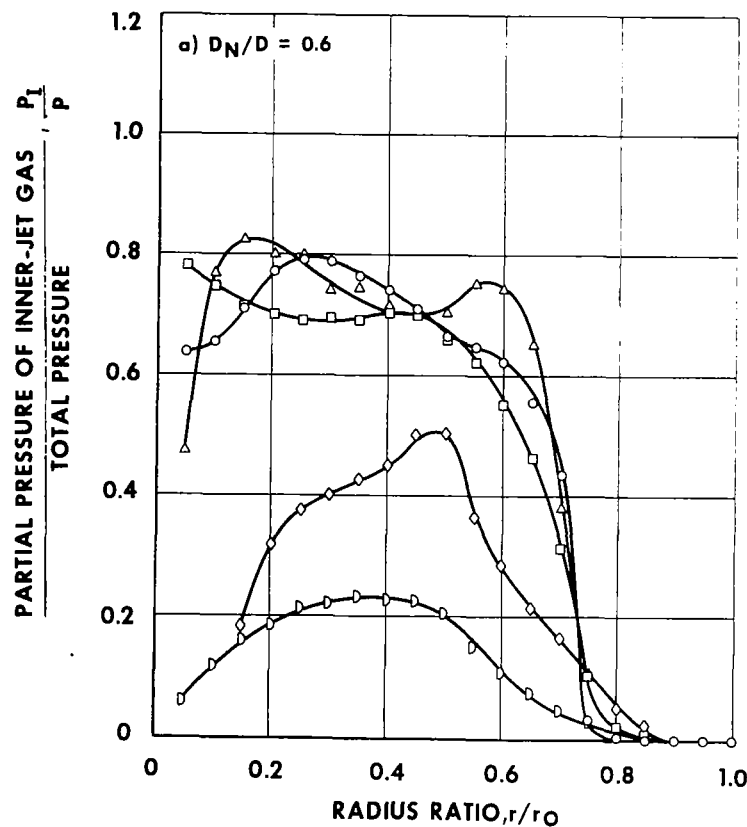| AXIAL STATION, z -IN.	0.75	2.25	3.75	5.25	6.75
SYMBOL	O	△	□	◇	⋄

FIG. 41

75

FIG. 42

EFFECT OF EXHAUST NOZZLE DIAMETER RATIO D_N/D ON AVERAGE PARTIAL PRESSURE OF INNER-JET GAS IN CHAMBER

D_N VARIED

$r_I/r_O = 0.7$ $L_N/D = 1.0$

INNER, BUFFER AND OUTER GASES - FREON-11, AIR, AIR; $\rho_I/\rho_{BAO} = 4.7$

SYMBOL	D_N/D	V_{BAO}/V_I	V_{BAO}-FT/SEC
o———o	0.6	19.9	40
△----△	0.2	19.8	51

AVERAGE PARTIAL PRESSURE OF CYLINDER OF INNER-JET GAS HAVING VOLUME $\pi r_I^2 L_C$

y-axis: $\dfrac{\bar{P}_I}{P}$, AVERAGE PARTIAL PRESSURE OF INNER-JET GAS / TOTAL PRESSURE

x-axis: $\dfrac{V_B}{V_{BAO}}$, BUFFER-STREAM VELOCITY / AVERAGE OUTER-STREAM AND BUFFER-STREAM VELOCITY
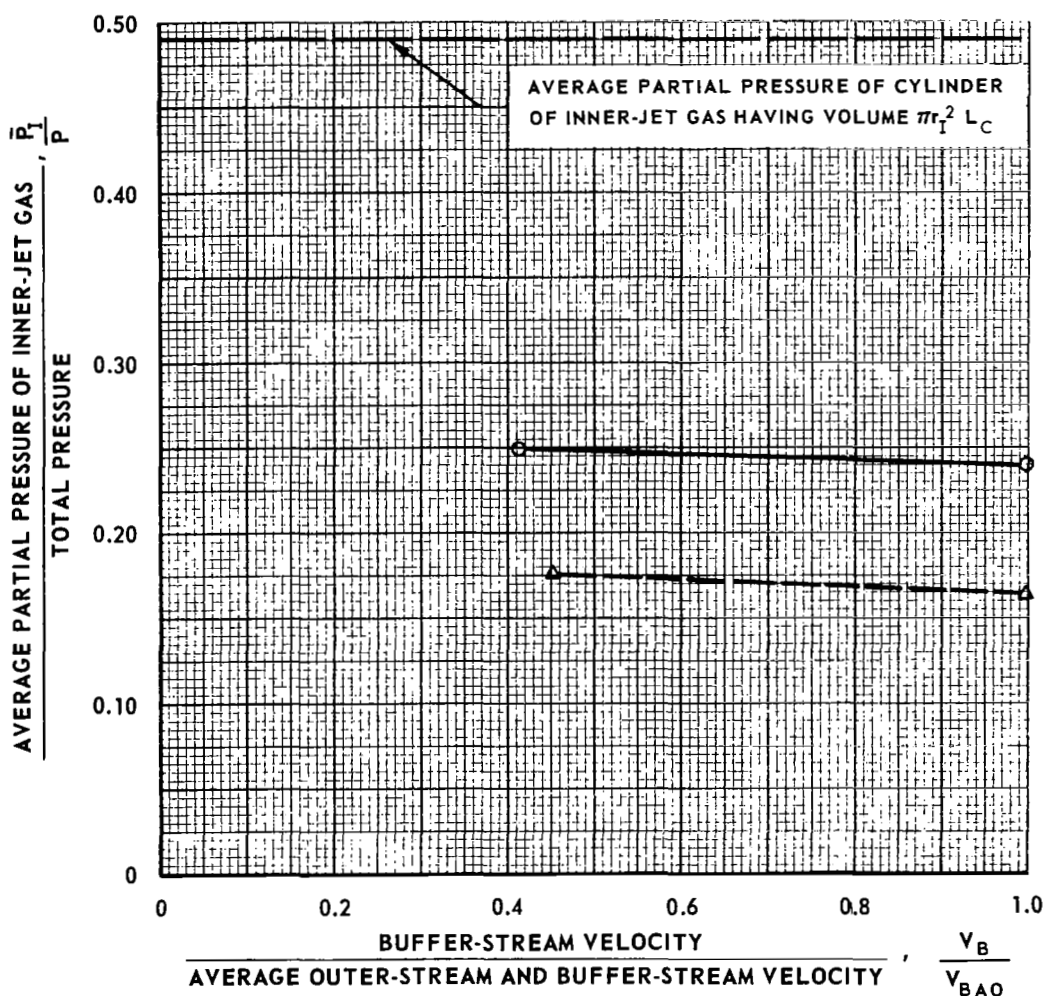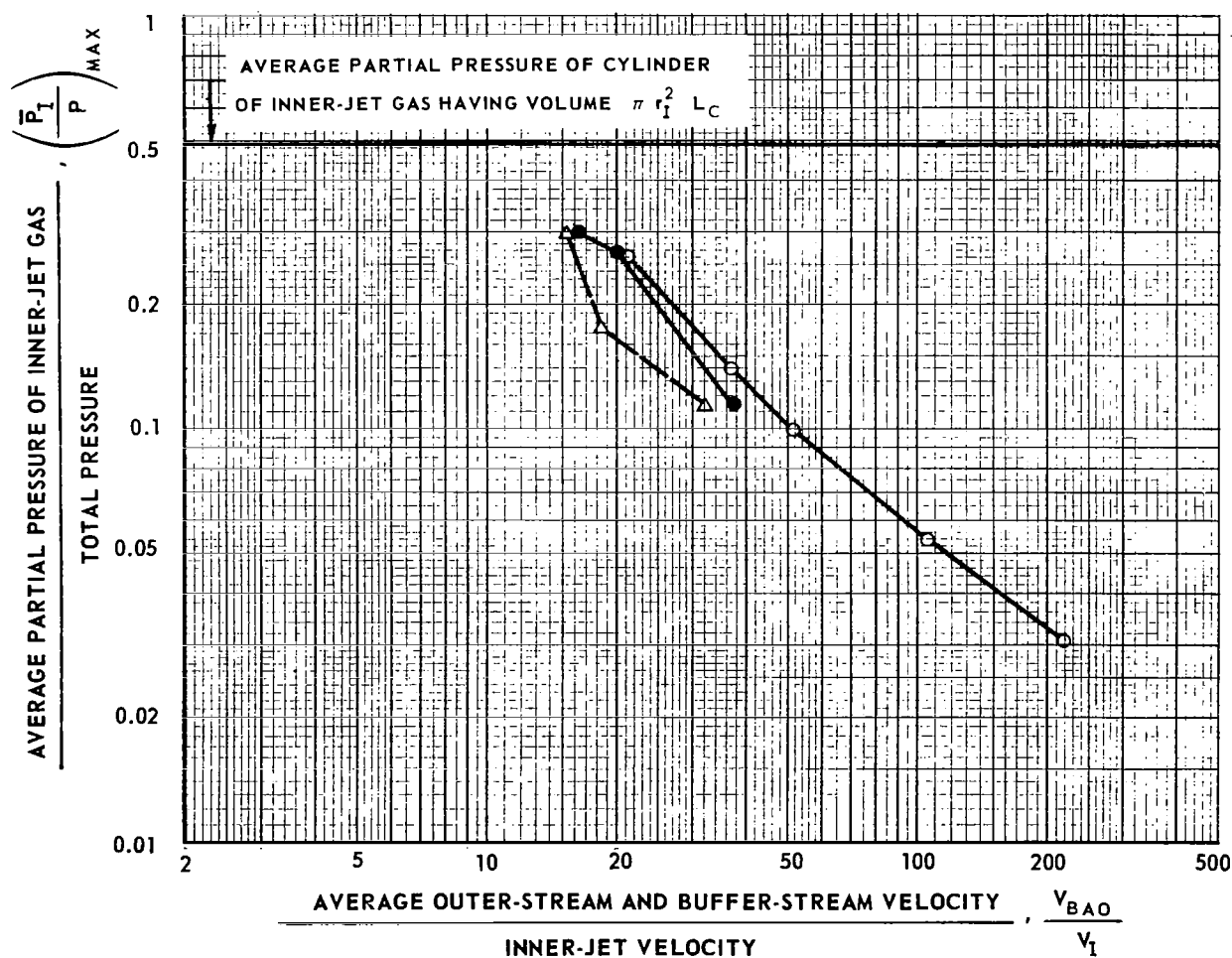
76

FIG. 43

EFFECT OF EXHAUST NOZZLE DIAMETER RATIO D_N/D ON MAXIMUM VALUES OF $\bar{P}_I/P$

D_N VARIED

$r_I/r_O = 0.7$ $L_N/D = 1.0$

INNER, BUFFER AND OUTER GASES - FREON-11, AIR, AIR; $\rho_I/\rho_{BAO} = 4.7$

MAXIMUM VALUES OF $\bar{P}_I/P$ OBTAINED FOR EACH VELOCITY RATIO, V_{BAO}/V_I

SYMBOL	D_N/D	V_{BAO} - FT/SEC
△— — —△	0.2	50
○————○	0.6	80
●————●	0.6	40

AVERAGE PARTIAL PRESSURE OF CYLINDER OF INNER-JET GAS HAVING VOLUME $\pi\, r_I^2\, L_C$

$\left(\dfrac{\bar{P}_I}{P}\right)_{MAX}$, $\dfrac{\text{AVERAGE PARTIAL PRESSURE OF INNER-JET GAS}}{\text{TOTAL PRESSURE}}$

AVERAGE OUTER-STREAM AND BUFFER-STREAM VELOCITY , $\dfrac{V_{BAO}}{V_I}$

INNER-JET VELOCITY

77

SKETCHES OF FLOW PATTERNS FOR $V_{BAO}/V_I \approx 18$

a) RECIRCULATION ZONE DIRECTLY BEHIND INLET

INNER-JET GAS	BUFFER VELOCITY
AIR	LOW
AIR	HIGH
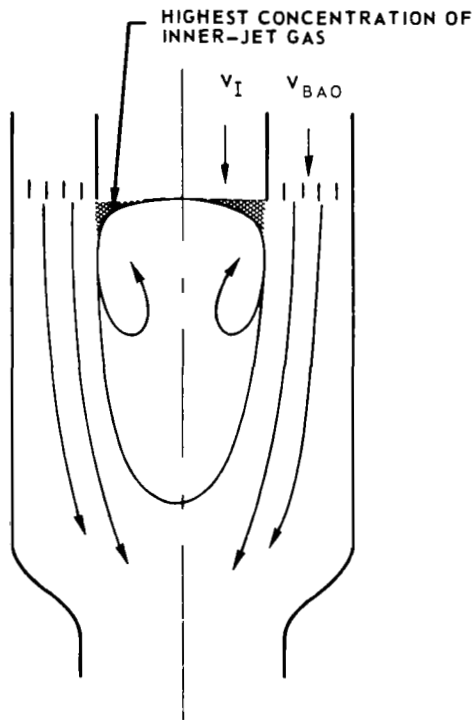
b) RECIRCULATION ZONE FORMS DOWNSTREAM OF INLET

INNER-JET GAS	BUFFER VELOCITY
AIR	MODERATE
FREON-11	HIGH
FREON-11	LOW
FC-77	LOW
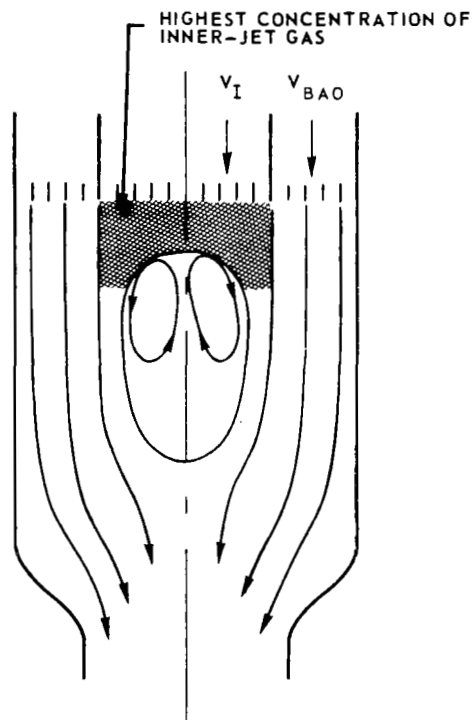
c) TURBULENT MIXING BETWEEN STREAMS WITHOUT RECIRCULATION

INNER-JET GAS	BUFFER VELOCITY
FREON-11	MODERATE
FC-77	HIGH
FC-77	MODERATE

HIGHEST CONCENTRATION OF INNER-JET GAS

V_I V_{BAO}

HIGHEST CONCENTRATION OF INNER-JET GAS

V_I V_{BAO}

HIGHEST CONCENTRATION OF INNER-JET GAS
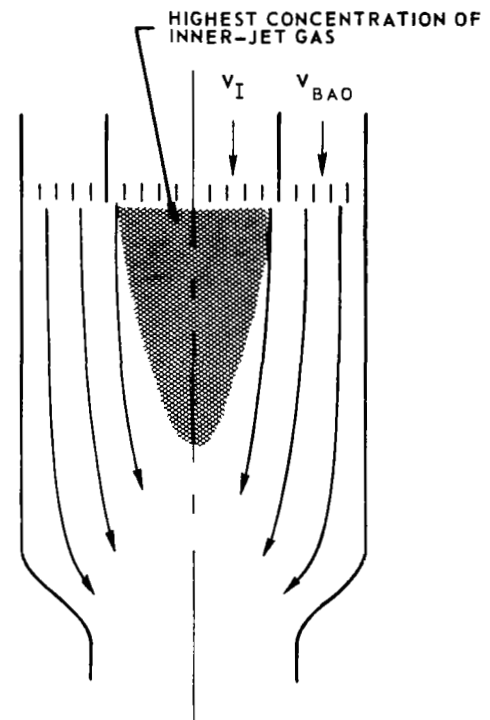
V_I V_{BAO}

78

FIG. 44

FIG. 45

SUMMARY OF EFFECT OF VOLUME FLOW RATE RATIO Q_{BAO}/Q_I
ON MAXIMUM VALUES OF $\bar{P}_I/P$

$L_N/D = 1.0$ $D_N/D = 0.6$

BUFFER AND OUTER GAS - AIR

$V_{BAO} \approx 80$ FT/SEC

DATA OBTAINED FROM FIGS. 32 AND 33

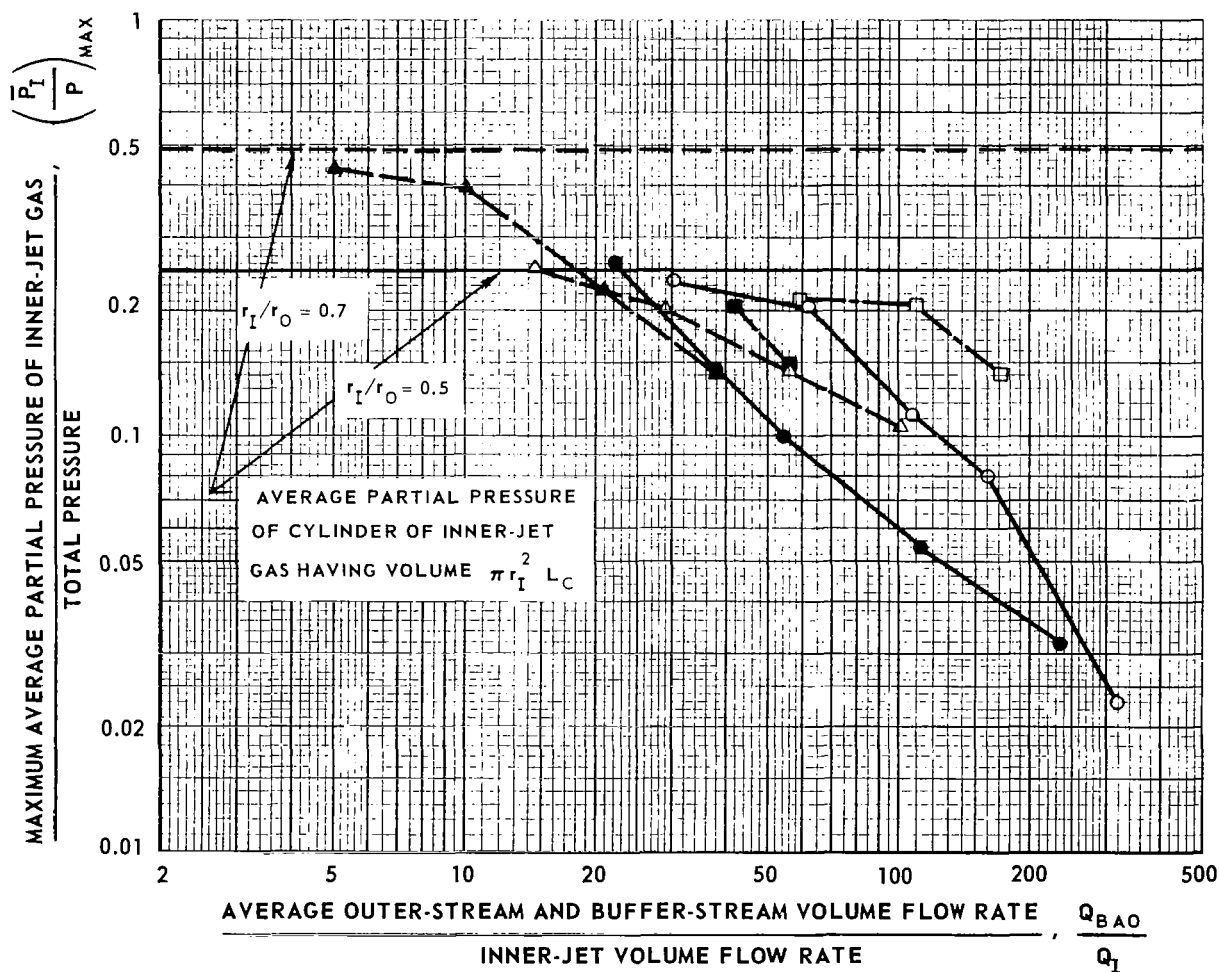| SYMBOL	INNER-JET GAS	INNER-JET GAS MOLECULAR WEIGHT	ρ_I/ρ_{BAO}	INLET MANIFOLD INNER-JET RADIUS RATIO
△— —△	AIR	29	1.0	0.5
▲— —▲	AIR	29	1.0	0.7
○——○	FREON-11	137	4.7	0.5
●——●	FREON-11	137	4.7	0.7
□— - —□	FC-77	400	14.0	0.5
■— - —■	FC-77	400	14.0	0.7

FIG. 46

SUMMARY OF EFFECT OF WEIGHT FLOW RATE RATIO
W_{BAO}/W_I ON MAXIMUM VALUES OF $\bar{P}_I/P$

$L_N/D = 1.0$ $D_N/D = 0.6$

BUFFER AND OUTER GAS - AIR

$V_{BAO} \approx 80$ FT/SEC

DATA OBTAINED FROM FIGS. 32 AND 33

SYMBOL	INNER-JET GAS	INNER-JET GAS MOLECULAR WEIGHT	ρ_I/ρ_{BAO}	INLET MANIFOLD INNER-JET RADIUS RATIO
△— — —△	AIR	29	1.0	0.5
▲— — —▲	AIR	29	1.0	0.7
○———○	FREON-11	137	4.7	0.5
●———●	FREON-11	137	4.7	0.7
□— · —□	FC-77	400	14.0	0.5
■— · —■	FC-77	400	14.0	0.7

MAXIMUM AVERAGE PARTIAL PRESSURE OF INNER-JET GAS $\left(\dfrac{\bar{P}_I}{P}\right)_{MAX}$, TOTAL PRESSURE

$r_I/r_0 = 0.7$

$r_I/r_0 = 0.5$

AVERAGE PARTIAL PRESSURE OF CYLINDER OF INNER-JET GAS HAVING VOLUME $\pi r_I^2 L_C$

AVERAGE OUTER-STREAM AND BUFFER-STREAM WEIGHT FLOW RATE / INNER-JET WEIGHT FLOW RATE , $\dfrac{W_{BAO}}{W_I}$
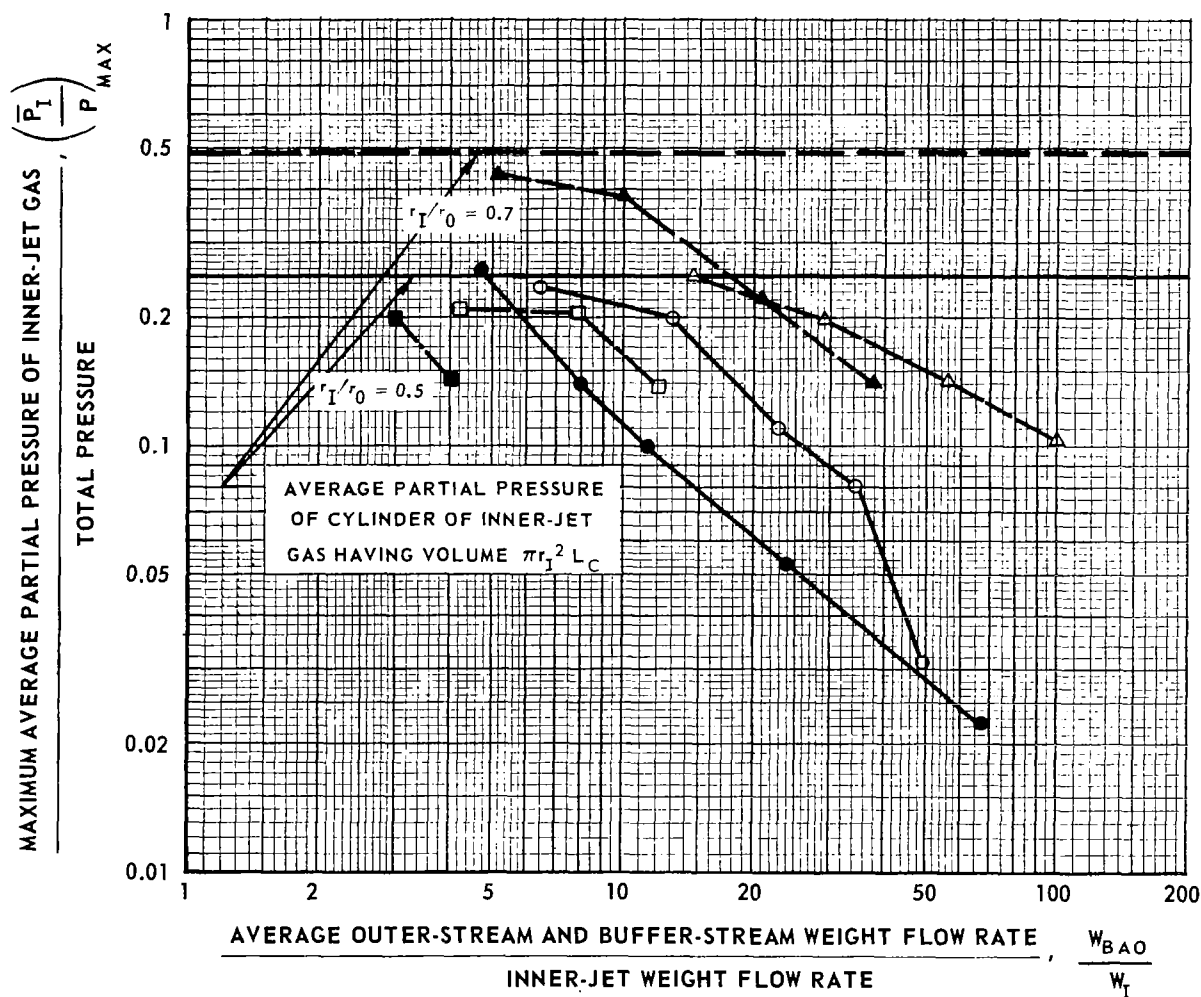
FIG. 47

SUMMARY OF EFFECT OF WEIGHT FLOW RATIO
W_{BAO}/W_I ON MAXIMUM VALUES OF $\overline{\rho}_I/\rho_{BAO}$

$L_N/D = 1.0$ $\qquad$ $D_N/D = 0.6$

BUFFER AND OUTER GAS - AIR

$V_{BAO} \approx 80$ FT/SEC

DATA OBTAINED FROM FIGS. 32 AND 33

SYMBOL	INNER-JET GAS	INNER-JET GAS MOLECULAR WEIGHT	ρ_I/ρ_{BAO}	INLET MANIFOLD INNER-JET RADIUS RATIO
△— —△	AIR	29	1.0	0.5
▲— —▲	AIR	29	1.0	0.7
○—○	FREON-11	137	4.7	0.5
●—●	FREON-11	137	4.7	0.7
□— --□	FC-77	400	14.0	0.5
■— --■	FC-77	400	14.0	0.7